Modeling Populations of Rotationally Mixed Massive Stars

Ines Brott

The chapters of this thesis have been published or are submitted to Astronomy & Astrophysics or The Astrophysical Journal. Papers and figures already published have been reprinted with permission of the corresponding journals under copyright of ESO or AAS, respectively.

Cover illustration: Dices rolling from a dice cup. In the background Sloan Digital Sky Survey images of the fields of N 11(front) and NGC 2004 (back). The stars marked with circles are studied in this thesis. The five-pointed star was a Sinterklaas gift in 2007. *Credits:* The Sloan Digital Sky Survey (`www.sdss.org`).

ISBN: 978-90-39355015

Printed by: Wöhrmann Print Service, Zutphen

Modeling Populations of Rotationally Mixed Massive Stars

De Modellering van Populaties door Rotatie Gemengde Zware Sterren
(met een samenvatting in het Nederlands)

Proefschrift

ter verkrijging van de graad van doctor aan de Universiteit Utrecht op gezag van de rector magnificus, prof. dr. J.C. Stoof, ingevolge het besluit van het college voor promoties in het openbaar te verdedigen op maandag 28 februari 2011 des middags te 12.45 uur

door

Ines Brott

geboren op 6 februari 1981 te Hamburg, Duitsland

Promotoren: Prof. dr. A. de Koter
Prof. dr. N. Langer

This research has been supported in part by the Nederlandse Organisatie voor Wetenschappelijk Onderzoek (NWO).

Contents

CHAPTER 1

Introduction

Star formation occurs over a wide range of masses, starting at a few tenths of a solar mass ($M_\odot$) up to perhaps even hundreds of $M_\odot$ (Crowther et al. 2010, also see Fig. 1.1). This thesis focuses on the most massive stars. They are also the brightest stars, visible up to vast distances in the local universe (Kudritzki et al. 2008) and in the integrated light of star-forming galaxies at high red shifts (Douglas et al. 2009).

It has been estimated that there are $\sim 10^{11}$ stars in our galaxy. Massive stars[1] represent only a small fraction of these. In other galaxies a similar situation is expected. Compared to stellar standards the typical lifetime of a massive star is very short, only a few million years. Even though the number of massive stars in the universe is small and their lives are very brief, massive stars have nevertheless a strong influence on their environment through their winds, radiation and explosive deaths. We give a few examples of this influence.

Stars more massive than about $8\,M_\odot$ end their lives in spectacular supernova explosions. Thereby, they feed back metal[2] enriched material into the interstellar medium, from which the next generation of more metal rich stars forms. In the early universe, the first generation of stars formed almost exclusively from hydrogen and helium. Star formation models predict that the first stars might have had masses between 60 and $300\,M_\odot$ (Bromm & Larson 2004). They synthesized in their core the

[1] Stars more massive than about $8\,M_\odot$

[2] The composition of a star is expressed as the mass fraction of hydrogen (X), the mass fraction of helium (Y) and the metallicity (Z). This last accounts for the mass fraction of all remaining elements.

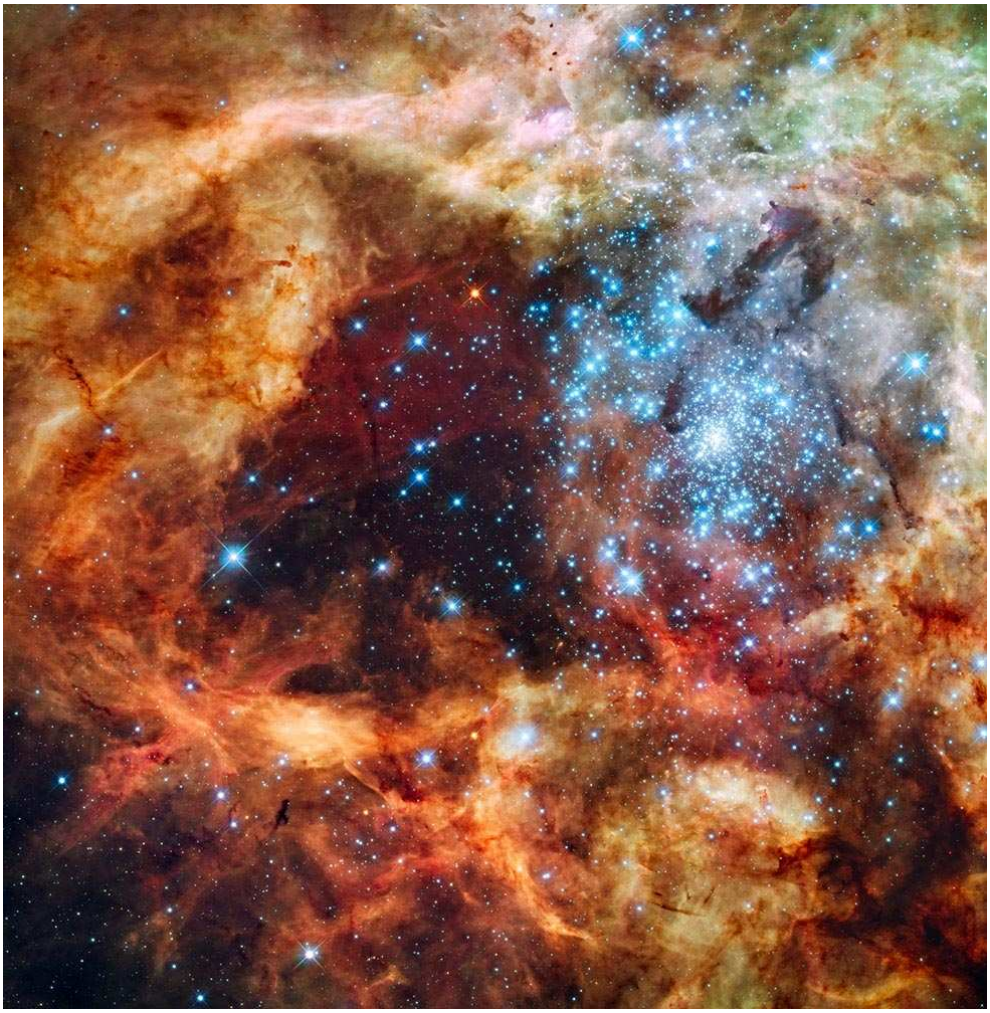

Figure 1.1: Optical image of the star forming region 30 Doradus in the Large Magellanic Cloud. The cluster in its center (R136) contains some of the most massive stars known (blue color). The current record holder R136a1 is in the cluster core, which is unresolved in this image. These Hubble observations were taken Oct. 20-27, 2009. Green color shows the glow of oxygen; and red fluorescing hydrogen. Credit: NASA, ESA, and F. Paresce (INAF-IASF, Bologna, Italy), R. O'Connell (University of Virginia, Charlottesville), and the Wide Field Camera 3 Science Oversight Committee.

first metals. Black holes left behind after the supernova (SN) explosion might have further contributed to the structure formation in the early universe (Bromm & Larson 2004; Bromm et al. 2009). It is also believed that the radiation emitted by the first stars contributed significantly to the re-ionization of the universe (Morales & Wyithe 2010).

In today's Universe massive stars continue their important role in the evolution of galaxies (McWilliam 2010). In addition to their contribution to the chemical evolution of galaxies, there is evidence that supernovae can trigger star formation in nearby giant molecular clouds (Marquez-Lugo & Phillips 2010). Also, the ionizing radiation of massive stars can trigger star formation by a process called radiation driven implosion (Bertoldi 1989; Lee & Chen 2007; Getman et al. 2009). In this scenario a nearby molecular cloud is ionized by a massive star. The ionization shock front embraces the surface of the cloud and compresses it until it reaches a critical density for gravitational collapse.

The radiation of massive stars can also stop star formation. The ionizing radiation of a nearby massive star can strip a forming proto-stellar core of its accretion disc (Balog et al. 2006), a process called disc evaporation. As massive stars form faster than low mass stars, this process is mostly affecting lower mass stars forming in a cluster where high mass stars have already formed. For a review see McKee & Ostriker (2007).

The Hertzsprung-Russell Diagram A star's two most directly observable characteristics are it's magnitude and spectral type. These two plotted against each other form the Hertzsprung-Russell diagram (HR-diagram, first produced by Russell in 1913 based on work of Hertzsprung in 1911). Stellar evolution theorists use a slightly different form of this diagram. If the distance to the star is known, e.g. for stars that belong to the same star cluster, the magnitudes can be translated into luminosities. The color or the spectral type of a star is related to its surface temperature, which can be determined with the help of stellar atmosphere models. Historically the spectral classes are labeled O, B, A, F, G, K and M with O-stars being the hottest stars ($T \gtrsim 35\,kK$) and M-stars the coolest. Our Sun has, with a surface temperature of 5700 K, the spectral type G. In this thesis we will mainly work on early B-type stars, referring to the spectral subtypes that are associated with the hotter members of the B-temperature range. During its life a star follows a unique track through the HR-diagram, determined by its initial properties mass, chemical composition and rotational velocity. Examples of this diagram can be seen in Fig.1.2.

Problems in Massive Star Evolution

Despite the importance of massive stars, their evolution is still poorly understood. For low and intermediate mass stars, evolutionary models have been quite successful in reproducing the main observable properties, e.g. see Gallart et al. (2005) for a review on the interpretation of color-magnitude diagrams using stellar evolution models, or Serenelli (2010) on the solar standard model. In contrast, for massive stars it remains a major challenge to even reproduce the distribution of stars in the Hertzsprung-Russell diagram. To be specific, stellar models predict a well-determined cool edge of the main-sequence band and a clear gap between core-hydrogen and blue core-helium burning stars. However, observational samples do not show this sharp transition (Fig.1.2). The gap predicted by stellar models is populated by many O and B supergiants whose evolutionary stage remains unclear (e.g. Fitzpatrick & Garmany 1990; Evans et al. 2006; Vink et al. 2010).

As a possible solution for this dilemma, rotation was introduced into stellar evolution models (i.e. Heger et al. 2000; Meynet & Maeder 1997). All stars rotate, a property which young stars inherit from the molecular clouds in which they are born. However, rotation has long been neglected as a second order effect in evolutionary calculations. The Sun is a very slow rotator, turning around its own axis once in about 27 days (Plyusnina 2010), which is equivalent to an equatorial rotation velocity of about 2 km/s. Massive main-sequence stars rotate on average with much higher velocities, i.e. of the order of 100 km/s (Hunter et al. 2008b; Martayan et al. 2006, 2007; Penny & Gies 2009). In this context helium and nitrogen surface abundances are of particular concern. In some massive O- and B-type stars and in giants and supergiants these elements have been found to be enriched (Gies & Lambert 1992; Herrero 1993; Vrancken et al. 2000; Przybilla et al. 2010). Rotationally induced mixing processes are thought to be responsible for these observations. Unfortunately abundance measurements have been restricted to low projected rotation rates, with the inference that enriched stars might be fast rotators viewed near pole-on. The physics of rotational mixing in evolutionary models for *rapid rotators* could well account for the observed range of enhancements.

This Thesis

Most of the work presented in this thesis focuses on evolutionary models of the hydrogen burning phase of massive rotating stars. We concentrate on the effects of rotation on surface abundances, particularly nitrogen. We present results for nitrogen measurements of the VLT-FLAMES Survey of Massive Stars (FLAMES Survey, see Sec. 1.2), for slow and fast rotating B-type stars. Our evolutionary models are com-

pared and calibrated against this sample. We employ detailed population synthesis models, allowing us to investigate the effect of different inclination angles and diverse selection effects on the sample. The sample of the FLAMES Survey gives the unique opportunity for quantitative tests of the current theory of rotational mixing.

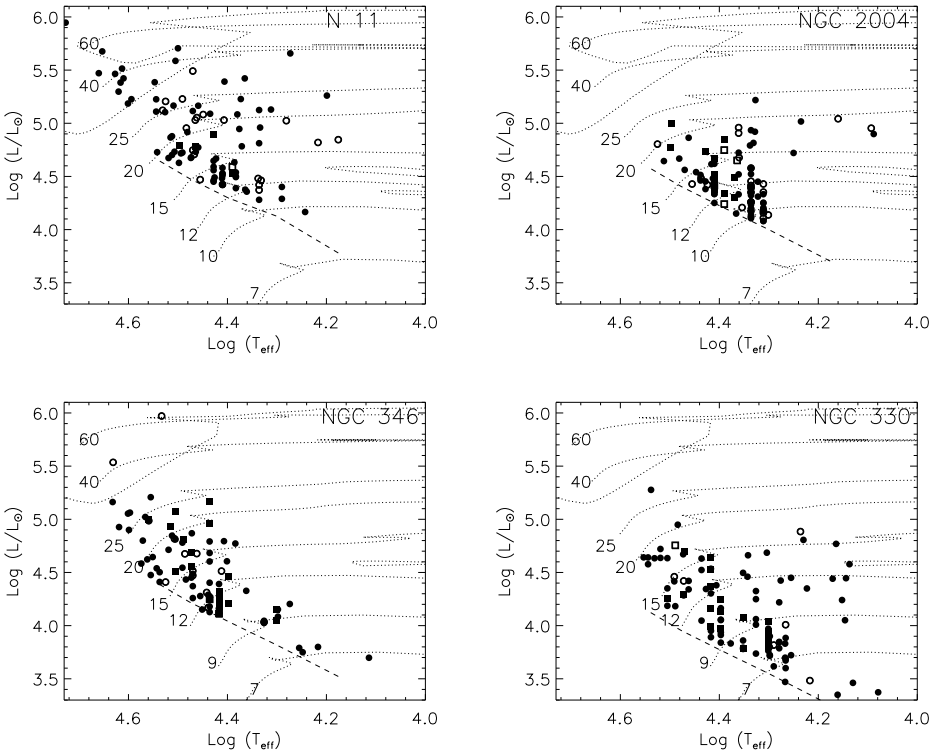

Figure 1.2: Hertzsprung-Russell diagrams of O- and early B- stars observed in the fields towards the clusters N 11 and NGC 2004 in the Large Magellanic Cloud (LMC), and NGC 346 and NGC 330 in the Small Magellanic Cloud (SMC). Open symbols denote objects showing evidence for binarity. Be-stars are plotted as squares. Evolutionary tracks for non-rotating models are shown as dotted lines. Models for LMC metallicity have been obtained from Meynet et al. (1994); Schaerer et al. (1993) and from Meynet et al. (1994); Charbonnel et al. (1993) for SMC metallicity. The dashed line indicates the magnitude limit for the observation in each region. Figure from Hunter et al. (2008b), reproduced with permission © ESO.

1.1 Evolution of Massive Stars

Stellar Evolution can be divided into the evolution of low mass and high-mass stars. High mass stars are stars initially more massive than about $8\,M_\odot$. These objects end their lives in spectacular supernova explosions, leaving behind a neutron star or black hole. Low mass stars end their evolution with the ejection of a planetary nebula and the production of a white dwarf. The evolution of rotating low mass stars has been reviewed by e.g. Pinsonneault (1997). Here we concentrate on the evolution of rotating massive stars.

1.1.1 Overview

Main-Sequence Evolution The life of a star is a constant battle against gravity. Nuclear fusion in the stellar core builds up an internal pressure gradient, balancing the gravitational force at the expense of a small fraction of the rest mass which is turned into energy. The fusion of hydrogen into helium assures the hydrostatic equilibrium for about 90% of the star's life. The energy released by nuclear reactions is exactly that required to balance gravity. If the equilibrium is perturbed, the star will readjust the nuclear reaction rates through compression or expansion.

In the HR-diagram, the star starts its evolution at the zero age main-sequence (ZAMS). During hydrogen burning the stellar luminosity increases slightly due to the increasing mean molecular weight when hydrogen is transformed into helium. The star reacts to the increased luminosity by increasing its radius and lowering its effective temperature. During hydrogen burning, the stars populate the main-sequence band in the HR-diagram.

The time spent on the main-sequence depends on the mass to luminosity ratio of the stars. Using the mass luminosity relation for ZAMS stars (Kippenhahn & Weigert 1990, p. 280) one finds that

$$\tau_H(M) \sim \frac{M}{L} \sim M^{1-\eta} \sim M^{-2.5} \tag{1.1}$$

where η is the average exponent in the mass-luminosity relation ($\eta \sim 3.5$). A typical main-sequence lifetime for a $60\,M_\odot$ star is of the order of 3×10^6 yrs while a $5\,M_\odot$ star lives of the order of 8×10^7 yrs.

Post Main-Sequence Evolution When the central hydrogen is exhausted as an energy source the star contracts to increase its internal temperature and density, until new nuclear energy sources can be accessed. The internal temperature structure first allows hydrogen to ignite in a shell around the core, while the core itself continues

to contract until the temperature is sufficient to convert helium into carbon. In later evolutionary stages first carbon, then neon, oxygen and finally silicon become the main energy source of the star, while less advanced burning stages continue in shells around the core.

After core hydrogen exhaustion, an overall contraction until the ignition of the hydrogen shell source causes the star to evolve briefly to higher surface temperatures. While the core continues contracting until helium ignition, the outer envelope is driven outwards by the hydrogen shell source. The expansion into a red super-giant is so rapid that there is little chance to observe such a star. In the HR-diagram the star evolves in a very short time towards cool temperatures. This phase is known as crossing the Hertzsprung Gap. After helium ignition the star becomes much more luminous and ascends the red super-giant branch. Depending on the exact model ingredients (Langer & Maeder 1995) the evolutionary model will execute a blue-loop and will return to hotter surface temperatures during helium burning. Subsequent burning phases are much shorter. The star will further increase its luminosity and ascend the super-giant branch again.

Supernova The temperatures in the cores of massive stars are high enough that elements with atomic masses up to iron can be synthesized. Of all elements, iron has the highest binding energy per nucleon. Therefore, no further energy can be gained by nuclear fusion. The iron core is supported by electron degeneracy and thermal pressures. The self-regulation process of the star causes the core to contract, increasing its central temperature and density. Higher temperatures offer the energy required to break up the iron into alpha particles, thus inducing energy loss. Increasing densities enable electron capture on protons, reducing the electron degeneracy pressure. The loss in pressure causes the core to contract, accelerating both processes even further (Fryer 2003). In the ensuing runaway process the star explodes as a supernova or a gamma ray burst, thereby distributing most of its material into the interstellar medium where it resides until the next generation of stars and planets is formed.

1.1.2 Evolution with Rotation

Mass loss and rotation affect massive star evolution and have a complicated interplay (Maeder 2000). In this thesis we focus on early B-stars at sub solar metallicity where mass loss is not very important. Therefore, we can single out the effects of rotation. The bulk of the stars discussed in this thesis experience relatively modest rotation, i.e. less than 70% of their break-up velocity. In the following paragraphs we will first discuss the case of moderate rotation before we turn to the discussion of rotation close to the break-up velocity.

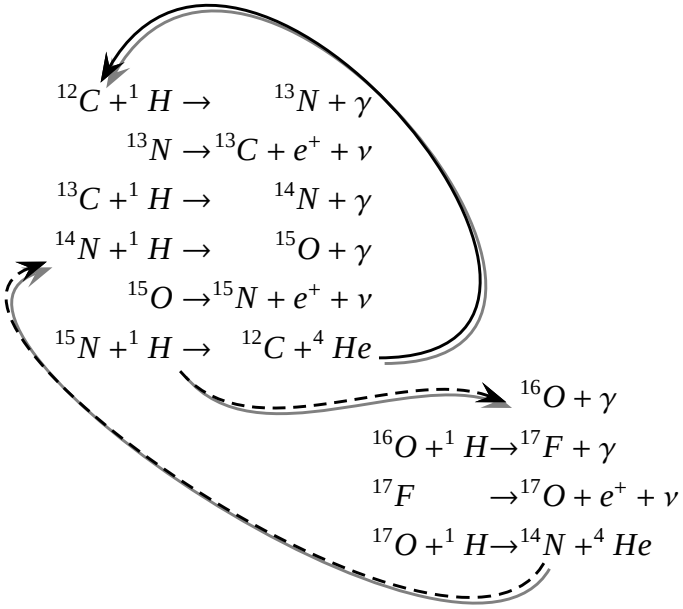

Figure 1.3: Schematic drawing of the CNO-cycle. The top part represents the main cycle (black arrow); the ^{16}O side branch (dashed arrows) is $\sim 10^4$ times less probable. Figure adapted from Kippenhahn & Weigert (1990)

Rotational Induced Mixing In the presence of rotation, the centrifugal force balances part of the gravitational force, thereby reducing the effective surface gravity. Thus the star 'feels lighter' and appears cooler and slightly less luminous than a non-rotating model of the same mass.

Since the radiative energy flux depends on the effective gravity (von Zeipel 1924), temperature and luminosity become latitude dependent. The resulting thermal imbalance drives large scale meridional currents. The Eddington-Sweet Circulation is the most important mixing process in rotating massive star models. Shear mixing can also become important in the presence of strong differential rotation. The presence of magnetic fields can keep the star largely in rigid body rotation, which reduces the influence of shear.

Rotational mixing is most important during the main-sequence evolution. Stars on the main-sequence have a wide range of rotational velocities (Hunter et al. 2008b, see also Chap. 2). When they reach the red super-giant branch, they become very slow rotators due to the significant increase in radius the stars experience. Also the timescale for post main-sequence evolution is much shorter than for hydrogen burn-

ing. Both effects render rotational mixing very inefficient.

Evolutionary models predict that rotational mixing enriches the stellar surface with nitrogen. Surface abundances of boron, carbon, oxygen and some other elements are also expected to change. In this thesis nitrogen is of particular interest, because its abundance is expected to be most influenced by rotational mixing. Nitrogen is synthesized during the CNO-cycle (see Fig. 1.3). In the initial phase of the cycle most initial C nuclei are transformed into ^{14}N. The slowest reaction of the cycle (^{14}N+^{1}H) acts as a bottleneck. While ^{14}N waits to be transformed to ^{15}O, it can be mixed into the stellar envelope. With the production of He, chemical gradients (namely the H-He gradient) become steeper, effectively hindering further mixing. From the lower envelope N is gradually mixed into the atmosphere over the main-sequence lifetime.

In addition to the surface enrichment with CN-processed materials, hydrogen is mixed from the envelope into the core. This has an effect similar to convective overshooting (see below), leading to a larger core size and, therefore, moderately longer lifetimes (on the order of a few percent) in rotating models.

The general picture of rotational mixing presented here is likely oversimplified, as we discuss in Chap. 5. For example, the efficiency of rotational mixing is still under debate, though in Chap. 2, we take a step toward its calibration.

Convection and Overshooting Convective bubbles reaching the surface manifest themselves in the granulation pattern on the solar surface. Convection is driven by buoyancy and appears when the temperature gradient is very steep, such that the convective cell rises faster than it can cool. This is true in environments where the opacity is high, such as the cores of massive stars and the envelopes of cool stars. It is a very fast and efficient way to transport matter so that the material inside a convective zone is always homogeneously mixed.

In stellar models convection is approximated by mixing length theory, which dates back to Prandtl (1925) who modeled convection in analogy to molecular heat transfer (see also Kippenhahn & Weigert 1990). Instead of molecules it uses macroscopic mass elements (or 'blobs'). The mass elements can travel a characteristic mean free path (the mixing length) after which they dissolve and deposit their heat in the surrounding material. The mixing length theory does not account for momentum conservation of the mass elements. To allow the convective cells to penetrate into non-convective regions the overshooting parameter α was introduced into the models. An overshooting core in massive star models mixes additional hydrogen into the center, prolonging the hydrogen burning phase of the star.

The overshooting parameter has to be calibrated against observations. Overshooting values have been determined from eclipsing binary stars (e.g. Schröder et al.

1997; Ribas et al. 2000; Claret 2007) and via asteroseismological measurements (e.g. Briquet et al. 2007). See also Stothers (1991) for a review of more tests of overshooting. In Chap. 2 we demonstrate a new method that uses the rotational velocity distribution of a sample of stars to determine the overshooting parameter.

Extreme Rotation Rates

Most stars do not show extreme rotation rates, but there is a small fraction of stars that show extreme rates, i.e. more than 70% of the critical rotation rate. Even though they are not important for our further discussion, some interesting effects can occur.

When the star rotates so fast that the gravitational force is balanced by the centrifugal force at the stellar equator, this defines the critical rotation rate. For our models around $20\,M_\odot$ this is typically $650\,km/s$ at the ZAMS. As the star evolves and expands the critical limit will move towards lower velocities. At rotation rates close to critical a star will deviate considerably from a spherical shape. Significant luminosity and temperature differences are expected between pole and equator due to the van Zeipel effect, giving rise to polar winds and equatorial outflows caused by critical rotation (Maeder 1999). Indeed Be-stars show indications of fast rotation and expelled matter. It is believed that the Be-phenomenon is connected to fast rotation in combination with stellar pulsations (see Porter & Rivinius 2003; Cranmer 2005).

Homogeneous Evolution In very fast rotating models, rotational mixing can become so strong that it effectively prevents the build up of chemical gradients within the star. These models also show significant helium enrichment at the surface. It is said the model is evolving 'chemically homogeneous' (Maeder 1987). In the HR-diagram these models evolve to the blue, stay compact and are very luminous. Even though such stars are not yet observed, they present a theoretical channel for the production of rapidly rotating massive helium stars, which have been suggested as progenitors of long γ-ray bursts (Yoon & Langer 2005). While the increase in lifetime is of the order of a few percent for moderate rotation, it can be as large as 50% for homogeneously evolving stars.

1.2 Observations

Most often, stars are not born in solitude but in clusters. This occurs when a giant molecular cloud becomes unstable and starts to collapse, fragmenting into many clumps that become single or multiple stellar systems. In addition to their chemical

composition, which is the same for all stars in the cloud, the newborn population inherits its mass- and velocity-distribution from the initial star formation phase. For a review on massive star formation see Zinnecker & Yorke (2007). The study of stellar populations enables us to sample stars with similar initial conditions at different stages of their evolution. Therefore, it is important to know the initial distributions of mass and rotational velocity of the observed population. These properties characterize the individual newborn stars.

The initial mass function appears to be surprisingly universal and given by $n(M) \propto M^{-2.35}$ (Salpeter 1955); see also Bastian et al. (2010) for a review. The initial velocity distribution is more complicated to obtain as only the velocity component perpendicular to the line-of-sight can be measured. In high metallicity regimes mass loss can efficiently remove angular momentum from the stars, so that there might be a significant difference between the present day and the initial velocity distribution. It is also unclear if the initial velocity distribution is the same for all masses. However, if reliable projected rotational velocities are measured for a large enough sample of stars one can model the initial velocity distribution by assuming a random orientation of the inclination angles in space (Dufton et al. 2006). The effects of mass loss get less important at lower metallicities and lower masses. It is, therefore, preferable to determine the initial rotational velocity distribution using a sample that is little influenced by mass loss. In this way, initial rotational velocity distributions have been determined by, e.g. Hunter et al. (2008b); Dufton et al. (2006) and Mokiem et al. (2006).

Binaries The binary population requires the additional specification of the mass ratio of the two components, their orbital separation and eccentricity. Sana & Evans (2010) report a binary fraction of massive stars that is as high as 44%. Triple systems (i.e McKibben et al. 1998) and more complicated configurations (e.g. in the dense cores of clusters like 30 Dor, see Fig. 1.1) are observed as well. Not mentioned so far is the risk of contamination of the rotational velocity distribution by post mass-transfer binaries. Stars in a binary system can be spun up by mass transfer (Langer et al. 2008). After mass transfer, a binary system is usually no longer detectable as such (de Mink et al. 2010).
In this thesis we limit ourself to the analysis of single stars.

The VLT-FLAMES Survey of Massive Stars

Determination of nitrogen abundances for a broad range of velocities is of the utmost importance for a quantitive test of the theory of rotational mixing, as rotational

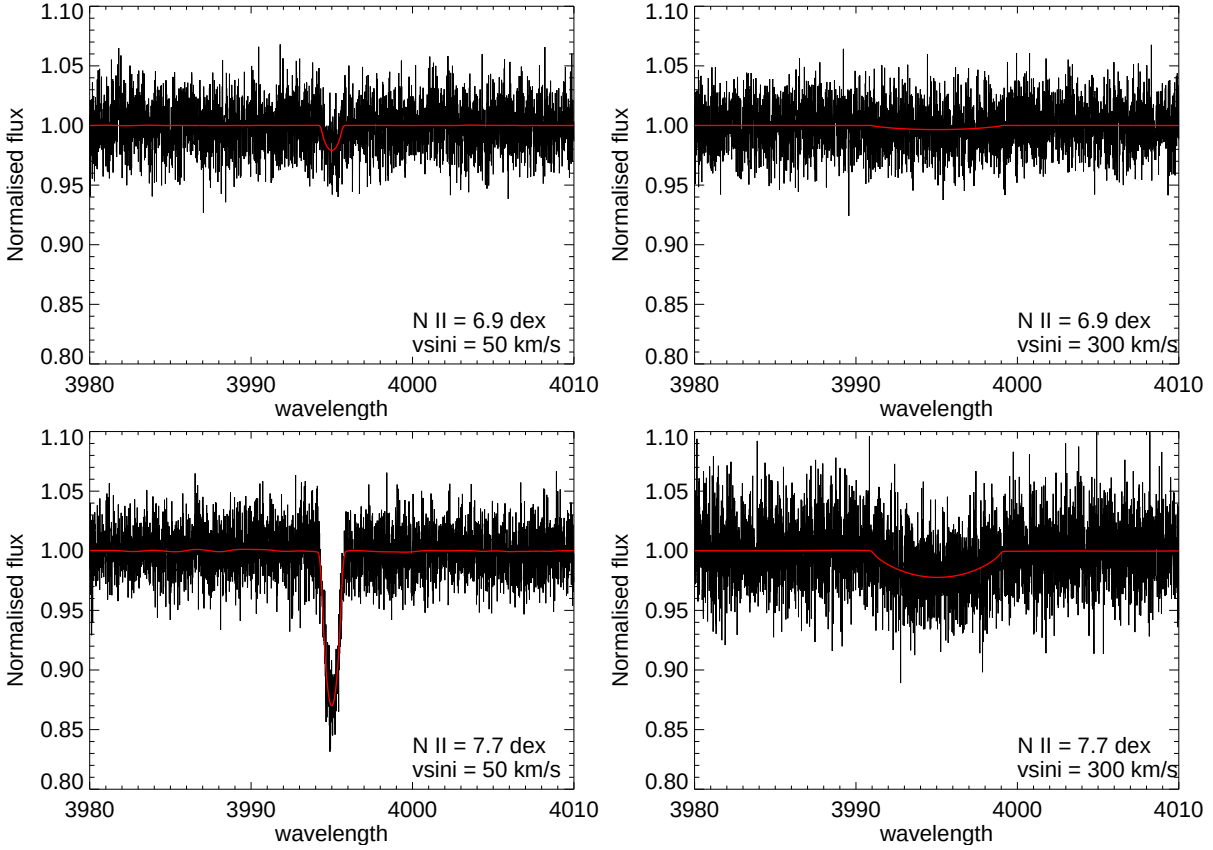

Figure 1.4: In red is shown the theoretical N II line at 3995 Å for nitrogen abundances of 6.9 dex (top) and 7.7 dex (bottom), for a projected rotational velocity of 50 km/s (left) and 300 km/s (right). In black is shown the same line for a S/N=50. These spectra are taken from a grid of non-LTE model atmospheres described by Dufton et al. (2005), calculated using the TLUSTY code (Hubeny & Lanz 1995).Figure: P. Dunstall, priv. comm.

mixing is expected to leave a stronger imprint on faster rotating stars.

Previous works, e.g. Gies & Lambert (1992); Herrero (1993); Reitermann et al. (1990); Korn et al. (2002), have been limited to the analysis of slowly rotating (mostly $v \sin i < 50$ km/s) stars. Even though first attempts of analyzing faster rotators have been made (Vrancken et al. 1997a; Korn et al. 2005), sample sizes have been too small for quantitative conclusions. An increase in the average nitrogen abundance of these slow rotators was used as an argument for the evidence of rotational mixing in these samples. The nitrogen enhanced stars in these samples would be concluded to be initial fast rotators that are observed pole on.

The VLT-FLAMES Survey of Massive Stars (Evans et al. 2005, 2006) undertook the effort to measure surface abundances and projected rotational velocities for more than 600 O and B-stars in the Magellanic Clouds and the Galaxy. A special effort was made *not* to exclude stars with larger projected rotational velocities from the analyzes but to determine their abundances, in particular nitrogen.

The FLAMES-sample provided an excellent testbed to a) re-calibrate the efficiency of rotational mixing in the evolutionary models and b) compare the predictions of our population synthesis models with the observations.
Fig. 1.4 illustrates the problematic nature of measuring abundances at high rotational velocities. It shows the N II line at 3995 Å for a abundance of 6.9 dex (typical for the LMC baseline abundance) and 7.7 dex (typical for a strongly enhanced star in the FLAMES sample). On the left the line is shown for a rotational broadening of 50 km/s, on the right for a rotational broadening of 300 km/s. Statistical noise is added to the spectrum with a S/N[3] of 50, which is the average noise level for observations in this sample. These spectra have been calculated using the TLUSTY code (Hubeny & Lanz 1995) and are described in Dufton et al. (2005) in detail. Rotation broadens spectral lines. At higher rotational velocity this can easily lead to the disappearance of weak lines in the noise level (Fig. 1.4, top right).

1.3 Overview of the Chapters of this Thesis

The VLT-FLAMES Survey of Massive Stars and its potential effects on our understanding of massive star evolution will be the subject of the major part of this thesis. In Chap. 2 we will introduce the grid of evolutionary models that has been calculated

[3]The signal to noise is a measure for how much of the signal has been corrupted by unwanted signal (noise). It is defined as μ/σ, i.e. the ratio of the signal mean (μ) over the standard deviation (σ) of the noise. In the case of a continuum-normalized spectrum, the signal-level is fixed to 1, reducing the S/N to $1/\sigma$.

for the analysis of the FLAMES Survey. Chap. 3 describes the preliminary analysis of early B-type stars in the LMC-subsample using the evolutionary models from Chap. 2. Chap. 4 presents the SMC and the Galactic samples and compares them to our models. We also present a refined comparison of the LMC sample, already described in Chap. 3 In Chap. 5 we present our newly developed population synthesis code STARMAKER which we use to simulate the population of stars in the LMC sample, to make a quantitative comparison with theoretical predictions. Chap. 6 investigates two alternative scenarios which could be responsible for a drop in B-star rotation rates at 22 kK. It is discussed if the drop can be caused by the end of the main-sequence or alternatively by an increased mass loss when stars evolve towards temperatures below 22 kK.

Chapter 2: Grids of Evolutionary Models and Isochrones

In this chapter we present a grid of more than 600 stellar evolutionary models, which have been evolved past core-hydrogen exhaustion. The models in our grid have initial masses between 5 and 60 $M_{\odot}$ and initial rotational velocities between 0 and ~550 km/s for SMC, LMC and Galactic chemical compositions. For these models we adopted an initial chemical composition tailored to the compositions of the specific environment, i.e. metallicities typically found in our sample stars. We pay particular attention to matching the CNO baseline abundances of our models to those from H II regions, as the amount of N enrichment during the subsequent stellar evolution depends critically on the initial abundances of the CNO elements. Of particular interest for Chap. 6 is the overshooting calibration in this grid, which we base on an observed drop in the projected rotational velocity as a function of surface gravity.

Also in this chapter, we present an extensive set of isochrones made from models of rotating stars. Isochrones for rotating stars cover an area in the HR-diagram instead of a line, allowing for interesting new views on stellar populations. These new isochrones also enable a refinement of current population synthesis models of young clusters that form the basis for a significant fraction of extragalactic research, demonstrating the far-reaching implications of this unique grid of stellar evolution models.

Chapter 3: Rotation and Nitrogen Enrichment as the Key to Understanding Massive Star Evolution

As described in Sec. 1.2, studies of nitrogen abundances in B-stars over a larger range of projected rotational velocities have never been attempted before. In this section we present nitrogen abundance determinations for the LMC sample of the FLAMES

Survey. The sample is compared to the evolutionary tracks described in Chap. 2. Already in this preliminary work it becomes evident that there are two groups of stars that are in contradiction to the expectations arising from stellar evolution models. We find a group of un-enriched stars with high projected rotational velocities. The surface gravities of these stars indicate that they are close to the end of hydrogen burning. As the projected rotational velocity yields only a lower limit on the true rotational velocity, a strong enrichment is expected for this group. We also find a group of enriched stars at very low projected rotational velocities. Even though some of these might be fast rotators seen pole on, it is extremely unlikely that all of them are seen pole on. Both groups challenge our understanding of rotational mixing, therefore, offering new insights into the underlying physical processes.

Chapter 4: Constraints on Stellar Evolution from the Chemical Compositions of Rapidly Rotating Galactic and Magellanic Cloud B-type stars

In this chapter we extend the analysis to the samples from the Small Magellanic Cloud and the Galaxy and compare them to the results from the LMC (Chap. 3). In the SMC sample we find a group of slowly rotating enriched stars that is comparable to the corresponding group in the LMC sample. No counterpart for the fast rotating non-enriched group can be identified, as for most fast rotators there are only upper limits on the nitrogen abundance available. An improvement compared to the previous chapter is the redefinition of the problematic group of un-enriched fast rotators. According to our evolutionary models, the lower part of the main-sequence is predicted to be too faint to be observed, given the magnitude limit of the sample. Therefore, young (unenriched) fast rotators are expected to be missing from the sample, which is in disagreement with observations detecting such a group.

In the Galactic sample we find no significant enrichment. However, only a small fraction of the fast rotators are evolved enough to show enrichment. A better insight into the true binary fraction of the problematic groups is required to confirm that those groups do not agree with evolutionary models of rotating single stars.

Chapter 5: Simulating a Population of LMC early B-type Stars as a Test of Rotational Mixing

In this chapter we present the newly developed population synthesis code STARMAKER. We apply this code to simulate the early B-type stars of the LMC subsample described in Chap. 4, as this subset has the best data quality. The grid of stellar evolution models described in Chap. 2 is used as input for our population synthesis simulation. The underlying star formation history and initial velocity distribution has

been carefully determined from the sample stars (Hunter et al. 2008b). To enable a fair comparison, we apply the same selection effects to our simulation that exist in the observed sample. Our simulations reproduce the fraction of nitrogen un-enriched stars, but predict twice as many enriched rapid rotators as found in the sample. The groups of un-enriched fast-rotators and enriched slow-rotators, (see Chap. 3) can not be reproduced by our single-star population synthesis. We argue that the group of enriched slow rotators is unlikely to be produced by binary evolution. Therefore, it is very likely important to account for binary evolution and the effects of magnetic fields to understand if rotational mixing is working in massive stars.

Chapter 6: The nature of B supergiants: Clues from a Steep Drop in Rotation Rates at 22 000 K – The possibility of Bi-stability braking

In this chapter we investigate the possibility that the observed drop in projected rotational velocity as a function of surface gravity or temperature can be caused by a sudden increase in the mass loss rate (the so called bi-stability jump around 22 kK, Vink et al. 2000, 2001). In Chap. 2 we use this drop to calibrate the overshooting parameter. In this scenario main-sequence stars can have any velocity (within the limits of the initial distribution), whereas a different population consists only of slow rotators. We find that the alternative mass loss scenario can cause a similar effect if the bi-stability jump appears on the main-sequence. In our models this is the case for models with initial masses above $30\,M_{\odot}$. At lower masses the mass loss scenario might work too, if an overshooting parameter much larger than what we use in our models (Chap. 2) is applied, in order to extend the main-sequence to temperatures below 22 kK. To settle this issue a simultaneous investigation of mass loss rates, rotational velocities and surface properties is required for a sample that contains more stars with masses above $30\,M_{\odot}$. The upcoming VLT-FLAMES Tarantula Survey (Evans et al. 2010) could provide these observations in the near future.

CHAPTER 2

Rotating Massive Main-Sequence Stars I: Grids of Evolutionary Models and Isochrones

I. Brott, S. E. de Mink, M. Cantiello, N. Langer, A. de Koter, C. J. Evans, I. Hunter, C. Trundle, J.S. Vink

Submitted to Astronomy & Astrophysics

Abstract We present a dense grid of evolutionary tracks and isochrones of rotating massive main-sequence stars. We provide three grids with different initial compositions tailored to compare with early OB stars in the Small and Large Magellanic Clouds and in the Galaxy. Each grid covers masses ranging from 5 to 60 $M_\odot$ and initial rotation rates between 0 and about 600 km/s.

To calibrate our models we used the results of the VLT-FLAMES Survey of Massive Stars. We determine the amount of convective overshooting by using the observed drop in rotation rates for stars with surface gravities $\log g < 3.2$ to determine the width of the main sequence. We calibrate the efficiency of rotationally induced mixing using the nitrogen abundance determinations for B stars in the Large Magellanic cloud.

We describe and provide evolutionary tracks and the evolution of the central and surface abundances. In particular, we discuss the occurrence of quasi-chemically homogeneous evolution, i.e. the severe effects of efficient mixing of the stellar interior found for the most massive fast rotators.

We provide a detailed set of isochrones for rotating stars. Rotation as an initial parameter leads to a degeneracy between the age and the mass of massive main sequence stars if determined from its observed location in the Hertzsprung-Russell diagram. We show that the consideration of surface abundances can resolve this degeneracy.

2.1 Introduction

Massive stars can be considered as cosmic engines. With their high luminosities, strong stellar winds and violent deaths they drive the evolution of galaxies throughout the history of the universe. Even before galaxies formed, massive stars are believed to have played an essential role in re-ionizing the universe (Haiman & Loeb 1997), with important consequences for its subsequent evolution. Massive stars are visible out to large distances in the nearby universe (Kudritzki et al. 2008), and as ensembles even in star-forming galaxies at high redshift (e.g. Douglas et al. 2009). Their explosions as supernovae or gamma-ray bursts shine through a major fraction of the universe, probing intervening structures as well as massive star evolution at the lowest metallicities (Savaglio 2006; Ohkubo et al. 2009). It is therefore of paramount importance for many areas within astrophysics to obtain accurate models of massive star evolution. In this paper we present an extensive grid of evolutionary models of rotating massive stars focusing on the main-sequence stage, which is at the root of understanding their subsequent evolution.

Basic concepts about massive main-sequence stars are long established and provide a good guide to their expected properties, most importantly the mass–luminosity relation (Mitalas & Falk 1984; González et al. 2005). However, two major issues have plagued evolutionary models of massive stars until today: mixing and mass loss (Chiosi & Maeder 1986). We concentrate here on the role of mixing in massive stars as, on the main sequence, the effects of mass loss remain limited in the considered mass and metallicity range.

Concerning thermally driven mixing processes, the occurrence of semiconvection and the related question of the appropriate choice of the criterion for convection does not alter the main sequence evolution of massive stars significantly (Langer et al. 1985). However, the efficiency of convective overshooting in massive main-sequence stars is still not well known. In particular, the cool edge of the main-sequence band is not well determined, as stars in observational samples are found in the gap predicted between main-sequence stars and blue core-helium burners (e.g. Fitzpatrick & Garmany 1990; Evans et al. 2006). Here we follow a promising approach to determine the cool edge of the main sequence band, and thus the overshooting efficiency, from

the rotational properties of B-type stars (see Hunter et al. 2008b; Vink et al. 2010).

Rotationally-induced mixing processes have been invoked in the past decade to explain the surface enrichment of some massive main-sequence stars with the products from hydrogen burning, in particular nitrogen (Heger et al. 2000; Meynet & Maeder 2000; Maeder 2000). Rotationally-induced mixing was further used to explain the ratio between O-stars and various types of Wolf-Rayet stars at different metallicities (Meynet & Maeder 2005), the variety of core collapse supernovae (Georgy et al. 2009) and the evolution towards long gamma-ray bursts (Yoon & Langer 2005). However, in view of the fact that all the mentioned observed phenomena have alternative explanations, a direct test of rotational mixing in massive stars appears of paramount importance.

In view of the recent results from the FLAMES Survey of Massive Stars (Evans et al. 2005), which provided spectroscopic data for large samples of massive main sequence stars, we pursued the strategy to compute dense model grids of rotating massive main sequence stars, and predict in detail and comprehensively their observable properties. This evolutionary model data [1], which was calibrated using results from the FLAMES Survey, is tailored to provide the first direct and quantitative test of rotational mixing in rapidly rotating stars(Hunter et al. 2008a, 2009a; Brott et al. 2010b, from here on Paper II).

Our new model grids deliver predictions for many observables, with a wide range of potential applications. Besides helium and the CNO elements, we show how the light elements lithium, beryllium and boron are affected by rotational mixing, as well as the elements fluorine and sodium. We also provide isochrones which predict complex structures near the turn-off point of young star clusters. In Sec. 2.2, we describe the set-up and calibration of our massive star models, Sec. 2.3 and 2.4 provide the evolutionary tracks in the HR diagram and the corresponding isochrones, and the surface abundances of all considered elements. We end with a brief summary in Sec. 2.5.

2.2 Stellar evolution code

We use a one-dimensional hydrodynamic stellar evolution code that takes into account the physics of rotation, magnetic fields and mass-loss. This code has been described extensively by Heger et al. (2000). Recent improvements are presented in Petrovic et al. (2005b) and Yoon et al. (2006).

To allow for deviations from spherical symmetry due to rotation in this one-dimensional code, we consider the stellar properties and structure equations on mass

[1] Our model data is made available through VizieR at `http://cdsarc.u-strasbg.fr/cgi-bin/...`

shells that correspond to isobars. According to e.g. Zahn (1992) turbulence efficiently erases gradients along isobaric surfaces and enforces shellular rotation (Meynet & Maeder 1997) allowing us to use the one-dimensional approximation. The effect of the centrifugal acceleration on the stellar structure equations is considered according to Kippenhahn & Thomas (1970) and Endal & Sofia (1976) as described in Heger et al. (2000).

2.2.1 Transport of chemicals and angular momentum

All mixing processes are treated as diffusive processes. Convection is modeled using the Ledoux criterion, adopting a mixing-length parameter of $\alpha_{\rm MLT} = 1.5$ (Böhm-Vitense 1958; Langer 1991). Semi-convection is treated as in Langer et al. (1983) adopting an efficiency parameter $\alpha_{\rm SEM} = 1$ (Langer 1991). We take into account convective core-overshooting using an overshooting parameter of 0.335 pressure scale heights i.e. the radius of the convective core is equal to the radius given by the Ledoux criterium plus an extension equal to 0.335 Hp, where Hp is the pressure scale height evaluated at the formal boundary of the convective core (see Sec. 2.2.4 for the calibration). Furthermore, we consider various instabilities induced by rotation that result in mixing: Eddington-Sweet circulation, dynamical and secular shear instability, and the Goldreich-Schubert-Fricke instability (Heger et al. 2000).

Transport of angular momentum is also treated as a diffusive process following Endal & Sofia (1978) and Pinsonneault et al. (1989) as described in Heger et al. (2000). The turbulent viscosity is determined as the sum of the diffusion coefficients for convection, semi-convection, and those resulting from rotationally induced instabilities. In addition, we take into account the transport of angular momentum by magnetic fields due to the Spruit-Tayler dynamo (Spruit 2002), implemented as described in Petrovic et al. (2005b). We do not consider possible transport of chemical elements as a result of the Spruit-Tayler dynamo because its validity is still controversial (Spruit 2006). We note that, while the dynamo process itself was confirmed through numerical calculations by Braithwaite (2006), it is still unclear under which conditions it can operate and whether it is active in massive stars (Zahn et al. 2007). Heuristically, angular momentum transport through magnetic fields produced by the Spruit-Tayler dynamo, as the so far only mechanism, appears to reproduce the rotation rates of white dwarfs and neutron stars quite well(Heger et al. 2005; Suijs et al. 2008).

In agreement with Maeder & Meynet (2005) we find that magnetic fields keep the star near rigid rotation throughout its main sequence evolution, suppressing the mixing induced by shear between neighboring layers. The dominant rotationally induced mixing process in our models is the Eddington-Sweet circulation, a large

scale meridional current that is caused by thermal imbalance in rotating stars between pole and equator (e.g. Tassoul 1978).

Some of the diffusion coefficients describing rotational mixing are based on order of magnitude estimates of the relevant time and length scales (Heger et al. 2000). To consider the uncertainties efficiency factors are introduced, which need to be calibrated against observational data. The contribution of the rotationally induced instabilities to the total diffusion coefficient is reduced by a factor $f_c = 0.0228$ (see Sec. 5.3.5 for the calibration) while their full value enters in the expression for the turbulent viscosity (see Heger et al. 2000, for details). The inhibiting effect of chemical gradients on the efficiency of rotational mixing processes is regulated by the parameter f_μ, see Heger et al. (2000). We adopt $f_\mu = 0.1$ after Yoon et al. (2006) who calibrated this parameter to match observed surface helium abundances.

2.2.2 Mass loss

We updated the treatment of mass loss by stellar winds by implementing the prescription of Vink et al. (2000, 2001), based on the method by de Koter et al. (1997), for winds from early O- and B-type stars. This mass loss recipe predicts a fast increase of the mass-loss rate as one moves to lower temperatures near 22 000 K. This increase is related to the recombination of Fe IV to Fe III at the sonic point and is commonly referred to as the bi-stability jump. These rates are derived for $12.5\,\mathrm{kK} \lesssim T_{\mathrm{eff}} \lesssim 50\,\mathrm{kK}$. We note that the formulae on the hot and cool side of the jump have *not* been derived for the intermediate temperature range between 22.5 and 27.5 kK. In this range, we thus perform a linear interpolation. In order to accommodate for a strong mass-loss increase when approaching the HD limit, we switch to the empirical mass loss rate of Nieuwenhuijzen & de Jager (1990), when the Vink et al rate becomes smaller than that from Nieuwenhuijzen & de Jager (1990) at any temperature lower than the critical temperature for the bi-stability jump. This ensures a smooth transition between the two mass loss prescriptions. This strategy also naturally accounts for the increased mass loss at the *second* bi-stability jump at ~12.5 KK.

To account for the effects of surface enrichment on the stellar winds, we follow the approach of Yoon et al. (2006). The mass-loss rate of Vink et al. (2000, 2001) is employed for stars with a surface helium mass fraction, Y_{s}, below 0.4. We interpolate between the mass-loss rate of Vink et al. (2000, 2001) and the Wolf-Rayet mass-loss rate of Hamann et al. (1995) reduced by a factor of 10 (Yoon et al. 2006) for $0.4 \leq Y_{\mathrm{s}} \leq 0.7$. When the helium surface abundance exceeds $Y_{\mathrm{s}} > 0.7$, we adopt the Wolf-Rayet mass-loss rate.

2.2.3 The initial chemical composition

We adopt three different initial compositions that are suitable for comparison with OB stars in the Small and Large Magellanic Cloud (SMC, LMC) and a mixture that is tailored to the Galactic sample of the FLAMES survey of massive stars (Evans et al. 2005), to which we will refer in this paper as the Galactic (GAL) mixture for brevity. In contrast with several previous studies we do not simply adopt Solar-scaled abundance ratios. Even though such mixtures may be sufficient to study the overall effects of metallicity, they are not accurate enough for direct comparison with observed surface abundances. For example, Kurt & Dufour (1998) find that the carbon to nitrogen ratio in HII regions in the LMC and SMC is considerably larger than the Solar ratio. In the stellar interior, carbon is converted into nitrogen, which can reach the surface due to mixing and/or mass loss. Brott et al. (2008) found that the surface nitrogen abundance can be enhanced by a factor of 11 with a realistic initial SMC mixture. A Solar-scaled mixture with the same iron abundance would lead to enhancement of only a factor of 4, for the same initial parameters. This demonstrates the need for tailored initial chemical mixtures.

Table 2.1: Initial abundances for C, N, O, Mg, Si, Fe adopted in our chemical compositions for the Magellanic Clouds and the Galaxy (see Sec. 2.2.3). All other elements are Solar abundances (Asplund et al. 2005) scaled down by 0.4 dex for the LMC and by 0.7 dex for the SMC.

	C	N	O	Mg	Si	Fe
LMC	7.75	6.90	8.35	7.05	7.20	7.05
SMC	7.37	6.50	7.98	6.72	6.80	6.78
GAL	8.13	7.64	8.55	7.32	7.41	7.40

For the initial abundances of C, N and O we use data from HII regions by Kurt & Dufour (1998). Surface abundances for these elements in B-type stars may no longer reflect the initial composition due to nuclear processing and mixing. For Mg and Si we use measurements of B-type stars as these stars are not expected to significantly alter the abundances of these elements during their main-sequence evolution. The B-type stars in different fields and clusters in the LMC show only small variations in Mg and Si of less than 0.02 dex (Trundle et al. 2007; Hunter et al. 2007, 2009a). Also for the SMC these authors find no evidence for any systematic differences. The Fe abundance for the SMC is taken from a study of A-supergiants by Venn (1999). For all the other elements we adopt Solar abundances by Asplund et al. (2005) scaled down by 0.4 dex for the LMC mixture and 0.7 dex for the SMC mixture. The initial abundances are summarized in Tab. 2.1. These mixtures have metallicities of Z =

0.0047 for the LMC and $Z = 0.0021$ for the SMC, where Z is defined as the mass fraction of all elements heavier than helium (see Table 2.2).

Choosing a chemical composition suitable for comparison with stars in the Milky Way is not straight forward due to the chemical gradients within the disk of our galaxy. We adopt an initial Mg and Si abundance based on the analysis of the Galactic cluster NGC6611 by Hunter et al. (2007). For C we adopted the NLTE corrected value from Hunter et al. (2007). N and O abundances are based on the average of HII-regions, see Hunter et al. (2008b, 2009a) and references therein. The Fe abundance is taken from measurements of A-supergiants by Venn (1995). For all other elements we have adopted Solar abundances by Asplund et al. (2005). The resulting metallicity of our Galactic mixture is Z = 0.0088, which is lower than the solar metallicity of Z = 0.012 found by Asplund et al. (2005) and the Solar neighborhood metallicity of Z = 0.014 measured by Przybilla et al. (2008). We point out we assumed the stellar wind mass loss rates as well as the opacities in our models to depend on the iron abundance, for which the spread in measurements is much smaller than for the total metallicity. Our wind mass loss rate scales with $(Fe_{Surf}/Fe_{\odot})^{0.85}$, where we use the iron abundance from Grevesse et al. (1996) as solar reference, for consistency reasons with older models.

For helium we assume that the mass fraction scales linearly with Z between the primordial helium mass fraction of Y = 0.2477 (Peimbert et al. 2007) at Z = 0 and Y = 0.28 at the Solar value (Grevesse et al. 1996). We adopt the OPAL opacity tables (Iglesias & Rogers 1996) using $(Fe_{Surf}/Fe_{\odot}) \times Z_{\odot}$ to interpolate between tables of different metallicities. The solar reference values are again taken from Grevesse et al. (1996).

Table 2.2: Resulting hydrogen (X), helium (Y) and metal (Z) mass fractions for the chemical mixtures used in our models.

	X	Y	Z
LMC	0.7391	0.2562	0.0047
SMC	0.7464	0.2515	0.0021
GAL	0.7274	0.2638	0.0088

2.2.4 Calibration of overshooting

Mixing beyond the convective stellar core can occur when convective cells penetrate into the radiative region, when they "overshoot" the boundary due to their non-zero velocity. This effect is accounted for through a parameter α which measures the extension of the affected region in units of the local pressure scale height. In general,

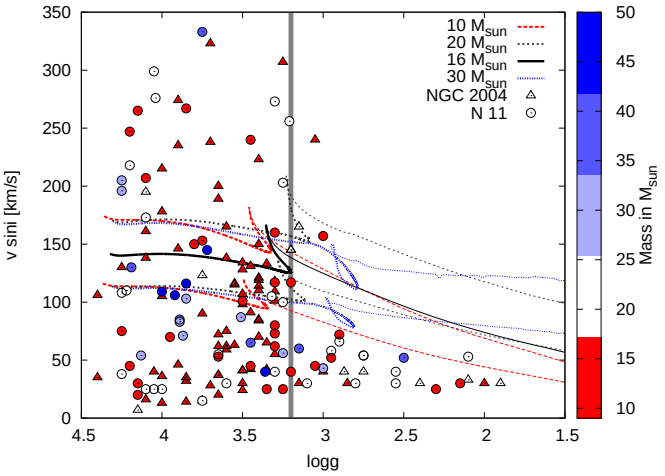

Figure 2.1: Projected rotational velocity versus surface gravity for stars in the FLAMES survey near LMC clusters NGC 2004 (triangles) and N11 (circles). Color coding indicates the stellar mass. We interpret the sudden transition at $\log g = 3.2$ (vertical line) as the end of the main sequence and use it to calibrate the amount of overshooting of our $16\,M_\odot$ model (black line), see Sec. 2.2.4. For comparison we plot several other models with different initial masses and rotation rates (dotted lines).

overshooting leads to larger stellar cores resulting in higher luminosities and larger stellar radii, especially towards the end of the main sequence evolution.

Various attempts have been undertaken to constrain the value of this parameter. Using eclipsing binary stars, Schröder et al. (1997) derived values between 0.25 and 0.32 for stars in the mass range of 2.5 to $7\,M_\odot$. Ribas et al. (2000) and Claret (2007) found α in the range of 0.1 to 0.6, with a systematic increase of the amount of overshooting with the stellar mass. Briquet et al. (2007) used asteroseismological measurements and obtained $\alpha = 0.44 \pm 0.07$ for the β-Cephei θ Ophiuchi. Another way to constrain the overshooting parameter is to fit the width of the main-sequence band for clusters with turn-off masses below approximately $15\,M_\odot$ (Mermilliod & Maeder 1986). Using non-rotating evolutionary models, Mermilliod & Maeder (1986) and Maeder & Meynet (1987) found an overshooting parameter between 0.25 and 0.3. This is supported by findings of Napiwotzki et al. (1991). In general, however, this method does not work well for masses above $5...10\,M_\odot$, since the red edge of the main sequence band remains mostly unidentifiable (Vink et al. 2010).

In this work we re-calibrate the overshooting parameter for our models using data of the FLAMES survey of massive stars. We use the fact that the properties of stars near the end of their main-sequence evolution depend on their core size. For larger

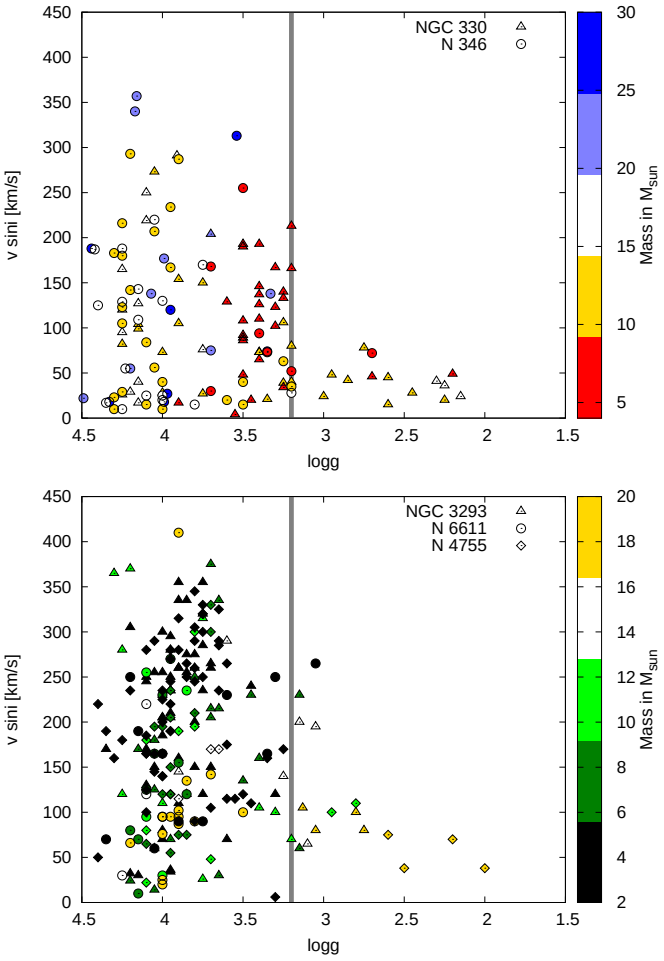

Figure 2.2: Similar to Fig. 2.1, but now for the SMC (top) and Galactic (bottom) samples of the FLAMES survey. The typical error in log g is about 0.15 dex. The drop in rotation rate, which may be interpreted as the end of the main sequence, occurs around log $g = 3.2$ (vertical line) independently of metallicity.

overshooting parameters, the end of the main sequence shifts to lower effective temperatures and lower surface gravities. After the end of their main sequence evolution, the rapid stellar expansion results in a strong spin down of the envelope. This phase of evolution occurs on the Kelvin-Helmholtz timescale, which is very short compared to the nuclear timescale. Observing stars during this phase is unlikely.

In Fig. 2.1 we plot the projected rotational velocity against the surface gravity for stars in the LMC sample of the FLAMES survey (adapted from Hunter et al. 2008b). Stars with surface gravities of $\log g > 3.2$ show a wide range of projected rotational velocities, $v \sin i$, in clear contrast with the stars with lower surface gravities which have projected velocities of about 50 km/s or lower. We interpret this transition as the division between main-sequence stars that are born with a wide range of rotational velocities and a different, more evolved, population that has experienced significant spin down. The surface gravity at which this transition occurs seems to be independent of mass, at least within the range available in this sample. To show this we color-coded the masses of the observed stars in Fig. 2.1.

In an alternate scenario discussed byVink et al. (2010), the population of slow rotators might be main-sequence stars, that have spun down due to increased mass loss (bi-stability breaking). However, this would require a huge overshooting, in order to extend the lifetime of main sequence stars at temperatures below the bi-stability temperature of about 22 kK. With the current overshooting calibration, bi-stability breaking plays a role only well above $30\,M_\odot$. The nature of the evolved slow rotators in Fig. 2.1 remains puzzling. The fact that all of them have a strong nitrogen surface enhancement might propose that they are post-red supergiants which acquired the nitrogen enhancement through the first dredge-up (Vink et al. 2010), but they might as well be products of binary interaction or of so far unidentified physical processes.

For the overshooting calibration we use a stellar model with a mass and rotation rate that are representative for the entire sample. The typical mass is about $16\,M_\odot$ (based on evolutionary masses; see Paper II) and the mean projected velocity of the stars in the sample with $\log g \geq 3.2$ dex is $\langle v \sin i \rangle = 110$ km/s. This corresponds to an average rotational velocity of $\langle v \rangle = 142$ km/s assuming a random orientation of the spin axes, i.e. $\langle \sin i \rangle = \pi/4$. Throughout the main-sequence evolution the equatorial velocity is expected to be nearly constant due to the reduced effect of stellar winds in the low metallicity environment of the LMC and due to coupling of the expanding envelope to the contracting core. Therefore, we use the typical velocity as an estimate of the average initial rotational velocity.

The full black line in Fig. 2.1 shows a model with the typical mass and rotation rate. The overshooting parameter has been adjusted to $\alpha = 0.335$, such that the end of the main sequence coincides with the drop in rotational velocities at $\log g = 3.2$. Fig. 2.1 demonstrates that the adopted amount of overshooting, derived for a $16\,M_\odot$ star, appears to be valid for the mass range 10 to $20\,M_\odot$. However, it is unconstrained outside this range, as for example the $30\,M_\odot$ tracks in Fig. 2.1 have no observed counterparts near the TAMS. We therefore use an overshooting parameter of $\alpha = 0.335$ for our entire grid. Given the uncertainty in the surface gravities ($\sim$0.15 dex),

we estimate the uncertainty of the overshooting parameter in the mass range 10 to $20\,M_\odot$ to be 0.1.

A priori we do not expect the overshooting parameter to depend on metallicity. To check this we show the projected rotational velocities against surface gravity for the SMC and Galactic sample of the FLAMES survey in Fig. 2.2. The drop in rotation rate occurs at the same surface gravity within the measurement errors. The Galactic sample shows a second feature around $\log g = 3.5$ caused mainly by stars below $5\,M_\odot$. Dufton et al. (2006) already described this stars as over-luminous for their age and a general disappointing agreement of the clusters HR-diagram with isochrones. When we vary the initial composition from SMC to the Galactic mixture, we find that the end of the main sequence for our $16\,M_\odot$ model shifts from $\log g \sim 3.3$ to 3.1, adopting the same value for the overshooting parameter. This shift is also within the measurement uncertainties. Therefore, adopting one fixed value for the overshooting parameter in our entire model grid is a reasonable assumption.

2.2.5 Calibration of the rotational mixing efficiency

As mentioned in the beginning of Sec. 2.2 we treat all mixing processes as diffusive processes, where the diffusion coefficient is taken as the sum of the individual diffusion coefficients for the various mixing processes. The contributions of all rotationally induced mixing processes are reduced by a factor, f_c, before they are added to the total diffusion coefficient for transport of chemicals. Pinsonneault et al. (1989) was the first to introduce this parameter. In order to explain the Solar lithium abundance they needed to reduce the efficiency of rotationally induced mixing processes by a factor $f_c = 0.046$. Based on theoretical considerations Chaboyer & Zahn (1992) proposed $f_c = 0.033$, which was adopted in the models of Heger et al. (2000). We note that we can not compare our efficiency parameter directly with these values due to differences in the implementation and the considered specific set of mixing and angular momentum transport processes.

We calibrate the mixing efficiency for our models using the B-stars in the LMC sample of the FLAMES survey. We aim to reproduce the main trend of the observed nitrogen surface abundances with the projected rotational velocity for the nitrogen enriched fast rotators. In Fig. 2.3 we present the data, indicating different regions or boxes which have been numbered for reference (Hunter et al. 2008a and Paper II). The majority of the sample, about 53% of the stars, is not significantly enriched in nitrogen, given the typical error of 0.2 dex for the nitrogen abundance measurements. This group is indicated as Box 5 in Fig. 2.3. Fast rotators with significantly enhanced surface abundances (> 7.2 dex; see Box 3) constitute 18% of the sample. A detailed discussion of the stars in Box 1 and 2, which deviate from the main trend, and of

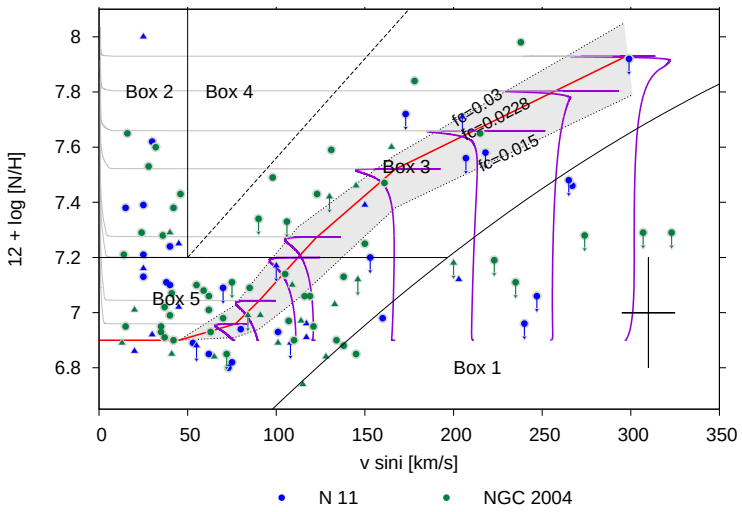

Figure 2.3: Nitrogen surface abundance versus projected rotational velocity for stars in the LMC sample of the FLAMES survey (Hunter et al. 2009a) in the N11 (blue) and the NGC 2004 (green) fields. Stars with evidence for a binary companion from radial velocity variations are plotted as triangles. Black solid lines indicate regions that are helpful as a reference in later discussion(see also Paper II). Evolutionary tracks of 13 $M_\odot$ models are plotted for various rotational velocities, shifted by a factor $\pi/4$ to account for random inclination angles. The red line marks the nitrogen abundance reached at the end of the main sequence for 13 $M_\odot$ models adopting a mixing efficiency of $f_c = 0.0228$ (our calibration). Thin dotted lines show the location of the line, if different values for f_c are adopted, e.g. $f_c = 0.015$ (lower line) and $f_c = 0.03$ (upper line).

observational biases and other factors that might influence this numbers are provided in Paper II and Hunter et al. (2008a).

For the calibration we use stellar models with a mass that is typical for the stars for which we have nitrogen surface abundance measurements, i.e. 13 $M_\odot$. We adjust the mixing efficiency such that the nitrogen surface abundances reached at the end of the main-sequence evolution follow the trend of the stars in Box 3 while we make sure that the slow rotators do not enrich more than 0.2 dex to match the stars in Box 5. We find that this is obtained for a mixing efficiency of f_c=0.0228. In Fig. 2.3 we plot evolutionary tracks for several 13 $M_\odot$ models with different initial rotation rates. Adopting this mixing efficiency, a model with the typical mass and average rotational velocity ($v_{\rm ZAMS}$ = 142 km/s) reaches a surface nitrogen enhancement of 7.2 dex at the end of its main sequence. To illustrate the sensitivity of the nitrogen surface abundances to the adopted mixing efficiency, we depict the surface abundances

reached at the end of the main sequence for $f_c = 0.015$ and $f_c = 0.03$ (dotted lines and grey band). As we have no reason to believe that the mixing efficiency f_c depends on metallicity, we adopt the same value for the SMC and the Galactic grid.

2.2.6 Grid of evolutionary tracks and isochrones: initial parameters and description of provided data

Using the calibration and the three initial compositional mixtures described above we computed a grid of evolutionary models. We adopt initial masses between 5 and 60 $M_\odot$ and initial equatorial rotational velocities ($v_{\rm ZAMS}$) ranging from 0 to about 600 km/s. For each initial composition we computed about 200 evolutionary tracks. The spacing between the initial parameters was chosen to provide a proper coverage of the parameter space and to provide extra resolution for massive fast rotating stars whose evolution depends sensitively on the initial rotation rate (see Fig. 2.4).

The results of our calculations are made available online through VizieR in table format. For each evolutionary track we provide the basic stellar parameters at different ages such as the mass, effective temperature, luminosity, radius and mass-loss rate as well as the surface abundances of various elements. We also list the central and surface mass fractions of the most important isotopes of these elements. In Table 2.3 we summarized all the provided data. The time steps are chosen to resolve the evolutionary changes of the main stellar parameters. Tracks with higher time resolution are available from the authors upon request.

Based on these evolutionary tracks we generated sets of isochrones, using our population synthesis code STARMAKER (Paper II). The isochrones cover the evolution until central hydrogen exhaustion for stellar masses between 5 and 60 $M_\odot$. We provide them for ages between 0 and 30 Myr at intervals of 0.2 Myr, for initial rotational velocities between 0 and 540 km/s with steps of 10 km/s and for three different initial compositions: SMC, LMC and a Galactic mixture. We provide the basic stellar parameters and surface abundances as listed in Tab. 2.4.

2.3 Evolutionary tracks and isochrones

2.3.1 Evolutionary tracks

Rotation affects evolutionary tracks in the Hertzsprung-Russell diagram (e.g. Maeder & Meynet 2000, and references therein). The centrifugal acceleration reduces the effective gravity resulting in cooler and slightly less luminous stars. However, rotation also induces internal mixing processes which can have the opposite effect, leading to more luminous and hotter stars. Which of these effects dominates depends on the

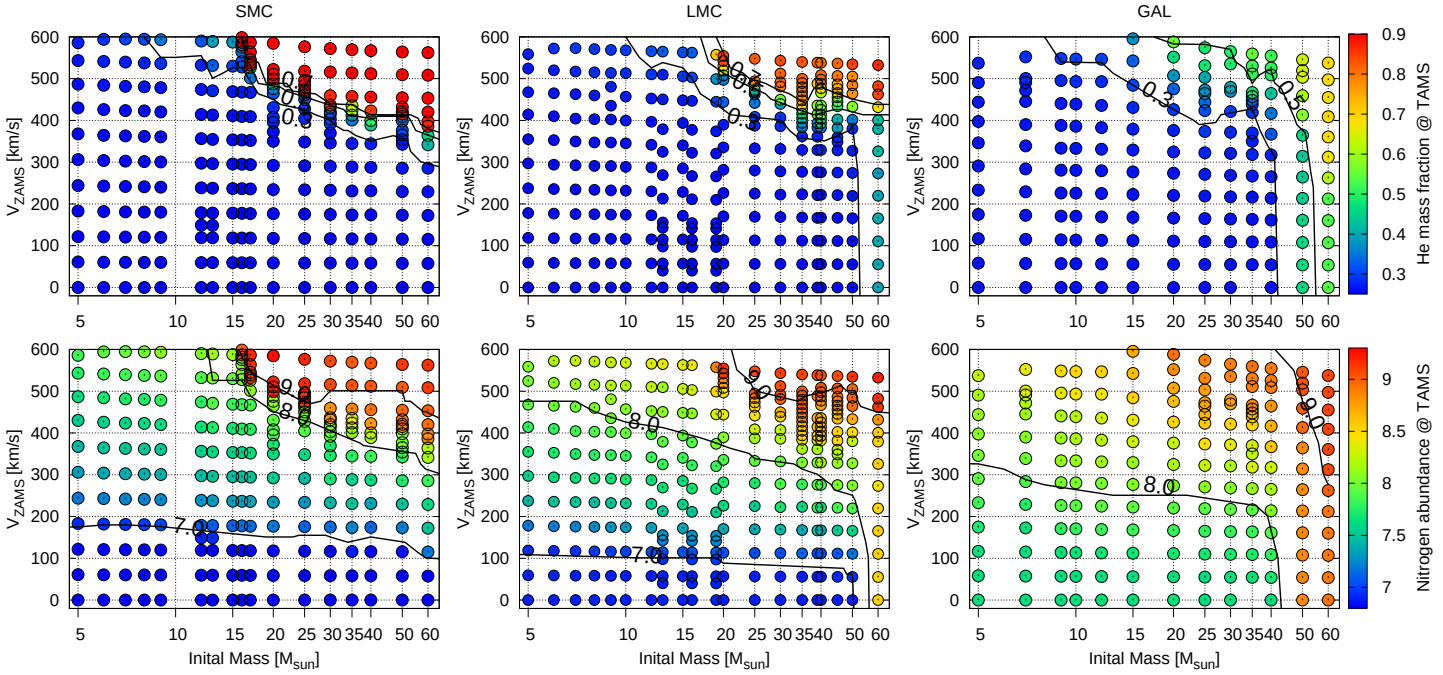

Figure 2.4: Surface abundance of nitrogen (bottom row) and helium (top row) reached at the end of the main sequence (colors and contours) in our models with different initial masses, rotational velocities and compositions. Each evolutionary sequence of our grids is represented by one dot in this diagram. See Sec. 2.2.6 for a description of the initial parameter space of our grid and Sec. 2.4 for a discussion of the abundances.

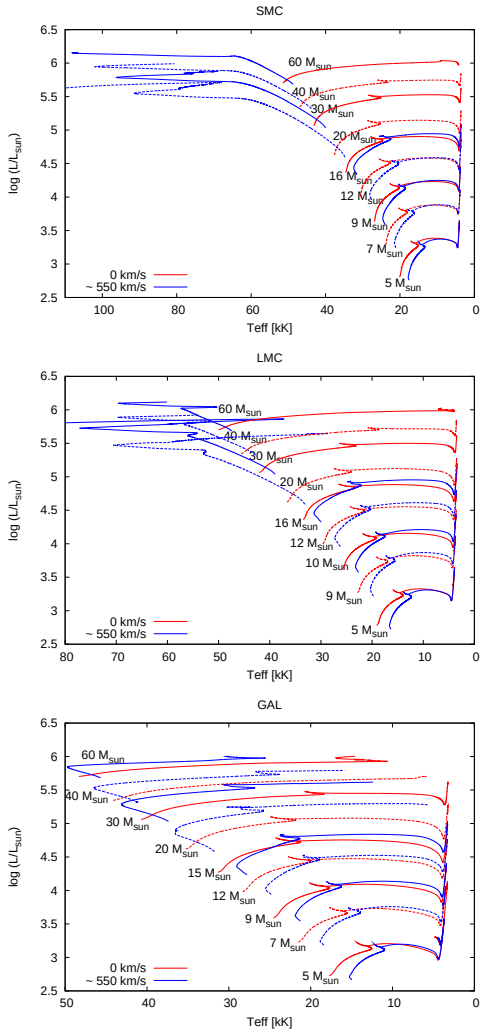

Figure 2.5: Evolutionary tracks for various masses and metallicities. Red tracks are the non-rotating models and in blue we show models rotating initially at about 550 km/s. For clarity we alternate different line styles. Note the different temperature ranges on the x-axis.

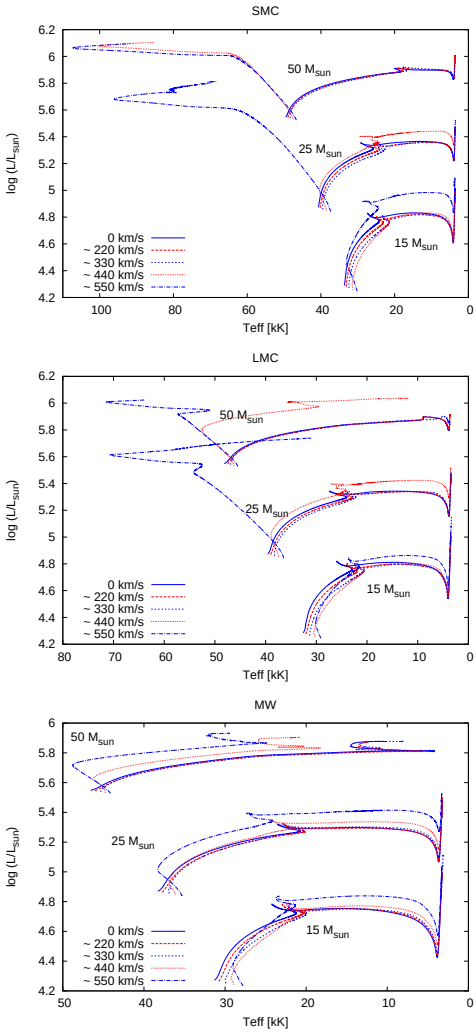

Figure 2.6: Evolutionary tracks for 15, 25 and 50 $M_{\odot}$ for SMC, LMC and Galactic composition (from top to bottom), for a range of initial rotational velocities (see legend).

Table 2.3: Description of the online tables containing the results of our evolutionary calculations as a function of time, for given initial composition, initial mass and initial rotation rate. The critical velocity is computed as $v^2_{\rm crit} = GM/R(1-\Gamma_{\rm e})$, where $\Gamma_{\rm e}$ denotes the Eddington factor due to electron scattering.

stellar parameters	surf. abun	surface & core isotope mass fractions
Age (t [yrs])	H	^{1}H
Mass (m [$M_\odot$])	He	^{3}He ^{4}He
Eff. temp. ($T_{\rm eff}$[K])	Li	^{7}Li
Luminosity (log($L/L_\odot$))	Be	^{9}Be
Radius (R [$R_\odot$])	B	^{10}B ^{11}B
Mass loss rate ($\dot{M}$ [$M_\odot$/yr])	C	^{12}C ^{13}C
Surface gravity (log g)	N	^{14}N ^{15}N
Surface velocity ($v_{\rm surf}$ [km/s])	O	^{16}O ^{17}O ^{18}O
Rotation period (P [days])	F	^{19}F
Critical velocity ($v_{\rm crit}$ [km/s])	Ne	^{20}Ne ^{21}Ne ^{22}Ne
Eddington factor ($\Gamma_{\rm e}$)	Na	^{23}Na
	Mg	^{24}Mg ^{25}Mg ^{26}Mg
	Al	^{26}Al ^{27}Al
	Si	^{28}Si ^{29}Si ^{30}Si
	Fe	^{56}Fe

initial mass, rotation rate, metallicity and the evolutionary stage. In this section we describe the effects of rotation on our models.

In rotating stars, the radiative energy flux depends on the local effective gravity (von Zeipel 1924), and temperature and luminosity become latitude dependent. The resulting thermal imbalance drives large scale meridional currents. In most stars, rotating at moderate rotation rates, the expected latitude dependence of temperature and luminosity is week (Hunter et al. 2009a). In models close to critical rotation, luminosity and temperature differences are expected to be more significant and may even give rise to polar winds and equatorial outflows caused by critical rotation (Maeder 1999). Temperatures, luminosities and gravities given for the models presented in this paper are surface averaged values.

Mass dependence of rotational mixing: For intermediate mass main-sequence stars the main effect of rotation is a reduction of the effective gravity by centrifu-

Table 2.4: Description of the online tables containing stellar parameters along isochrones computed for different initial rotational velocities as provided by our population synthesis code (Paper II). See also Tab. 2.3.

stellar parameters	surf. abun
Age (t [yrs])	H
Mass (m [$M_\odot$])	He
Effective temperature ($T_{\rm eff}$[K])	B
Luminosity ($\log(L/L_\odot)$)	C
Radius (R [$R_\odot$])	N
Mass loss rate ($\dot{M}$ [$M_\odot$/yr])	O
Surface gravity ($\log g$)	Ne
Surface velocity ($v_{\rm surf}$ [km/s])	Na
Rotation period (P [days])	Mg
Critical velocity ($v_{\rm crit}$ [km/s])	Si
Eddington factor (Γ_e)	^{1}H (mass fraction)
initial mass and velocity	^{4}He (mass fraction)

gal acceleration. Fig. 2.5 shows that, during the main-sequence evolution, the tracks of the fast rotating 5 $M_\odot$ stars are about 2000 K cooler compared to the non-rotating counterparts. Rotational mixing does affect the surface abundances of those elements that are so fragile that the relatively low temperatures in the stellar envelope are sufficient to induce nuclear reactions on them. However, the mixing is not efficient enough to significantly alter the structure of the star. As a consequence, the effect of rotation on the corresponding evolutionary tracks in the Hertzsprung-Russell diagram remains limited.

In rapid rotators more massive than about 15 $M_\odot$, the effect of rotational mixing becomes more important than that of the reduced effective gravity: towards the cool edge of the main sequence band, the rotating stars become more luminous than the non-rotating ones. The main effect of rotation is an effective increase of the size of the stellar core, similar to the effect of overshooting (Sec. 2.2.4). This can be seen in Fig. 2.5 when one compares the tracks of the 15 and 16 $M_\odot$ models near the end of their main-sequence evolution. The larger core mass in the fast rotating models results in a higher luminosity.

In the most massive stars at low metallicity ($\gtrsim 16\,M_\odot$ for the SMC, $M \gtrsim 19\,M_\odot$ for the LMC), and for the extreme rotators shown in Fig. 2.5, mixing induced by

rotation is so efficient that almost all the helium produced in the center is transported throughout the entire envelope of the star. During their main-sequence evolution they become brighter and hotter, evolving up- and blue-wards in the Hertzsprung-Russell diagram. After all hydrogen in the center has been converted to helium, the star contracts, reaching effective temperatures of up to 100,000 K. This type of evolution is referred to as “quasi-chemically homogeneous evolution” (Maeder 1987; Yoon & Langer 2005; Woosley & Heger 2006). The blue-ward and red-ward evolution after the exhaustion of hydrogen in the center is analogous to the "hook" at the end of the main sequence seen in tracks of non-rotating stars. Note that all models have been computed beyond central hydrogen exhaustion, in most cases up to the ignition of helium. This allows us to later compare the main sequence surface abundances with those resulting from the first dredge-up in the red supergiant regime.

Metallicity dependence of rotational mixing: Fig. 2.6 depicts evolutionary tracks of models with various initial rotation rates. The most striking feature in these diagrams is the bifurcation of the evolutionary tracks occurring at high masses and low metallicity, most clearly visible at SMC metallicity. Stars that rotate faster than a certain threshold are so efficiently mixed that they evolve almost chemically homogeneously. Stars that rotate slower than this threshold build a chemical gradient at the boundary between the convective core and the radiative envelope. This gradient itself has an inhibiting effect on the mixing processes, strongly reducing the transport of material from the core to the envelope. The minimum rotation rate required for chemically homogeneous evolution decreases with increasing mass (Yoon et al. 2006).

At high metallicity, rotational mixing is less efficient. In addition, mass and angular momentum loss due to stellar winds becomes important, slowing down the rotation rate and therefore the efficiency of the mixing processes. The fastest rotating stars at high metallicity initially evolve blue- and up-ward in the Hertzsprung-Russell diagram, see in the lower panel of Fig. 2.6. However, the combined effects of spin down by a stellar wind and the build up of an internal chemical gradient reduces the efficiency of internal mixing processes. The star switches onto a red-ward evolutionary track, similar to that of a non rotating star. However, its larger core mass results in a higher luminosity compared to the slower rotating counterparts.

2.3.2 Isochrones

While for a given metallicity, a classical isochrone can be represented by a single line in the Hertzsprung-Russell diagram, the isochrones of rotating stars span an area for a given age and initial composition. This is shown in Fig. 2.7. The isochrone

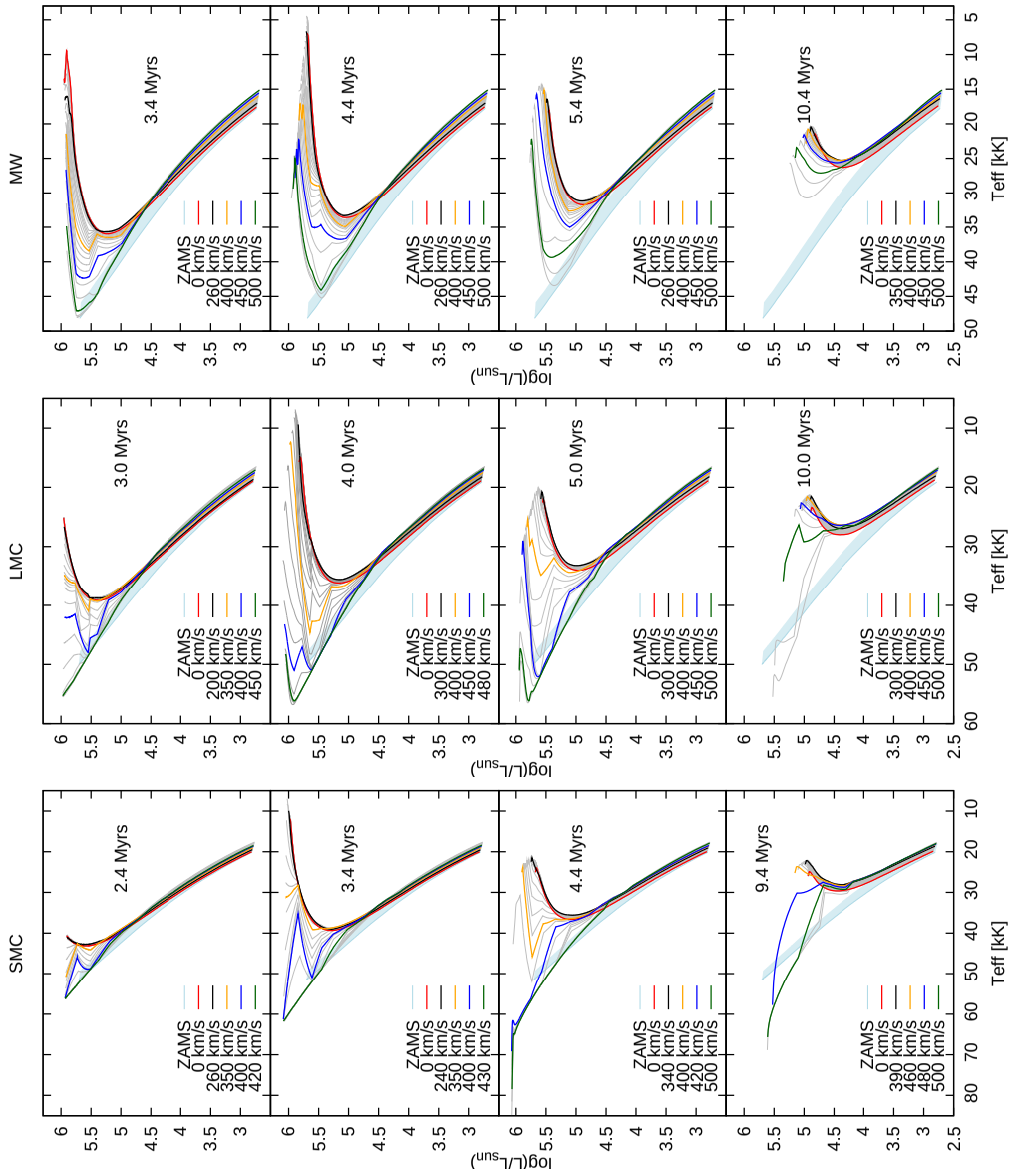

Figure 2.7: Isochrones for SMC (left panels), LMC (center) and galaxy (right) composition. Each panel shows isochrones for a given age and initial rotational velocity ranging from 0 to 540 km/s in steps of 20 km/s, with an increased resolution of 10 km/s between 350 and 450 km/s (grey lines). In red we show the isochrone for non rotating models, for other colors see the legend and the main text. We show the area spanned by the zero-age isochrones as a light blue band. The age in the second row has been chosen such that the isochrones span the largest range in effective temperature, 1 Myr earlier is shown in the first row, 1 and 5 Myr later are shown in the third and fourth row.

constructed from non-rotating evolutionary models is plotted in red. The isochrone corresponding to the fastest initial rotational velocity for which the models do not yet follow a blue-ward evolution in the HRD is plotted in black. The isochrone with the slowest initial velocity that shows a clear blue-wards evolution is shown in green. In blue and yellow we have selected two isochrones from the transition region that may help the reader to asses the sudden transition from classical to chemically homogeneous evolution.

For rotational velocities above 350 km/s, when the most massive stars undergo chemically homogeneous evolution, the isochrones deviate strongly from the non-rotating case. The maximum spread in effective temperature occurs around 4 Myr (second row in Fig. 2.7). At lower metallicity the isochrones split into more clearly separated branches. At SMC metallicity (e.g. the third panel in the first column in Fig. 2.7) the isochrone based on models rotating initially at 500 km/s moves straight to the blue. In contrast, the comparable LMC isochrone returns to the red for stars above $\sim$50 $M_\odot$. This behavior is directly related to the feature in the evolutionary LMC tracks in Fig. 2.6, see for example the 50 $M_\odot$ track for 550 km/s. At Galactic metallicity the blue-ward evolution does not appear in the models. Nevertheless, the area spanned by the isochrones extends over a wide range of effective temperatures.

Between about 5 and 10 Myr the most massive non-rotating stars have evolved off the main sequence. However, at low metallicity, the most massive fast rotators, which undergo chemically homogeneous evolution are still in their main-sequence phase at this time, forming a blue straggler-like blue population (see the bottom panels of Fig. reffig:aiso). If homogeneously evolving stars exist in nature they would most likely be found in low metallicity star clusters with ages between 5 and 10 Myr.

2.4 Surface Abundances

2.4.1 Abundances as a function of time

A direct observable consequence of rotationally induced mixing is the enrichment or depletion of certain elements in the atmospheres of main-sequence stars. In Fig. 2.9–2.11 we show the evolution of the surface abundance of various elements as a function time. The effects of rotational mixing are more pronounced at lower metallicity, at higher masses and for higher rotational velocity (see also Fig. 2.4 and Sec. 2.3).

As is usual in observational work, we express the surface abundances relative to the abundance of hydrogen. When stars become significantly hydrogen depleted at the surface, using hydrogen as a reference element may not be the most logical choice. Changes in the abundance may partially reflect changes in the reference ele-

ment hydrogen. We plot the abundances in red when these effects become important (i.e. when the helium mass fraction at the surface becomes larger than 40%) .

Most of our stellar models evolve to the red supergiant stage directly after the end of core hydrogen burning. This leads to a large vertical step in the surface abundances of many elements in Fig. 2.9-2.11, which is due to the convective dredge-up in the red supergiant stage. In the following, we discuss the evolution of the surface abundances of various groups of elements, focusing on the changes occurring over the course of the main-sequence evolution.

Helium

Even though helium is the main product of hydrogen burning, the abundance of helium at the surface remains remarkably constant in most evolutionary tracks during the main-sequence phase. For the 12 $M_\odot$ models the enhancement is less than 0.2 dex. Only the fast rotators of 30 and 60 $M_\odot$ show significant helium surface enrichments, especially at low metallicity (Fig. 2.9-2.11). These behaviors can be understood as the combination of two effects. Firstly, the production of helium occurs on the nuclear timescale. This occurs slower than, for example, the production of nitrogen or destruction of Li. Secondly, with the production of helium a steep gradient in mean molecular weight is established at the boundary between the core and the envelope. Such gradients inhibit the efficiency of mixing processes and prevent the transport of helium to the surface. Significant amounts of helium can be transported to the surface in models were mixing processes are efficient enough to prevent the build-up of a chemical barrier between core and envelope.

The fragile elements, Li, Be, B and F

The elements Li, Be, B are destroyed by proton captures at temperatures higher than 2.5×10^6 K for lithium, 3.5×10^6 K for beryllium, 5×10^6 K for boron (McWilliam & Rauch 2004, p. 123). These elements can only survive in the outermost layers. In rotating stars the surface abundances of these elements decrease gradually as the outer layers are mixed with deeper layers in which these elements have been destroyed. The decrease is most rapid for the most fragile element, lithium. The surface abundance of fluorine behaves similarly. It can survive temperatures of up to about 20×10^6K. We note that the rates of the reactions in which fluorine is involved are quite uncertain (Arnould et al. 1999).

In addition, stellar winds can affect the surface abundances especially for the most massive stars at high metallicity. Due to mass loss deeper layers are revealed in which the fragile elements have been destroyed. For non-rotating stars a sudden drop in the

surface abundances of the fragile elements is visible in Fig. 2.9-2.11, when mass loss has removed the layers in which these elements can survive. In rotating models the change is more gradual.

After the end of the main-sequence, dredge-up leads to a further decrease of the surface abundances of these elements. However, for some models with masses between 20 and 40 $M_\odot$ we find that small amounts of Li and Be are produced in the hydrogen burning shell by the p-p chain. As a result of the interplay between a convective zone on top of the shell source and the convective envelope reaching into these layers after hydrogen exhaustion, we find that the surface abundances of these elements can be significantly increased in these models. Even though the possible production of these elements by massive stars has several interesting applications, the robustness of the predictions for these elements requires further investigation.

Carbon, nitrogen, oxygen and sodium

Carbon, nitrogen and oxygen take part as catalysts in the conversion of hydrogen into helium. Although their sum remains roughly constant, nitrogen is produced when the cycle settles into equilibrium, at the expense of carbon and, somewhat later, oxygen. The CN-equilibrium is achieved very early in the evolution, before a strong mean molecular weight gradient has been established between the core and the envelope. Therefore, rotational mixing can transport nitrogen throughout the envelope to the stellar surface. While the surface abundance of nitrogen increases, carbon is depleted. Since full CNO-equilibrium is achieved only after a significant amount of hydrogen has been burnt in the core, changes in the oxygen surface abundance are only found in later stages in the more massive and faster rotating models.

Sodium is produced in the extension of the CNO-cycle, the NeNa-chain. The changes in the surface abundances of sodium resemble the changes is nitrogen, even though the enhancements are smaller and appear a little bit later at the stellar surface, see Fig. 2.9-2.11.

The relative increase of the nitrogen abundance depends on the initial amount of carbon available for conversion into nitrogen. These amounts are different for the different mixtures. The C/N ratio in the SMC and LMC composition are similar (7.4 and 7.1, respectively), while the ratio in our Galactic composition is smaller (3.1). In Fig. 2.8 we show the evolution of the surface nitrogen abundance in models of 15 and 40 $M_\odot$ with initial rotation rates of 0 and 270 km/s for SMC, LMC and Galactic composition. The initial abundance of nitrogen in the Magellanic clouds is much lower than in the Galactic mixture. Nevertheless, the rotating SMC and LMC models reach surface nitrogen abundances at the TAMS which are higher than in the initial Galactic mixture.

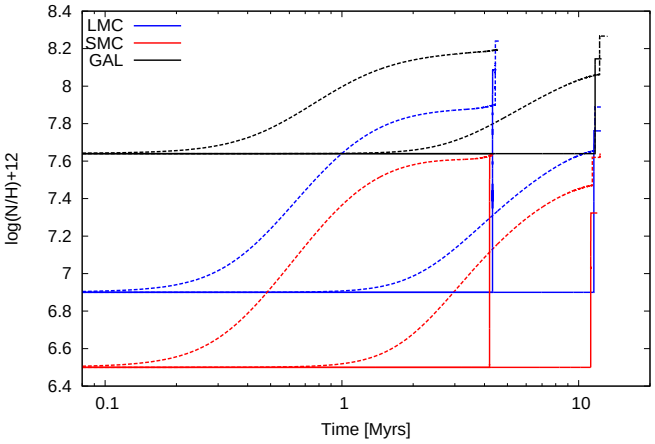

Figure 2.8: Nitrogen as a function of time at SMC, LMC and Galactic metallicity. The models are of 15 and 40 $M_\odot$. Full lines represent non-rotating models, dashed lines models rotating initially at ~270 km/s.

2.4.2 Surface abundances for selected ages

Due to the effects of rotation, the age or mass of a star can no longer be determined uniquely from its position in the Hertzsprung-Russell diagram by fitting evolutionary tracks or isochrones. This holds especially for stars that are located near the zero-age main sequence. A young, unevolved, slowly rotating star may have the same effective temperature and luminosity as a less massive, fast rotating, evolved star. A determination of the surface composition and to some extent the projected rotational velocity may help to lift this degeneracy.

In the panels of Fig. 2.12-2.14 we show which abundance distributions are predicted at a given time, as function of the considered mass and rotational velocity. Models of more massive stars show more pronounced surfaces abundances changes for a given age. The kinks in the lines of 400 km/s at LMC and Galactic composition occur due to difficulties in the interpolation between stars that follow blue-ward and red-ward evolutionary tracks effects.

These plots also show the effect of rotation on the main sequence life time. For example, Fig. 2.14 shows that the lines representing models with initial rotation rates of 400 and 500 km/s predict that stars of 50 and 60 $M_\odot$ are still present at 4 Myr, whereas non-rotating models predict that they have left the main sequence. On a much smaller scale this effect is also visible if one compares lines for rotation rates between 0 and 300 km/s based on models that follow normal evolutionary tracks.

The steep drop in the boron abundance along the isochrones based on non-rotating models is related to the stellar wind mass loss. For example, at LMC composition, the drop occurs around $35\,M_\odot$, indicating that the winds efficiently remove the outer layers of stars of $35\,M_\odot$ and higher (see also Sec. 2.4.1).

2.5 Summary

In this paper we have presented an extensive grid of models for rotating massive main sequence stars. We provide three sets of initial compositions that are suitable for comparison with early OB stars in the SMC, the LMC and the Galaxy. The models cover the main-sequence evolution and in most cases these have been computed up to helium ignition. In terms of overshooting and rotational mixing efficiency, our models have been calibrated against the FLAMES survey of massive stars. We are using a new method to calibrate the amount of overshooting that makes use of the observed drop in projected rotation rates for stars with surface gravities lower than $\log g = 3.2$ dex. Interpreting this drop as the end of the main sequence, we find an overshooting parameter of 0.34 ± 0.1 pressure scale heights.

We have also presented a detailed set of isochrones based on models of rotating massive main sequence stars. Whereas classical isochrones can be represented by a single line in the Hertzsprung-Russell diagram, the isochrones of rotating stars span a wide range of effective temperatures at a given luminosity. Therefore, the mass and age of an observed star can no longer be determined uniquely from its location in the Hertzsprung-Russell diagram. We also provided detailed predictions for the changing surface abundances of rotating massive main sequence stars. While we believe that the data provided here can be useful to many future studies of massive stars, we make use of it in (Paper II) for undertaking a quantitative test of rotational mixing of massive stars in the LMC.

Acknowledgements We thank Georges Meynet, the referee of this paper, for many helpful comments and suggestions.

This work has been performed within the framework of the FLAMES consortium of massive stars and has made use of the VizieR catalogue access tool, CDS, Strasbourg, France. SdM acknowledges support for this work provided by NASA through Hubble Fellowship grant HST-HF-51270.01-A awarded by the Space Telescope Science Institute, which is operated by the Association of Universities for Research in Astronomy, Inc., for NASA, under contract NAS 5-26555.

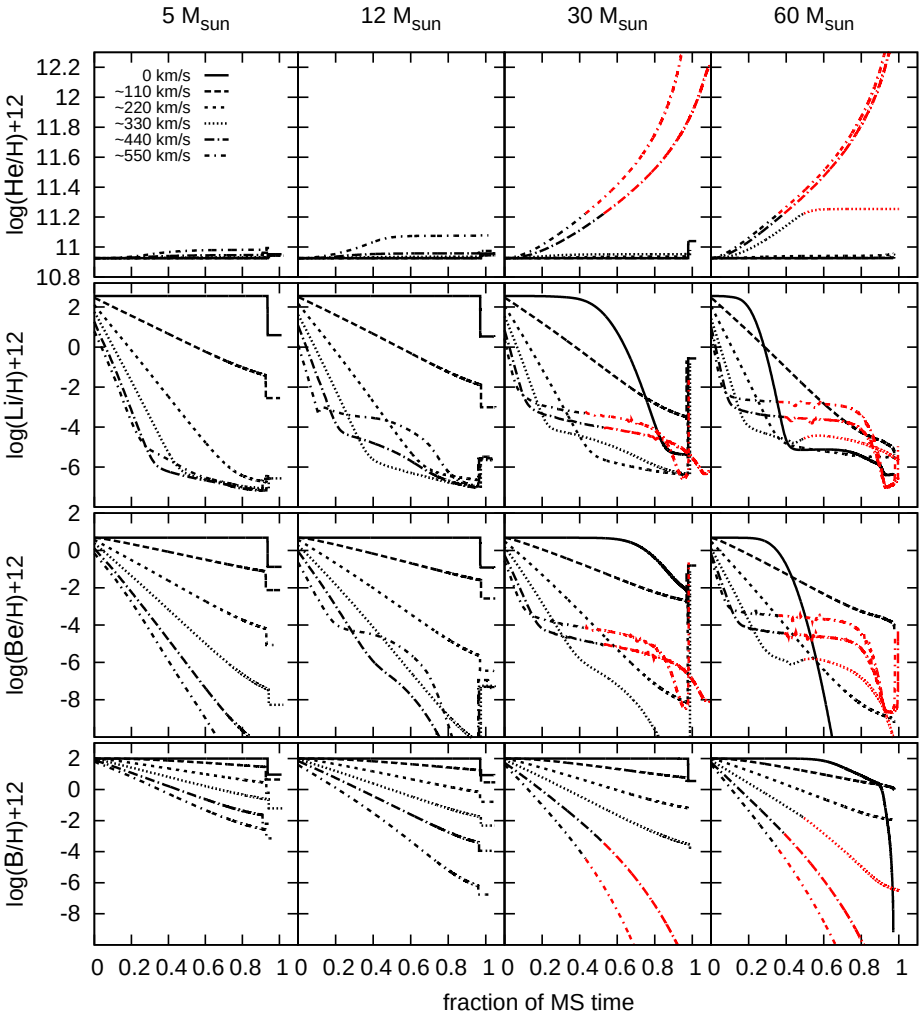

Figure 2.9: Change of the surface abundances of helium, lithium, beryllium and boron along evolutionary tracks of SMC composition as a function of time, expressed as a fraction of the main-sequence lifetime. Different line styles represent different initial rotational velocities (see legend). For models where the surface helium mass fraction exceeded 40%, the abundances are plotted in red, to indicate that the reference element hydrogen is depleted significantly (see also Sec. 2.4).

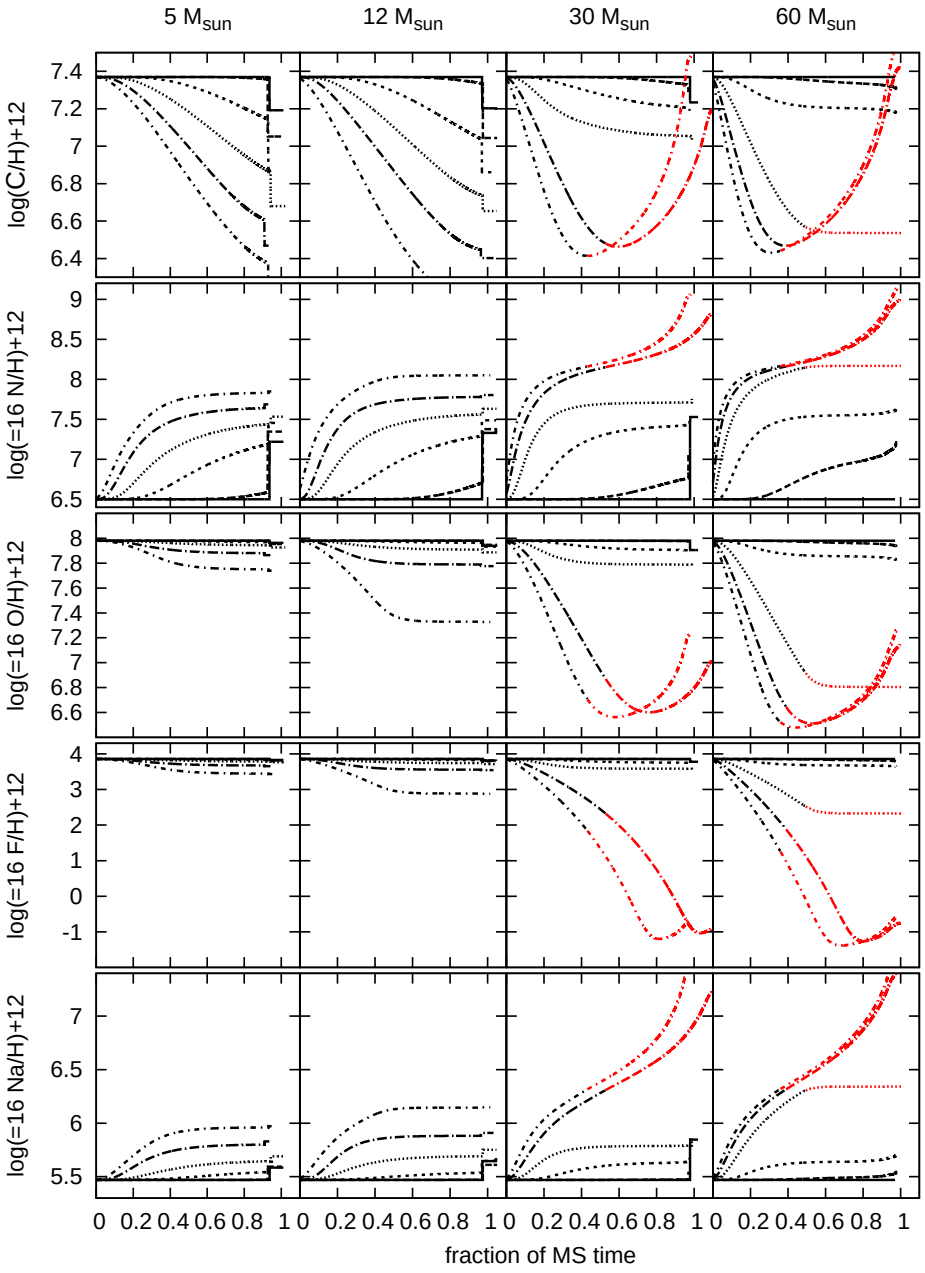

Figure 2.9: Surface abundances of rotating models at SMC metallicity, continued. Shown are carbon, oxygen, nitrogen, fluorine and sodium (from top to bottom) as a function of time, expressed as a fraction of the main-sequence lifetime.

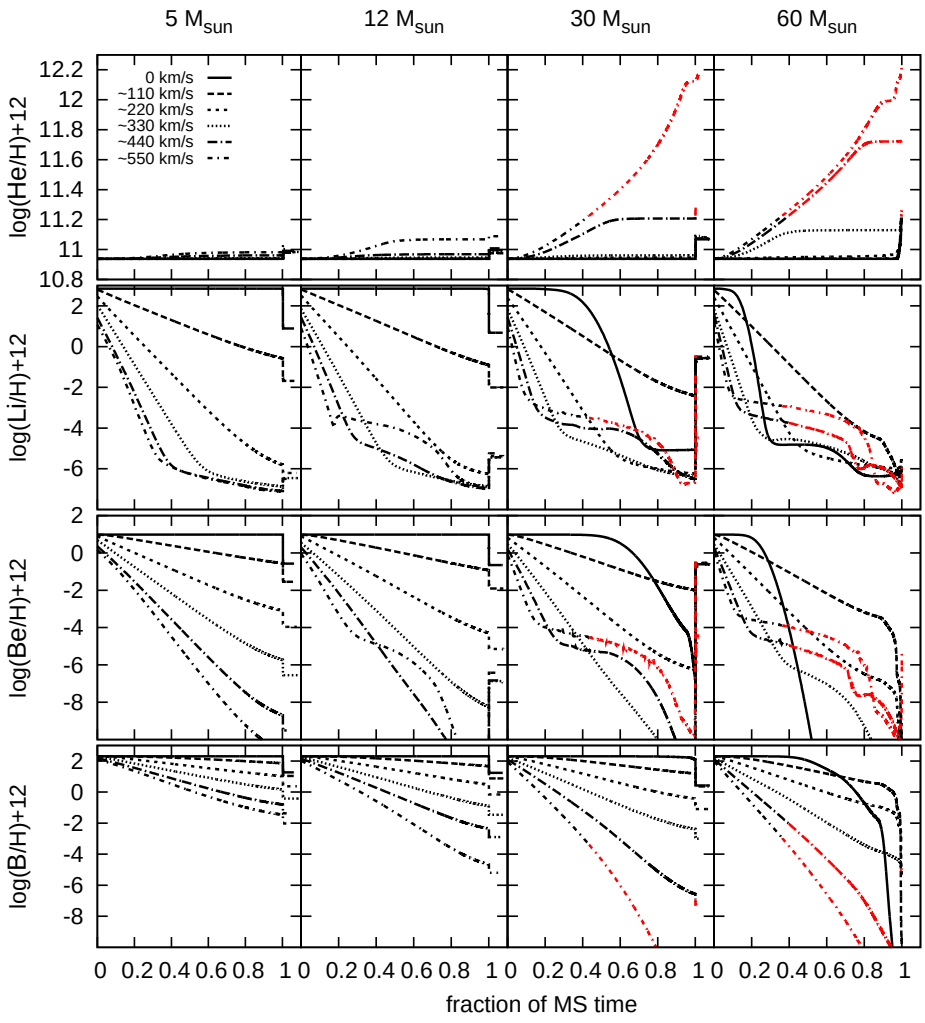

Figure 2.10: Like Fig. 2.9, for stellar models of LMC composition.

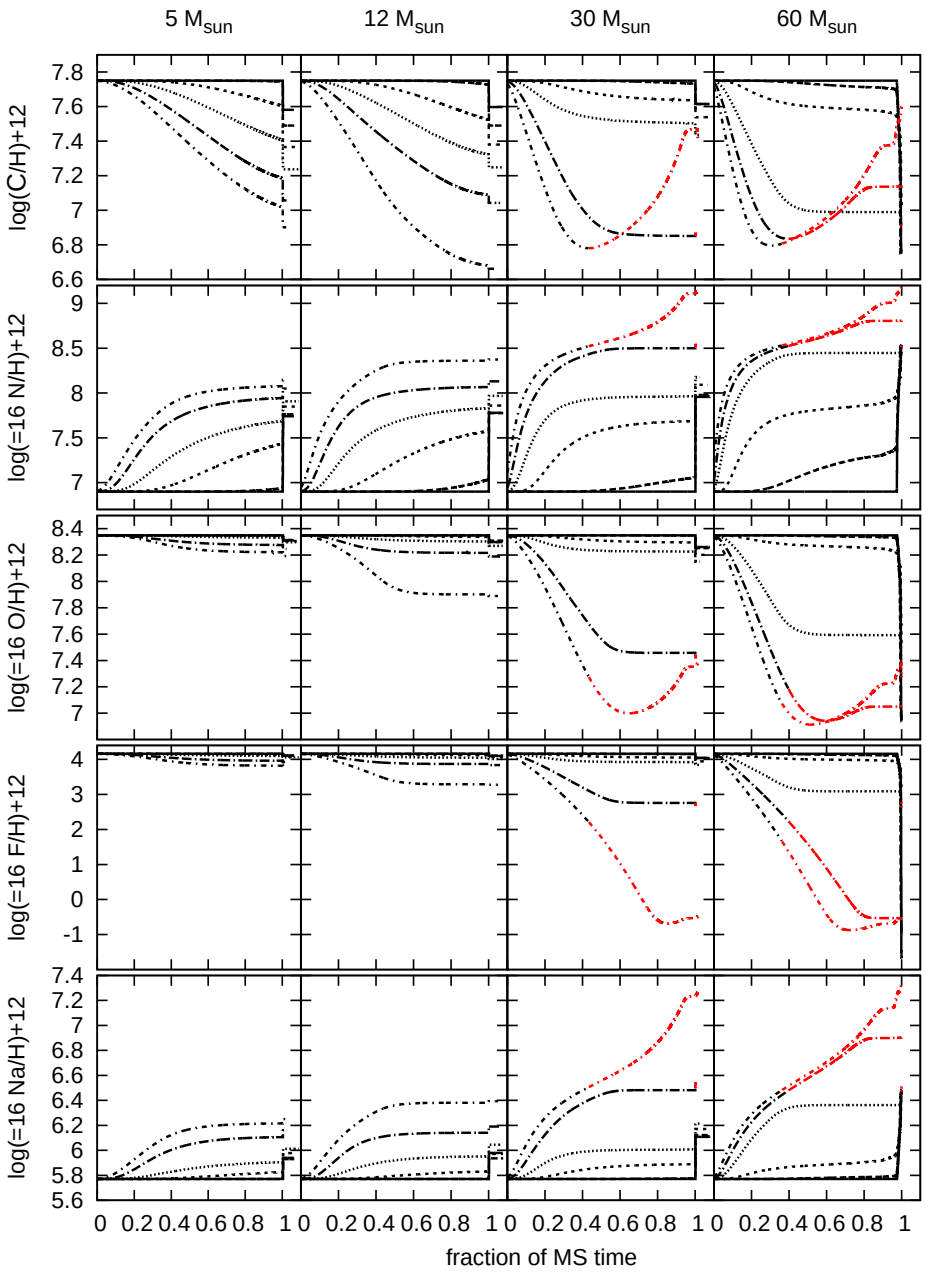

Figure 2.10: continued: Like Fig. 2.9, for stellar models of LMC composition.

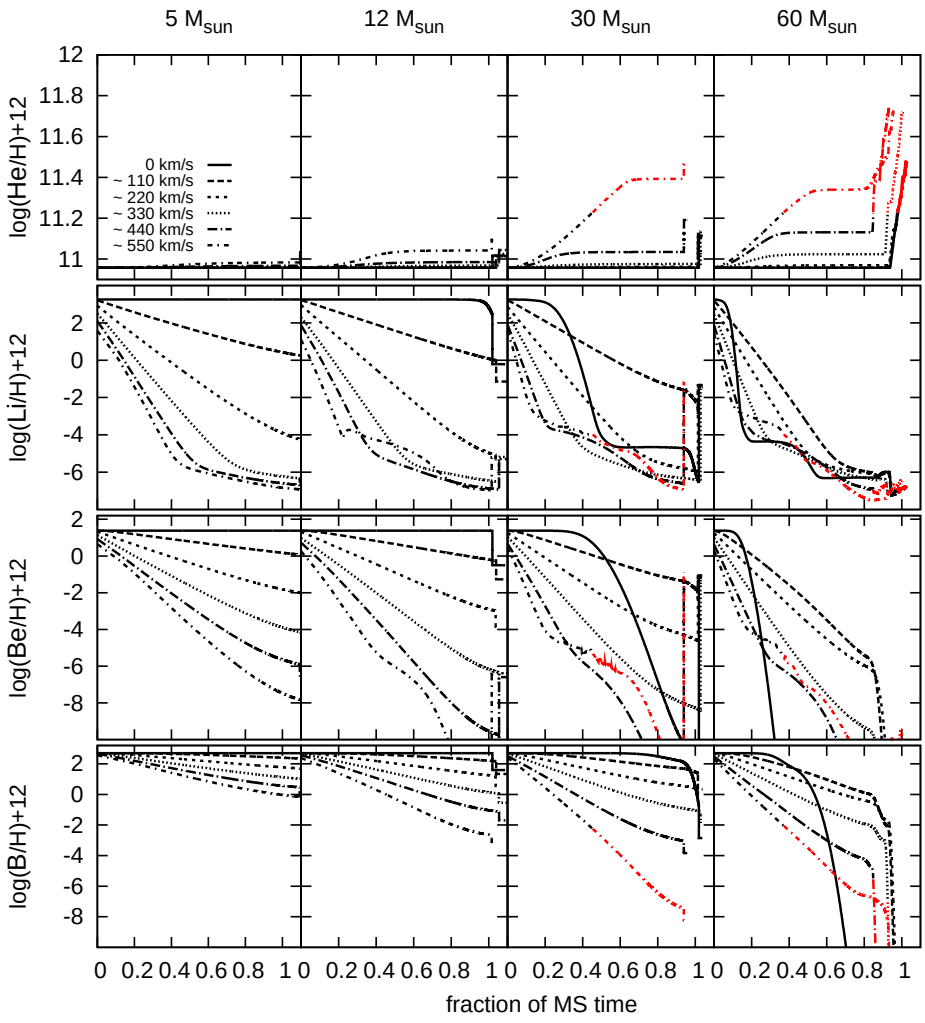

Figure 2.11: Like Fig. 2.9 for stellar models with a Galactic initial composition.

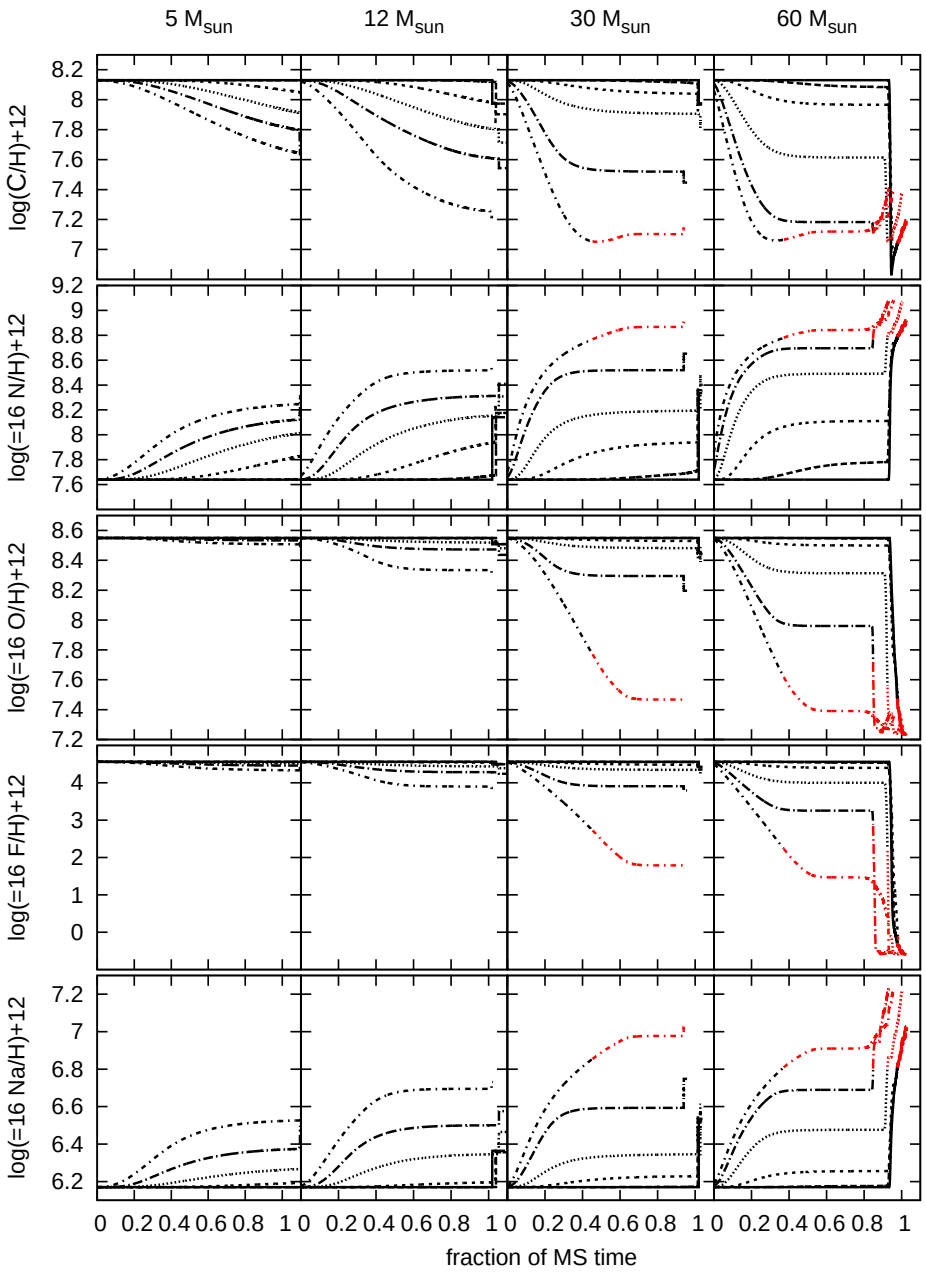

Figure 2.11: continued: Like Fig. 2.9, for stellar models of Galactic composition.

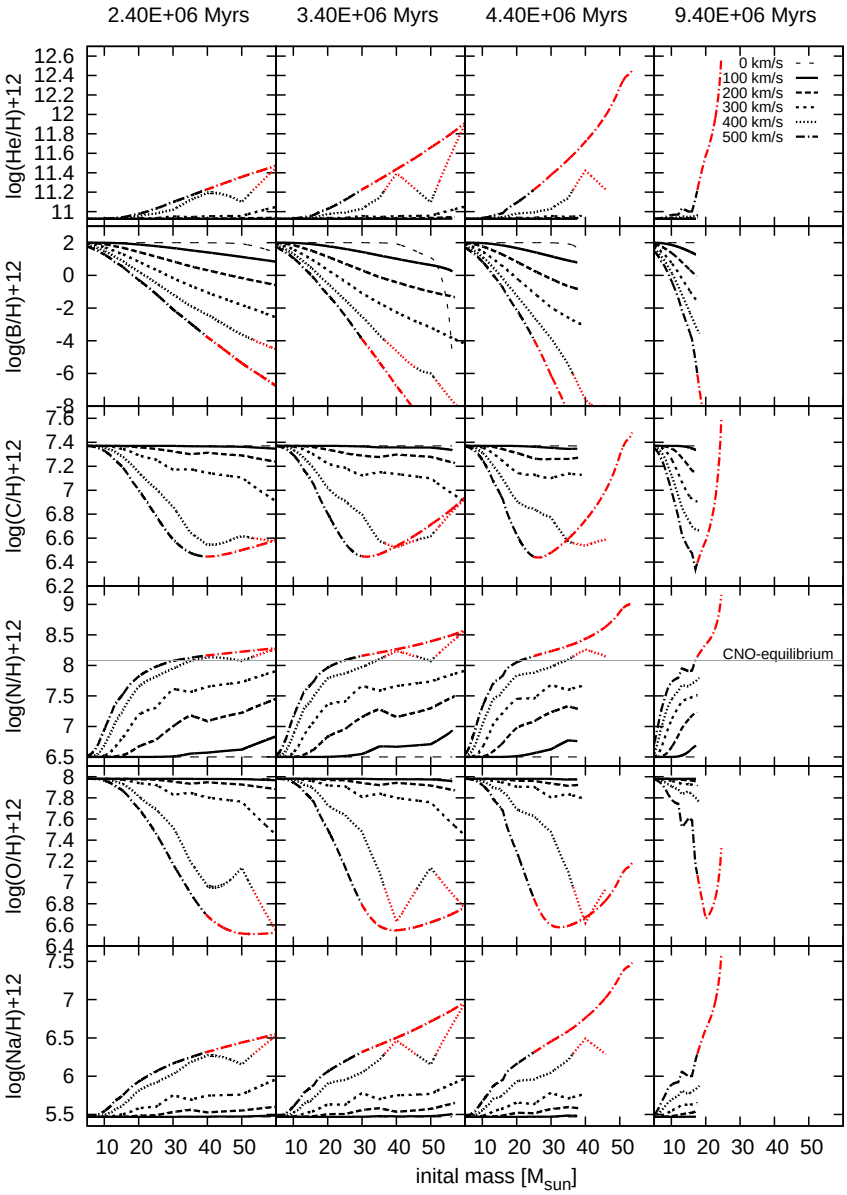

Figure 2.12: Surface abundances for a fixed age, as a function of initial mass and rotational velocity, for SMC metallicity. From top to bottom are shown helium, boron, carbon, nitrogen, oxygen and sodium abundances.

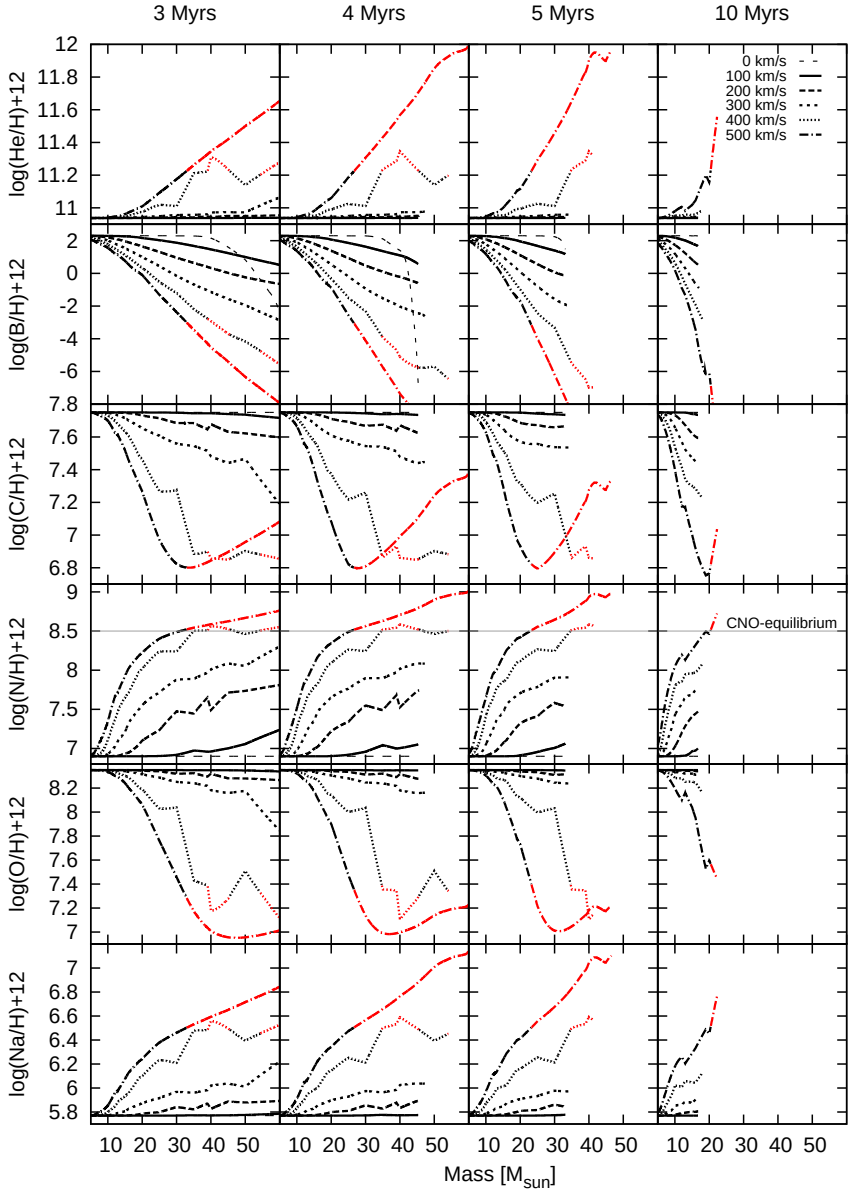

Figure 2.13: Surface abundances for a fixed age, as a function of initial mass and rotational velocity, for LMC metallicity. From top to bottom are shown helium, boron, carbon, nitrogen, oxygen and sodium abundances.

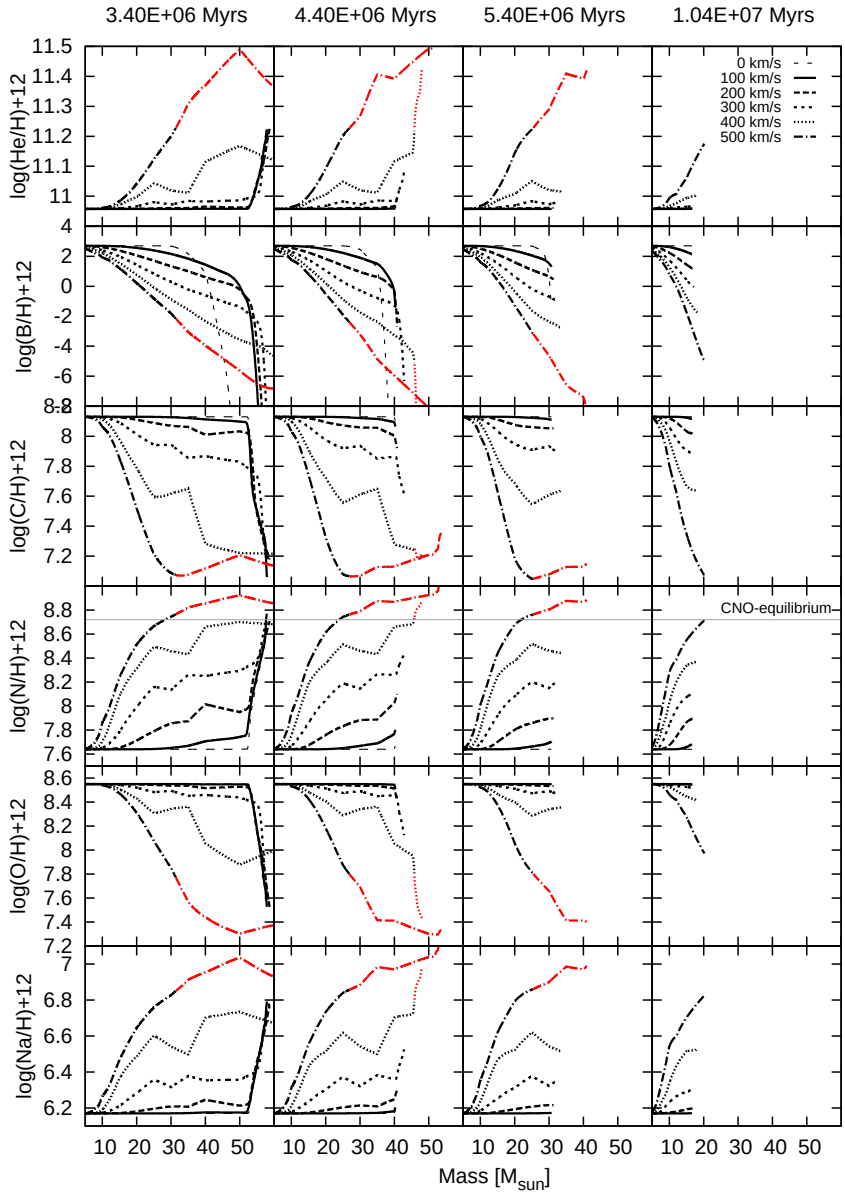

Figure 2.14: Surface abundances for a fixed age, as a function of initial mass and rotational velocity, for Galactic metallicity. From top to bottom are shown helium, boron, carbon, nitrogen, oxygen and sodium abundances.

CHAPTER 3

The VLT-FLAMES Survey of Massive Stars: Rotation and Nitrogen Enrichment as the Key to Understanding Massive Star Evolution

I.Hunter, **I.Brott**, D.J. Lennon, N. Langer, C. Trundle, A. de Koter, C.J. Evans and R.S.I. Ryans

Published in The Astrophysical Journal Letters, 2008, 676, L29-L32

Abstract Rotation has become an important element in evolutionary models of massive stars, specifically via the prediction of rotational mixing. Here, we study a sample of stars, including rapid rotators, to constrain such models and use nitrogen enrichments as a probe of the mixing process. Chemical compositions (C, N, O, Mg and Si) have been estimated for 135 early B-type stars in the Large Magellanic Cloud with projected rotational velocities up to $\sim$300 km s^{-1} using a non-LTE TLUSTY model atmosphere grid. Evolutionary models, including rotational mixing, have been generated attempting to reproduce these observations by adjusting the overshooting and rotational mixing parameters and produce reasonable agreement with 60% of our core hydrogen burning sample. We find (excluding known binaries) a significant population of highly nitrogen enriched intrinsic slow rotators ($v \sin i \lesssim$50 km s^{-1}) incompatible with our models ($\sim$20% of the sample). Furthermore, while we find fast rotators with enrichments in agreement with the models, the observation of evolved ($\log g < 3.7$dex) fast rotators that are relatively unenriched (a further $\sim$20% of the sample) challenges the concept of rotational mixing. We also find that 70% of

our blue supergiant sample cannot have evolved directly from the hydrogen burning main-sequence. We are left with a picture where invoking binarity and perhaps fossil magnetic fields are required to understand the surface properties of a population of massive main sequence stars.

3.1 Introduction

Stellar rotation in massive stars has been adopted in recent theoretical models to, for example, predict the correct blue to red supergiant ratio (Maeder & Meynet 2001), the progenitors of gamma-ray bursts through homogeneous evolution (Yoon & Langer 2005) and Wolf-Rayet populations as a function of metallicity (Meynet & Maeder 2005; Vink & de Koter 2005). However, the consequent surface enrichment of helium and nitrogen through rotational mixing is poorly constrained by observations (Daflon et al. 2001), with the mixing typically calibrated from either studies of main-sequence stars with low projected rotational velocities (Korn et al. 2002) or evolved supergiant stars (Venn 1999). The former are biased towards slow rotators while the latter have evolved beyond the core hydrogen burning phase. The analysis of an unbiased sample of fast rotating core-hydrogen burning stars in order to properly calibrate the predicted rotational mixing efficiency was a strong driver for a large survey of O- and early B-type stars in our Galaxy and the Magellanic Clouds (Evans et al. 2005). Hunter et al. (2007) and Trundle et al. (2007), hereafter Paper I and II respectively, have presented chemical abundances for the narrow lined objects (predominately slow rotators) in the LMC sample. Here we extend the study with the chemical analysis of the faster rotating stars.

3.2 Observations and model atmosphere analysis

High-resolution (R$\sim$20 000) spectra from the Fibre Large Array Multi-Element Spectrograph (FLAMES) at the European Southern Observatory Very Large Telescope were obtained for some 750 O- and early B-type stars located towards clusters in our Galaxy and the Large and Small Magellanic Clouds (LMC and SMC respectively). A discussion of target selection, observational details and initial data reduction can be found in Evans et al. (2005). In this letter we discuss the LMC early B-type stars, using nitrogen as a probe of chemical enrichment.

A grid of non-LTE TLUSTY model atmospheres (Hubeny & Lanz 1995) has been used to calculate the atmospheric parameters and chemical compositions (C, N, O, Mg and Si) of our targets as described in Papers I, II and Hunter et al. (2008b), hereafter Paper III. We have fitted the lines with rotationally broadened profiles to

estimate the equivalent widths (EWs), since at significant rotational velocities (>50 $\mathrm{km\,s^{-1}}$) the line shape is rotationally dominated. For those objects in which no nitrogen features could be identified, an upper limit to the nitrogen abundance was estimated by placing an upper limit on the equivalent width of the strongest N II line in our spectral range, which is located at 3995Å (Paper I).

The mean abundances of C, O, Mg and Si are in excellent agreement (within 0.05 dex) with the LMC baseline abundances given in Paper I. However the mean nitrogen abundance is 0.36 dex higher than its baseline abundance indicating that nitrogen enrichment has occurred in many of the stars. Additionally the scatter in the nitrogen abundances is over a factor of two larger than that of the other elements, indicating that different levels of enrichment explain the mean nitrogen abundance, rather than systematic errors. Since nitrogen is an important element in the CNO-cycle, the surface nitrogen enrichments can be used as a measure of the mixing efficiency. Note that although a corresponding carbon depletion of up to ~0.2 dex would be expected, within the uncertainties in determining carbon abundances (see Paper I), such an effect would be difficult to observe. In Fig. 3.1 the nitrogen abundances are plotted as a function of the projected rotational velocity with the sample being split into two groups; core hydrogen burning objects with surface gravities ≥3.2 dex and supergiants having surface gravities <3.2 dex (see Paper III).

3.3 Stellar evolution models

Comparison with published stellar evolution models such as the Geneva models (Maeder & Meynet 2001) is complicated as no rotating models at the LMC metallicity are currently available. Additionally, the initial chemical composition for evolutionary models is often scaled from solar composition, and this is not appropriate for all elements, in particular nitrogen.

New evolutionary models have been calculated (Brott et al. in prep.) using the stellar evolution code of Yoon et al. (2006), which includes rotation (Heger et al. 2000) and angular momentum transport by magnetic torques (Spruit 2002). Only two differences apply here: we updated the mass loss prescription and now use the recipe of Vink et al. (2001), and we disregard the magnetically induced chemical diffusion term of (Spruit 2002), which — in contrast to the magnetic angular momentum transport — is not observationally supported, and appears controvercial at present (Spruit 2006).

As initial composition we adopted the LMC C, N, O, Mg and Si abundances given in Paper I and all the other metal abundances decreased by 0.4 dex from the solar composition of Asplund et al. (2005). Based on the recent discussion of the pri-

mordial helium abundance (Peimbert et al. 2007), we have updated the initial helium mass fraction for our LMC models to Y= 25.6%, which together with the metallicity of the adopted chemical composition (Z= 0.5%), results in a hydrogen mass fraction of X= 73.9%.

In Paper III we determined that the end of core hydrogen burning occurs at a logarithmic surface gravity of ~3.2 dex. We find that a convective core overshooting of 0.335 pressure scale heights is required to reproduce this result. While this value is larger than what is typically assumed, with consequences for the post-main sequence evolution which still remain to be investigated, it provides the only way to understand the sharp drop in the rotational velocity distribution of our sample at a surface gravity of 3.2 dex. Evolutionary models neglecting overshooting indicate that the surface nitrogen enrichment is smaller by less than 0.15 dex at core hydrogen exhaustion for a rapid rotator. Hence, our principal conclusions are not significantly affected by the adopted amount of overshooting.

The efficiency of rotationally induced mixing in our models is controlled by the parameter f_c, which is the ratio of the turbulent viscosity to the diffusion coefficient that describes the transport of angular momentum by rotationally induced hydrodynamic instabilities (Heger et al. 2000). The mean projected rotational velocity of the stars shown in Fig. 3.1 is 110 km s^{-1}, with the mean surface nitrogen abundance being 7.2 dex. Although this mean projected rotational velocity is lower than that observed for cluster stars (see, for example, Huang & Gies 2006a) there is no bias towards stars with low rotational velocities. Our stars are a relatively unbiased sample of the true populations, as explained in Evans et al. (2006). This population is dominated by field stars, which are known to rotate slower than cluster stars, and our velocity distribution is comparable to the Galactic field stars of Abt et al. (2002a). Additionally Be-type stars are excluded, hence our mean velocity is representative only for normal B-type stars and there is no velocity bias for these B-type stars.

The parameter f_c has been calibrated to reproduce the mean surface nitrogen abundance of the core-hydrogen burning stars at core hydrogen exhaustion for a 13 $M_\odot$ model (the mean mass of our non-supergiant stars) initially rotating at 140 km s^{-1} ($110\times4/\pi$ to account for random angles of inclination). We find f_c=2.28×10^{-2}, compared to 3.33×10^{-2} adopted previously (Heger et al. 2000). Using these parameters, we computed a grid of models for masses representative of our sample and a range of initial rotational velocities.

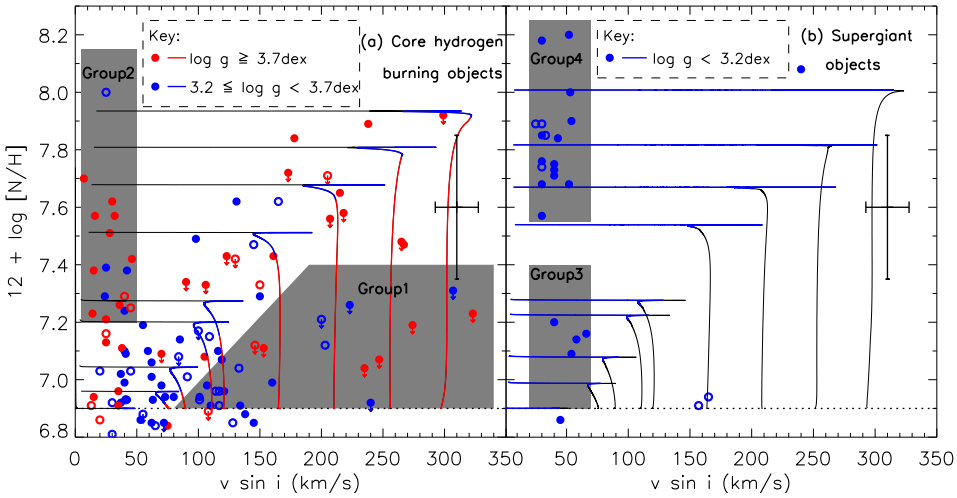

Figure 3.1: Nitrogen abundance (12 + log [N/H]) against the projected rotational velocity ($v \sin i$) for core hydrogen burning (a) and supergiant (b) objects. Open symbols: radial velocity variables; downward arrows: abundance upper limits; dotted line: LMC baseline nitrogen abundance. The mean uncertainty in the nitrogen abundance is 0.25 dex while that in $v \sin i$ is 10% and these are illustrated. These errors are largely independant of rotational velocity since the systematic uncertainties are comparable to the measurement errors. The bulk of the core hydrogen burning objects occupy a region at low $v \sin i$ and show little or modest nitrogen enrichment. The tracks are computed for an initial mass of 13 $M_\odot$ (a) and 19 $M_\odot$ (b), corresponding to the average mass of our non-supergiant and supergiant stars, respectively, and their rotational velocity has been multiplied by $\pi/4$. Although the plot contains stars with a range of masses, comparison of the tracks shown in (a) and (b) show that any mass effect is negligible compared to the abundance uncertainties. In (a) the surface gravity has been used as indicator of the evolutionary status and the objects (see legend) and tracks have been split into red and blue to indicate younger and older stars respectively. However, this is illustrative only, since the evolutionary status is obviously continuous and not discrete. Gray shading in panel (a) highlights two groups of stars which remain unexplained by the stellar evolution tracks. In panel (b), gray shading highlights the apparent division of the supergiants into two distinct groups. The surface gravity estimates of many of the objects in Group 3, and the two apparantly rapidly rotating unenriched supergiants, are consistent with being in the core hydrogen phase within their uncertainties.

3.4 Discussion and conclusions

In Fig. 3.1 the nitrogen abundances are plotted against the projected rotational velocities for our sample stars, and compared with the evolutionary models. Given the large

number of objects in our sample, it is reasonable to assume a random distribution of inclination angles, and hence the rotational velocity of the tracks has been scaled by $\pi/4$. Although we have attempted to contrain the evolutionary tracks to the observations, we are able to reproduce agreement for only 60% of the data (excluding known radial velocity variables).

However, two groups of core hydrogen burning stars in Fig. 3.1(a) stand out as being in conflict with the evolutionary models. Group 1 contains fast rotators which have little chemical mixing. In particular, this group includes fast rotating single stars with surface gravities indicating that they are near the end of core hydrogen burning (excluding radial velocity variables this is ∼20% of the core hydrogen burning sample.) The gravities used to discriminate these stars have not been corrected for the fact that we may observed them almost equator-on, i.e. their true polar gravities could be larger, meaning that they are less evolved than our derived gravities imply. However, applying the surface gravity corrections described in Huang & Gies (2006b) would increase the gravities by up to ∼0.3 dex for our faster rotators. As the zero age main-sequence gravity of our 13 $M_{\odot}$ models is about 4.3 dex, and since most of the stellar expansion on the main sequence occurs towards the end of core hydrogen burning, this gravity uncertainty can not reconcile the situation.

The second discrepant group of stars in Fig. 1a are the 15 slow rotators ($v \sin i$ <50 km s^{-1}) that show significant nitrogen enrichment (Group 2). This group also forms ∼20% of the non-binary core hydrogen burning sample. Although it could be argued that they may be fast rotators observed pole-on, statistically this is unlikely. In order to reproduce their mean nitrogen abundance requires a rotational velocity of ∼200 km s^{-1}. Using simple geometry to calculate the solid angle restriction that we must impose, i.e. $4\pi(1 - cos\theta)$, and assuming that we need 15 stars to have this velocity, we expect less than one star to appear with such a low rotational velocity due to random inclinations. The simple corollary of this is that if we have 15 stars with velocities ∼200 km s^{-1} populating Group 2 through random angles of inclination, over 300 similary enriched stars with $v \sin i$ values between 150 and 200 km s^{-1} would be expected. Such a population clearly does not exist.

Evolved rapid rotators with low nitrogen enrichment (Group 1) may be produced by close binaries with an initial period small enough to ensure tidal locking and slow rotation but large enough for highly non-conservative mass transfer, i.e. with an amount of mass accreted which is sufficient to spin-up the star but insufficient to enrich it significantly (Petrovic et al. 2005a). However, for many of the evolved stars in Group 1, there is no indication of binarity. The single star nature for these objects would pose a serious challenge to the theory of rotational mixing.

While binaries might be able to populate Group 2 (Langer et al. 2008), another explanation may be more likely. Morel et al. (2006) have analyzed ten slowly rotat-

ing Galactic early β-Cephei B-type stars and found a highly enriched group (four out of ten) of which three have detected magnetic fields. Although pulsations in these stars may cause an apparent surface enrichment, Bourge et al. (2007) report that only slight nitrogen enrichments would be expected. As such, assuming that the effect of pulsations is negligible, there appears to be a correlation between magnetic fields and nitrogen enrichment. Indeed, Wolff et al. (2007) have attributed the large number of slow rotators often seen in massive star populations to magnetic locking of the star to the accretion disk during the star formation process and Abt et al. (2002b) also show a correlation between slow rotation and magnetic fields for magnetic A- and B-type stars. Hence we postulate that the highly enriched slow rotators in the LMC are analogs of the enriched Galactic magnetic stars. This would imply that, independent of metallicity, a significant fraction of early B-type stars are intrinsically magnetic, analogous to the well known situation for lower mass stars. In this context, the identification of three He-rich slowly rotating OVz stars in NGC 346 (Mokiem et al. 2006) suggests that the phenomenon of intrinsic magnetic fields in massive stars may not be confined to the B-star regime. If these magnetic fields are of fossil origin, i.e. possessing long-term stability (Braithwaite & Spruit 2004), in contrast to the fields produced by the (Spruit 2002) mechanism, one may speculate that stars in Group 2, and their Galactic counterparts, might be the progenitors of magnetars, analogous to the suggestion of Ferrario & Wickramasinghe (2006) that magnetic white dwarfs evolve from magnetic A, F and late B stars. While the fossil field hypothesis might well explain the slow rotation, the physical process which leads to the enrichment of nitrogen in the stars of Group 2 remains to be identified.

The nitrogen abundances of the supergiants (Fig. 3.1(b)) appear to fall into two distinct groups, one group having a level of nitrogen enhancement consistent with that seen for the majority of the core hydrogen burning objects (<7.2 dex; Group 3), and a second having a much greater level of enrichment (>7.6 dex; Group 4). It should be noted that although the Group 4 objects appear to be well fitted by evolutionary tracks with initial rotational velocities of 200-300 $\mathrm{km\,s^{-1}}$, such a rotational velocity distribution for supergiants is inconsistent with that for core-hydrogen burning objects and rotation does not increase the blue-supergiant lifetime. Hence, the enrichments of the supergiants in Group 4 (70% of the non-binary supergiant sample) are incompatible with the theory of rotational mixing. Additionally it should be noted that the lowest gravity stars (<2.8 dex) are all enriched in nitrogen, implying that some evolutionary process not accounted for in the models is responsible for the enrichment.

The simplest way to interprete this would be to characterize Group 3 as pre-red supergiant objects, and Group 4 as post-red supergiant objects. The nitrogen abundances and rotational velocities in Group 4 are indeed consistent with the predictions for a blue loop stage (Heger & Langer 2000). However, we note that our models do

not return to the high effective temperatures of the stars in Group 4 and hence their position on the H-R diagram cannot be reproduced. As several of the enriched objects show evidence of binarity, mass transfer may also be important (Wellstein et al. 2001).

To conclude, our study can not provide unambigous evidence for rotational mixing acting in massive stars. The fast rotators in our sample can be interpreted in two ways. Firstly as rotationally mixed stars, if the relatively non-enriched stars (Group 1) can be explained by binary effects. However, if it were confirmed that these Group 1 stars are single stars, then the enriched rapid rotators may need to be understood as binary products — and rotational mixing would be inefficient, or much more complex than described by the present-day shellular models. Additionally, the population of intrinsically slow rotators with nitrogen enhancements of up to a factor of ~6 implies that studies of nitrogen enhancements with stellar samples which are restricted to low projected rotational velocities — which applies to most previous works — are not suited for constraining, or motivating, the adoption of rotational mixing in massive stars. Finally our supergiant sample implies that these stars cannot be considered as representative of the amount of mixing that occurs during the hydrogen burning main-sequence and hence should not be used to constrain this process. In summary, our study provides a challenge to rotational mixing, and provides evidence for two other processes affecting the rotation and the surface abundances of populations of massive stars, likely binarity and magnetic fields.

Acknowledgments We are grateful to staff from the European Southern Observatory for assistance in obtaining the data, and to STFC (UK Science and Technology Facilities Council) and NWO (Netherlands Science Foundation) for financial support. IH acknowledges financial support from DEL (Dept. of Employment & Learning Northern Ireland). SJS acknowledges the European Heads of Research Councils and European Science Foundation EURYI Awards scheme and the EC Sixth Framework Programme. We would also like to thank the referee for highly constructive comments which significantly improved this manuscript.

Facilities: ESO (VLT-FLAMES, 2.2m-WFI).

CHAPTER 4

The VLT-FLAMES Survey of Massive Stars: Constraints on Stellar Evolution from the Chemical Compositions of Rapidly Rotating Galactic and Magellanic Cloud B-type Stars

I. Hunter, **I. Brott**, N. Langer, D.J. Lennon, P.L. Dufton, I.D. Howarth, R.S.I. Ryan, C. Trundle, C. Evans, A. de Koter and S.J. Smartt

Published in Astronomy & Astrophysics, 2009, 496, 841- 853

Abstract We have previously analysed the spectra of 135 early B-type stars in the Large Magellanic Cloud (LMC) and found several groups of stars that have chemical compositions that conflict with the theory of rotational mixing. Here we extend this study to Galactic and Small Magellanic Cloud (SMC) metallicities.

We provide chemical compositions for ∼50 Galactic and ∼100 SMC early B-type stars and compare these to the LMC results. These samples cover a range of projected rotational velocities up to $\sim 300\,\mathrm{km\,s^{-1}}$ and hence are well suited to testing rotational mixing models. The surface nitrogen abundances are utilised as a probe of the mixing process since nitrogen is synthesized in the core of the stars and mixed to the surface.

In the SMC, we find a population of slowly rotating nitrogen-rich stars amongst the early B type core-hydrogen burning stars, which is comparable to that found previously in the LMC. The identification of non-enriched rapid rotators in the SMC is not possible due to the relatively high upper limits on the nitrogen abundance for the fast rotators. In the Galactic sample we find no significant enrichment amongst the core

hydrogen-burning stars, which appears to be in contrast with the expectation from both rotating single-star and close binary evolution models. However, only a small number of the rapidly rotating stars have evolved enough to produce a significant nitrogen enrichment, and these may be analogous to the non-enriched rapid rotators previously found in the LMC sample. Finally, in each metallicity regime, a population of highly enriched supergiants is observed, which cannot be the immediate descendants of core-hydrogen burning stars. Their abundances are, however, compatible with them having gone through a previous red supergiant phase. Together, these observations paint a complex picture of the nitrogen enrichment in massive main sequence and supergiant stellar atmospheres, where age and binarity cause crucial effects. Whether rotational mixing is required to understand our results remains an open question at this time, but could be answered by identifying the true binary fraction in those groups of stars that do not agree with single-star evolutionary models.

4.1 Introduction

Rotation is generally considered to be of critical importance for theoretical models of massive star evolution and, specifically, rotationally-induced mixing, where material is mixed from the stellar core into the photosphere (Heger & Langer 2000; Meynet & Maeder 2000). For example, rotation has been used as an explanation of blue to red supergiant ratios (Maeder & Meynet 2001) and of Wolf-Rayet populations as a function of metallicity (Meynet & Maeder 2005; Vink & de Koter 2005). Additionally, for a single massive star to end its life with an associated long gamma-ray burst, chemically homogeneous evolution through rapid rotation may be required (Yoon & Langer 2005; Woosley & Heger 2006).

Stellar evolution models including rotation predict a surface enrichment of helium and nitrogen with an associated carbon and oxygen depletion during the main sequence evolution. Massive star surface abundance anomalies (particularly nitrogen) have long been observed, by, for example, Walborn (1970), Dufton (1972) and, more recently, Gies & Lambert (1992), Kilian (1992), Bouret et al. (2003), Dufton et al. (2005), Lennon et al. (2003), Trundle & Lennon (2005), Korn et al. (2002) and Venn (1999). However, the majority of these analyses have focused on one of two groups: narrow lined main-sequence stars (i.e. stars with low projected rotational velocities) or blue supergiants. For example, Kilian considered 21 main sequence Galactic objects all with projected rotational velocities of less than 63 $\mathrm{km\,s^{-1}}$.

The magnitude of the predicted mixing has generally been compared to and calibrated against these two groups. It follows from the stellar evolution models that

the more rapidly a star rotates, the more mixing will occur, and hence the greater the nitrogen (and helium) surface enrichment that should be observed. Unfortunately spectroscopic studies of rapidly rotating stars are relatively rare. Lennon et al. (1991) studied the O9.5V star HD 93521 with a projected rotational velocity of approximately 400 km s^{-1}. They deduced an enhanced helium abundance that they ascribed to rotational mixing. Howarth & Smith (2001) analysed spectra of three rapidly rotating O-type stars (including HD 93521) using models that allowed for variations in temperature and gravity across the stellar surface and again found evidence for helium enhancements. By contrast, Villamariz & Herrero (2005) obtained a normal helium abundance together with a nitrogen enrichment for one of the stars (ζ Oph) discussed by Howarth and Smith.

Vrancken et al. (1997b) analysed the spectra of two B-type targets in NGC 2244, with projected rotational velocities between 200 and 300 km s^{-1}. The analysis was undertaken differentially with respect to a cluster member with a small projected rotational velocity. No significant abundance anomalies were identified with indeed the two fast rotators being found to have a small *underabundance* of nitrogen. Daflon et al. (2001) analysed twelve Galactic stars in Cygnus associations with projected rotational velocities between 60 and 150 km s^{-1}. On average they had subsolar abundances that agreed with those found for a sample of eight stars with very low projected rotational velocities. However two targets (with projected rotational velocities of 100 and 142 km s^{-1}) showed relative nitrogen enhancements of nearly a factor of two. Korn et al. (2005) analysed three LMC targets with projected rotational velocities of approximately 130 km s^{-1} but again found no evidence for either enhanced helium or nitrogen abundances.

The measurement of surface abundances of a large sample of core-hydrogen burning, rapidly rotating, massive stars is clearly necessary for both testing and calibrating the mixing theory and this was one of the primary drivers of the VLT-FLAMES survey of massive stars. This Large Program on the VLT with the FLAMES instrument (PI.: S.J. Smartt) focused on OB-type stars in the Galaxy and Magellanic Clouds (Evans et al. 2005, 2006, hereafter Paper I and Paper II). Over 700 O- and B-type stars were observed across these three metallicity regimes. Both the large number of objects and the different metallicity regimes allow many of the theoretical predictions of evolutionary models to be tested.

The principle outcomes of this survey related to rotation are as follows. Mokiem et al. (2006, 2007) have analysed the O-type stars in the sample (~50 objects) and used their mass-loss rates to derive the wind-momentum luminosity relation. They show that at lower metallicity stars rotate faster since they have lower mass loss rates. Dufton et al. (2006, hereafter Paper III) have shown that Galactic cluster stars (observed in the survey) rotate significantly faster than stars in the Galactic field. This

was consistent with studies of stars in the double cluster h and χ Persei (Slettebak 1968; Strom et al. 2005) and other clusters (Wolff et al. 2007; Huang & Gies 2006a). Hunter et al. (2008b, hereafter Paper IV) have derived rotational velocities for the Magellanic Cloud B-type stars from the survey and show that stars at low metallicity rotate faster than in higher metallicity regimes. For two clusters (NGC 330 and NGC 2004), these results complement the recent studies of Martayan et al. (2006, 2007), who also utilised the FLAMES spectrograph albeit at lower spectral resolution. Additionally in Paper IV, it was suggested that the observed population of B-type supergiants cannot be explained by normal single star evolution and either binarity or blue-loops needed to be invoked to model the population.

Hunter et al. (2007, hereafter Paper V) have performed a detailed chemical composition analysis of approximately 50 narrow-lined B-type stars from the survey and utilised these objects to estimate the baseline chemical compositions of the Magellanic Clouds, thereby complementing previous studies mainly of H II regions (summarized, for example, by Garnett (1999). Additionally as found from H II region analyses and other more limited stellar samples (for example Korn et al. 2002), they confirmed that for both Magellanic Clouds the assumption that all elements can be scaled from the solar composition by the same factor is incorrect. Trundle et al. (2007, hereafter Paper VI) have extended this sample of narrow lined stars to ∼100 objects and, utilising the same methods, have derived temperature scales for Galactic and Magellanic Cloud stars, which imply that stars at lower metallicity have higher effective temperatures for a given spectral type, in broad agreement with previous studies (Martins et al. 2002, 2005; Crowther et al. 2002, 2006; Massey et al. 2004, 2005). Hunter et al. (2008a, hereafter Paper VII) have presented chemical compositions for 135 B-type stars in the Large Magellanic Cloud (LMC) with a broad range of rotational velocities (up to $\sim$350 km s^{-1}). This was the first significant abundance analysis of rapidly rotating early B-type stars and they utilised the nitrogen abundances to test the theory of rotational mixing, finding the theory to be unable to explain several aspects of the sample. In particular they found populations of unenriched fast rotators, highly enriched slow rotators and supergiants that are highly enriched compared to normal core-hydrogen burning objects (see Sect. 4.4). In this paper we utilise identical methodologies to Paper VII and extend the chemical composition analysis to the Galactic and Small Magellanic Cloud (SMC) samples from the FLAMES large survey and compare these to the LMC stars.

In Sect. 4.2 we briefly describe the survey and the selection criteria for the objects that are analysed here. In Sect. 4.3 a summary of the analysis methodology is presented and the chemical compositions of the objects in each metallicity regime are compared and discussed. In Sect. 4.4 the nitrogen abundances of the sample are used to test the validity of the conclusions made in Paper VII and to further constrain the

theory of rotational mixing. Finally in Sect. 4.5 we present our principle findings and lay out the challenges for future theoretical models.

4.2 Observations

The observations of the Galactic and Magellanic Cloud stars from the VLT-FLAMES survey of massive stars have been described in detail in Paper I and Paper II respectively. To summarise, the majority of the data were obtained using the Fibre Large Array Multi-Element Spectrograph (FLAMES) on the 8.2 m European Southern Observatory Very Large Telescope (ESO-VLT) at Paranal, Chile. These data were supplemented by UVES and FEROS observations of the brighter targets. Approximately 300 Galactic objects were observed and these are associated with the clusters NGC 6611, NGC 3293 and NGC 4755. Due to the distance of the Magellanic Clouds and constraints on fibre placement with the FLAMES instrument, it was not possible to solely observe cluster objects and hence the observed Magellanic Cloud samples are dominated by the field populations (see Paper IV). These field samples were centred towards N 11 and NGC 2004 in the LMC and NGC 346 and NGC 330 in the SMC, with over 400 objects being observed. The signal-to-noise (S/N) ratios of the SMC spectra were generally in the range 25-150 while the other spectra were in the range 50-200[1].

In Fig. 4.1 (only available online) we provide the observed spectra for a subset of the LMC stars. The strongest nitrogen line (at 3995Å) has been highlighted and the Hα profile is also shown where available. Panels (a) to (d), (e) to (h) and (i) to (l) show objects with low projected rotational velocities (less than 100 km s^{-1}), high projected rotational velocities (greater than 200 km s^{-1}) and supergiants respectively. In each of these groups two relatively nitrogen normal and two nitrogen rich stars are displayed. Inspection of the spectra reveals that apart from the nitrogen lines there is no apparent difference between the spectra of nitrogen rich and nitrogen normal stars.

4.2.1 Selection criteria

Paper IV presents atmospheric parameters and projected rotational velocities for the SMC sample of stars from the FLAMES survey. We have examined the B-type stars in this sample of objects and estimated chemical compositions where possible. Following the methodology adopted for the LMC sample, upper limits to the nitrogen abundances have been estimated when no nitrogen lines were observed for the SMC

[1]The reduced spectra are publicly available at http://star.pst.qub.ac.uk/~sjs/flames/

objects. Stars were excluded from the analysis if asymmetries in the line were obvious or if the upper limits to the equivalent width estimates for the nitrogen lines lead to abundance estimates that did not provide a useful constraint. Note that due to spectral contamination issues Paper IV does not provide atmospheric parameters for the double-lined spectroscopic systems or the Be-type stars and hence no attempt has been made to derive abundances for these objects here. Additionally, due to limitations in the model atmosphere grid used to derive the abundances, the majority of the O-type stars (i.e. stars hotter than 35 000 K) have not been analysed (see Sect. 4.3). These selection criteria are consistent with those for the LMC sample (Paper VII). We note that the two B8 supergiants analysed in Paper VI, NGC2004-005 and NGC2004-007, were excluded as their oxygen abundances may be unreliable.

In addition to the Magellanic Cloud samples, we require a Galactic comparison sample. However, given that we are primarily interested in using nitrogen to constrain the possible enrichment process (see Sect. 4.1), chemical compositions are only presented for those Galactic stars with atmospheric parameters in Paper III and measurable nitrogen features. Although this introduces a bias towards slow rotators in the Galactic sample, the upper limits to the nitrogen abundances for the faster rotators were too high to be useful when comparing with evolutionary models. For the Galactic sample nitrogen lines were observable at projected rotational velocities up to $\sim$250 km s^{-1}. In Fig. 4.2 the projected rotational velocity distributions of the selected stars in the three regions are plotted. Despite the selection criteria, the three distributions are similar although we observe a smaller proportion of slowly rotating Galactic objects. This may be due to Galactic cluster stars rotating faster than field stars (see Strom et al. 2005; Huang & Gies 2006a; Wolff et al. 2007, Paper III). Hence our Galactic and Magellanic Cloud samples can be considered to be comparable, with our selection criteria compensating for the intrinsic differences between the Galactic cluster and the Magellanic Cloud field star velocity distributions.

Papers V and VI have presented the abundances for the majority of the slow rotators in these samples and these abundances have been adopted here. Those stars which have previously been identified as radial velocity variables (Papers I, II, III and IV) are considered to be binaries in the subsequent discussion.

4.2.2 Equivalent width measurements

As discussed in Papers V and VI the equivalent widths (EWs) of the absorption lines for the narrow lined stars were measured by fitting Gaussian profiles to the observed features. The uncertainties in these measurements are typically estimated to be of the order of 10% for well defined lines (Paper V). However, for faster rotating stars (typically those with projected rotational velocities greater than 50 km s^{-1}) the rotational

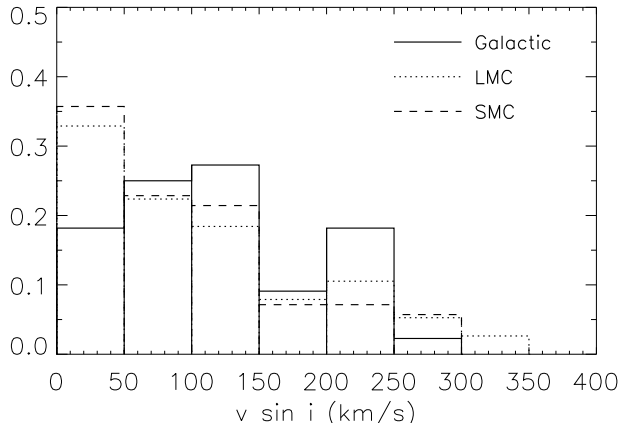

Figure 4.2: Histogram of the projected rotational velocity distribution of the Galactic, LMC and SMC samples, normalised to the number of stars in the sample. The three samples have similar distributions save for a slight deficit of slow rotators in the Galactic sample.

broadening dominates over the other broadening mechanisms and the use of a Gaussian profile is no longer satisfactory. Hence we have utilised rotationally broadened profiles to estimate the equivalent widths of the faster rotators in our sample.

The measurement of the metal line equivalent widths for the fast rotators is not as straightforward as the measurements for the slowly rotating stars analysed in Papers V and VI and many of the associated problems and uncertainties are discussed in Vrancken et al. (1997b). For example, at high rotational velocities part of the line can be 'hidden' in the continuum. This obviously will affect the estimation of the continuum level, the line strength and the line width and can bias the measurements towards lower equivalent widths. However, a priori knowledge of the projected rotational velocity can help to alleviate these problems. The rotational velocity of the fast rotators have been estimated from the helium lines (Papers III and IV) where these problems are less important due to the strength of these lines. In the estimation of the equivalent widths of the metal lines we have forced the fits to the lines to have a width equivalent to the projected rotational velocity, and hence the line width is not underestimated. Additionally, in defining the continuum level the continuum is set beyond the region of the broad lines and is fitted with a low order polynomial.

In Fig. 4.3 examples are shown to demonstrate the accuracy of the equivalent width measurements in fast rotating stars for lines of different strength and spectra of differing quality. A theoretical line profile of a known equivalent width has been rotationally broadened and random noise is added to the spectra. This line is then

fitted with a rotationally broadened profile. The centroid and width of the line are known quantities and hence these parameters can be constrained. We can therefore estimate the uncertainty in the equivalent width measurements, excluding continuum fitting, to be of the order of ~20%. Although we have carefully defined the continuum region to be beyond the region of the line, we estimate, by performing repeated fits to a sub-sample of spectra, that the normalisation procedure contributes an additional error of ~20% to the equivalent width measurements. Hence for the faster rotators in our sample the equivalent width errors can be considered to be of the order of 20-40%.

The blending of lines in rotationally broadened spectra also affects the equivalent width measurements. We again define the continuum beyond the range of the blended lines and fit the blended lines simultaneously using multiple rotationally broadened profiles. By constraining the fitted lines to have the appropriate centroids, rotational broadening errors in the fitting procedure can be minimised. If this procedure does not result in a visually satisfactory fit the lines have not been included for further analysis. However, weak absorption features which are not included will obviously affect the measured equivalent widths especially for the faster rotators and would bias the measurements to higher equivalent widths. Comparison of the abundances between the slow rotators (where blending is not an issue) with the faster rotators reveals no trend with rotational velocity. Hence we can conclude that while weak absorption lines may bias our equivalent width measurements, such a bias is negligible within the other uncertainties in our analysis.

The absorption lines used in this analysis are summarized in Paper V with only measurable C, O, Mg and Si lines being included. However, given that we are primarily interested in the nitrogen abundances, even upper limits to the nitrogen abundance of a star can be useful for constraining the chemical mixing processes in the Magellanic Cloud data sets. Hence, as discussed in Sect. 4.2.1 for the Magellanic Cloud samples, upper limits to the equivalent width of the N II 3995Å line (which is the strongest nitrogen feature in our spectra) and to the corresponding nitrogen abundance were estimated. Examples of the fitting of upper limits are also shown in Fig. 4.3. The equivalent widths of the lines included in this analysis along with the estimated abundances (see Sect. 4.3.2) are given in Table 4.1 (only available online).

4.3 Analysis

4.3.1 Atmospheric parameters and rotational velocities

The atmospheric parameters and rotational velocities have been estimated in Papers III and IV and for completeness a brief overview of the method is given here. The

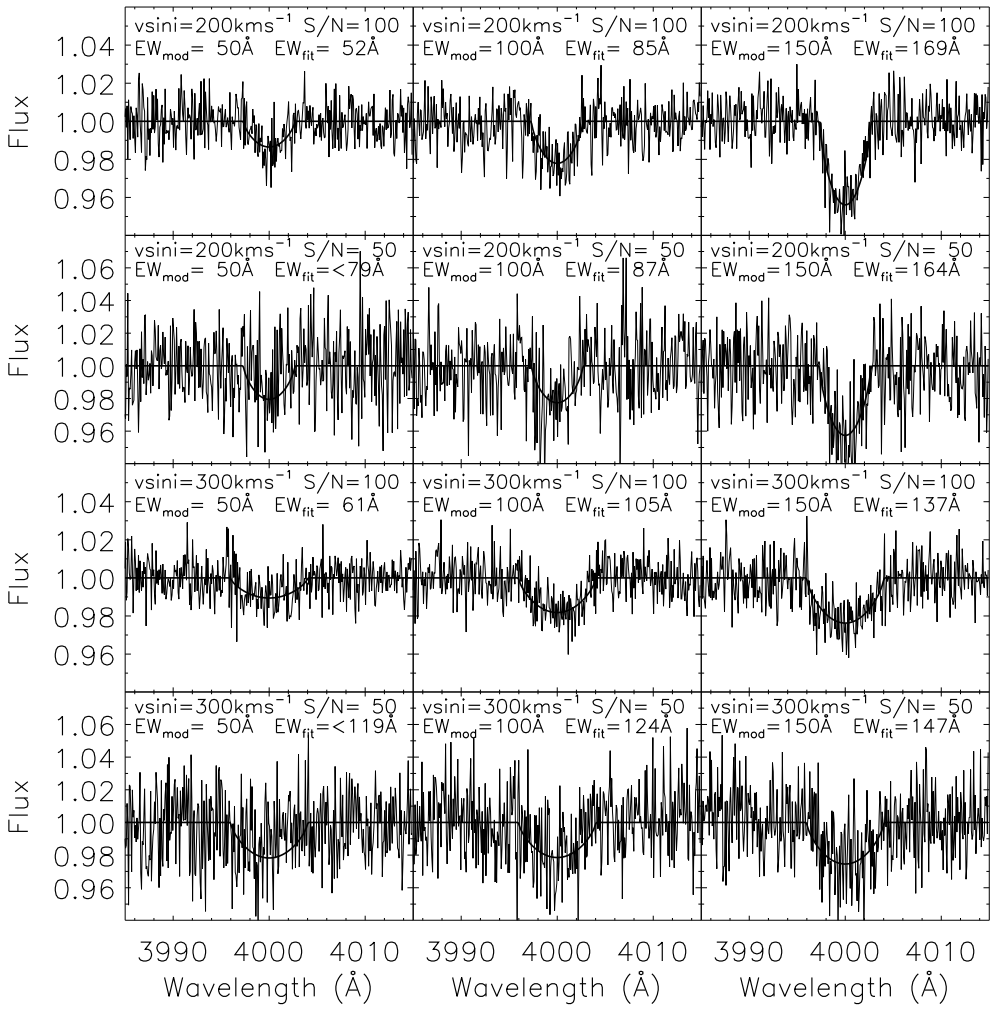

Figure 4.3: Examples of the quality of the equivalent width measurements for fast rotators at differing S/N ratios. The theoretical spectra of an absorption line (with an equivalent width of EW_{mod}) is rotationally broadened and noise added to the spectra. Using our IDL fitting routine the equivalent width of this simulated line is then measured (EW_{fit}). It should be noted that at a S/N ratio of 50, an absorption line of 50 mÅ could not be observed at these rotational velocities and therefore upper limits to the equivalent width are given.

non-LTE TLUSTY model atmosphere grid (see Hubeny & Lanz 1995, and references therein) has been used and is described in detail in Dufton et al. (2005)[2]. This grid covers the effective temperature range 12 000–35 000 K and allows for the analysis of all the B-type stars observed in the VLT-FLAMES survey, both the core-hydrogen burning and supergiant objects.

As described in Papers III and IV the hydrogen and helium lines were utilised to estimate the effective temperatures and surface gravities of the majority of the sample. For those stars where the helium lines were not temperature sensitive, effective temperatures were estimated based on spectral type using the effective temperature calibrations from Paper VI. The hydrogen lines were used to constrain the surface gravities in all cases.

For the narrow-lined spectra, where two ionization stages of silicon could be observed, the effective temperature was determined from the silicon ionization balance. The majority of these stars have been analysed in Papers V and VI. For those stars in which two ionization stages were available, but which lay outside the selection criteria of these papers, the effective temperatures (and if necessary the surface gravities) have been re-determined, rather than using those estimated in Papers III and Paper IV. However these parameters are in good agreement with those previously determined.

Rotational velocities have generally been estimated from the profile fitting methodology, where a theoretical spectrum is rotationally broadened to fit the observed spectrum. Again these values are given in Papers III and IV. We note that for several cases it was found that the rotational velocity estimated from the helium lines (Papers III and IV) did not well fit the metal lines and in these few cases the projected rotational velocity has been re-determined from the metal lines and is preferred. For the supergiants in the sample, where macroturbulent broadening can dominate over rotational broadening, the Fourier Transform technique has been utilised. This technique has the advantage that rotational broadening can be separated from other broadening mechanisms (see Simón-Díaz & Herrero 2007, Paper IV).

4.3.2 Abundance determinations

Carbon, nitrogen, oxygen, magnesium and silicon abundances have been estimated using the atmospheric parameters and EW measurements. In order to constrain the microturbulence, it has been assumed that the silicon abundance should be invariant across each metallicity regime and the microturbulent velocity has been fixed to achieve this where possible. A detailed description of this methodology is given in Paper V. The chemical composition of each star is given in Table 4.2 (only available online). This table lists the stellar identifier (from Papers I and II), atmospheric

[2]See also http://star.pst.qub.ac.uk

parameters (effective temperature, surface gravity and microturbulence), projected rotational velocity and chemical composition (C, N, O, Mg and Si) along with the number of absorption lines observed for each species.

Abundance uncertainties have been estimated using a similar method to that described in Paper V. Random uncertainties have been estimated from the scatter in the line-by-line abundances of each element and hence include both uncertainties in the EW measurements and random errors in the atomic data. For those objects where only one line was observed, the random uncertainties were assumed to be equivalent to the scatter in the oxygen abundances. If only a few oxygen features were observed (and hence it was not possible to estimate this scatter), a random uncertainty of 0.2 dex was assumed, which is typical for stars with many observed oxygen lines. Systematic errors in the abundances were estimated by considering the uncertainties in each of the atmospheric parameters. For stars where the effective temperature was constrained from the silicon ionization balance an uncertainty of 1 000 K was adopted, otherwise an uncertainty of 1 500 K was assumed. However in contrast to Paper V we consider that the effective temperature and surface gravity estimates are correlated in order to improve our error estimates, with an increase of 1 000 K resulting in a higher gravity estimate of 0.1 dex. In addition we adopt measurement errors in the surface gravity to be 0.05 dex for stars with gravities of less than 3.0 dex and 0.1 dex otherwise. Similarly the microturbulence was better estimated at small values and an uncertainty of $3\,\mathrm{km\,s^{-1}}$ has been adopted for values of less than $10\,\mathrm{km\,s^{-1}}$ with $5\,\mathrm{km\,s^{-1}}$ being taken otherwise. The systematic and random uncertainties were summed in quadrature to give the uncertainties quoted in Table 4.2 (only available online)

The derived carbon abundances are known to be susceptible to non-LTE effects (see Sigut 1996; Nieva & Przybilla 2006, 2008) and these are not fully taken into account by the rather simplistic model ion that was included in our TLUSTY calculations. Paper V discussed adding a correction of 0.34 dex (from Lennon et al. 2003) to the derived carbon abundances from the 4267Å line. This was to achieve better agreement between the estimated carbon abundance of B-type stars and those of H II regions. However, since the non-LTE effects will be temperature dependent, such a correction will also be temperature dependent. Here we adopt a more sophisticated method.

Sigut (1996) utilises a more complex model atom than does our TLUSTY grid. We have compared abundances from our grid with those calculated by Sigut over a range of effective temperatures by adopting the equivalent widths that Sigut used to reproduce a carbon abundance of 8.55 dex (Grevesse et al. 1994). The results are shown in Fig. 4.4. It is clear that there are differences of up to 0.3 dex and we have applied corrections to the abundances from the 4267Å line in order to reproduce the

temperature independent trend of Sigut. Our adopted carbon abundances are solely from these corrected estimates for this line. We note that the calculations of Sigut apply only at a surface gravity of 4.00 dex, a microturbulence of $5\,\mathrm{km\,s^{-1}}$ and solar metallicity and hence the extrapolation to other parameters and metallicity regimes should be treated with caution.

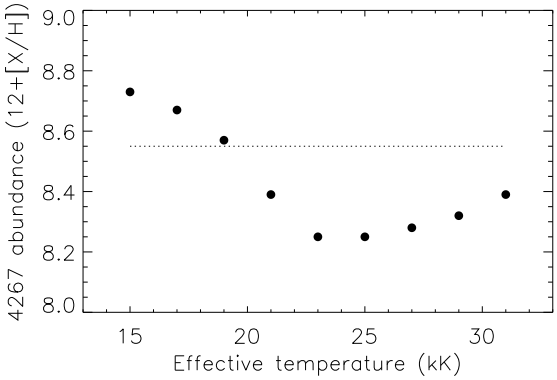

Figure 4.4: Comparison between the abundance estimated from the C II 4267Å line using the TLUSTY grid (points) and that adopted by Sigut (1996); for a gravity of 4.00 dex, microturbulence of $5\,\mathrm{km\,s^{-1}}$ at solar metallicity; dashed line). Corrections have been applied to remove the temperature dependence of the TLUSTY carbon abundances.

4.3.3 Chemical compositions

In each metallicity regime, the sample of stars is composed of objects in at least two fields or clusters (see Sect. 4.2). Papers V and VI have presented a detailed abundance analysis of the narrow-lined targets in each field and show that, within the same metallicity regime, there are no systematic differences between the abundances from each field. This is consistent with each Magellanic Cloud being homogeneously mixed and with the Galactic clusters having similar galactocentric distances (the Galaxy is known to have a metallicity gradient, see, for example, Rolleston et al. (2000). In this context we combine the targets in each metallicity regime in order to increase the sample size. In Table 4.3 the average abundances for each metallicity regime are given. These are compared to the baseline chemical compositions from H II regions and the solar composition as recently determined by Asplund et al. (2005).

Table 4.3: Mean abundances (excluding upper limits) for each metallicity region given on the scale 12+log[X/H][1]. Solar and H II region abundances are given for comparison.

Species	Solar[2]	Galaxy		LMC		SMC	
		B-stars	H II regions[3]	B-stars	H II regions[4]	B-stars	H II regions[4]
Carbon[5]	8.39	8.00±0.19 (56)	–	7.70±0.19 (132)	7.81±0.22	7.30±0.28 (81)	7.20±0.02
Nitrogen[6]	7.78	7.62±0.12 (45)	7.57±0.30	7.13±0.29 (83)	6.92±0.14	7.24±0.31 (36)	6.56±0.07
Oxygen	8.66	8.63±0.16 (54)	8.70±0.30	8.34±0.13 (133)	8.37±0.09	7.99±0.21 (80)	8.02±0.04
Magnesium	7.53	7.25±0.17 (52)		7.05±0.14 (134)		6.72±0.18 (72)	
Silicon	7.51	7.42±0.07 (56)		7.17±0.10 (135)		6.77±0.09 (88)	

[1] Values in brackets indicate the number of stars for which abundances were estimated.

[2] Asplund et al. (2005).

[3] Average of solar neighbourhood regions from Shaver et al. (1983)

[4] Kurt & Dufour (1998)

[5] The carbon abundances have been corrected, see text.

[6] Supergiants have been excluded from the mean nitrogen abundances.

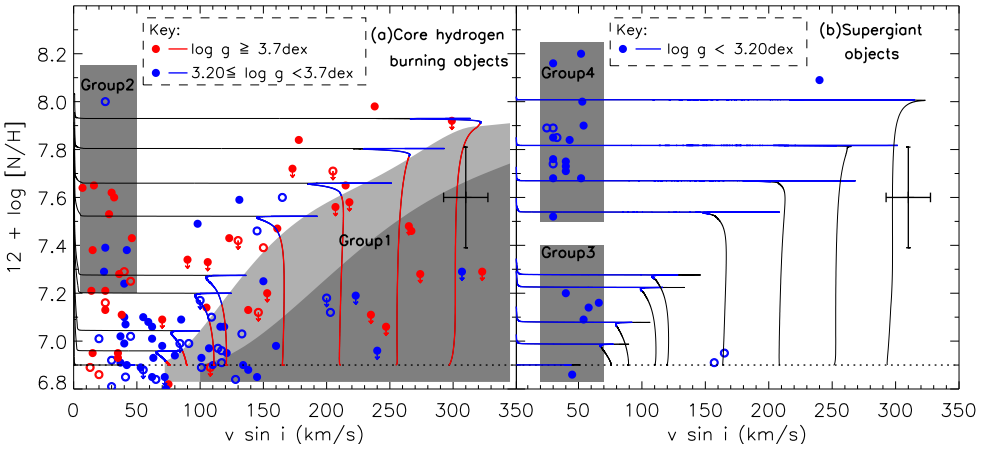

Figure 4.5: Nitrogen abundance (12+log[N/H]) as a function of projected rotational velocity for the LMC sample of stars. This plot has been taken from Paper VII. The mean error bars of the nitrogen abundances and projected rotational velocities are indicated. Core-hydrogen burning objects (a) and supergiants (b) are defined based on their surface gravity. In panel (a) the core-hydrogen burning objects are sub-divided to indicate objects in the first part or latter part of the core hydrogen burning phase, red and blue symbols respectively, approximately 70% and 30% of the main-sequence lifetime. Open symbols represent radial velocity variables. Downward arrows indicate upper limits to the nitrogen abundances. The dotted line indicates the LMC baseline nitrogen abundance as determined from H II region analyses and unmixed B-type stars (Paper V). The rotational velocity of the evolutionary models have been scaled by $\pi/4$ to take into account random angles of inclination. The individual groups of objects have been discussed in Paper VII and are summarized in the text although we have redefined the Group 1 stars (see text). The evolutionary models in (a) and (b) have initial masses of $13\,M_\odot$ and $19\,M_\odot$ respectively. We note that a minor error in the temperature scale adopted in Paper VII was discovered and hence several of the points in the figure have been corrected. However this is an effectively negligible correction as the mean nitrogen abundance and the number of stars in each group remain unchanged.

The mean oxygen abundances of the three regions are in excellent agreement with the H II region abundances. Our Galactic nitrogen abundance is also in good agreement with that from H II regions. However, the mean nitrogen abundance of the SMC from B-type stars is clearly larger than that from H II regions. The LMC nitrogen abundance from B-type stars is also greater than that from H II regions and, although these mean LMC values can be reconciled within the uncertainties, it is clear from Sect. 4.4 that there is a mix of normal and significantly enriched stars. In addition, the scatter in the stellar nitrogen abundance is larger than that for other

elements and we conclude that this is not dominated by observational scatter, but due to significant abundance differences amongst the sample stars (see Sect. 4.4).

Our Magellanic Cloud carbon abundances are in good agreement with those from H II regions implying that our correction to the carbon abundance may be reasonable. However, obtaining a Galactic H II region carbon abundance from the literature is highly problematic. For example, Dufour et al. (1982) give a value of 8.46 dex for the Orion nebula whereas Walter et al. (1992) find a range of 7.94–8.78 dex for the same region depending on the consideration of temperature fluctuations. Given the additional problem of determining accurate stellar carbon abundances it is difficult to confirm the validity of our mean Galactic carbon abundances.

4.4 Results

Chemical compositions are presented for 53 Galactic and 96 SMC stars and compared with the results for the 135 LMC stars from Paper VII. In order to investigate the role of rotational mixing, a large population of fast rotators is necessary. Our targets have projected rotational velocities up to $\sim$300 km s^{-1} and hence are well suited to such a comparison. In particular the nitrogen abundance can be used as a tracer of surface enrichments and our discussion will only consider this element. While in principle associated carbon depletions would be expected, these would be of the order of the uncertainties in our carbon abundance estimates. We adopt the baseline nitrogen abundances of the three regions from Paper V, which are based on H II regions and unenriched B-type stars. In Paper VII the distribution of the nitrogen abundances of the LMC stars as a function of their projected rotational velocity was described. In Fig. 4.5 the plot from Paper VII is shown and the principle conclusions are summarized below.

- The majority of the core-hydrogen burning stars show little nitrogen enrichment and the efficiency of rotational mixing in the evolutionary models has been constrained to fit the mean nitrogen abundance of this population. Many of the nitrogen abundances for the faster rotators are upper limits. We find that the rotational mixing models provide a reasonable fit to half of our core-hydrogen burning data-set, but is in conflict with the rest of the stars (Groups 1 and 2).

- Group 1 consists of non-enriched fast rotators, of which many are in the late stage of core-hydrogen burning (with relatively low gravity) and hence a significant nitrogen enrichment would be expected. This group has been redefined

since Paper VII. The observed sample was magnitude selected thereby excluding low mass stars close to the beginning of their core-hydrogen burning phase. We therefore should be biased against young unenriched stars, indicated by the dark shaded area of Group 1 (plotted for the mean mass of the sample, $13\,M_{\odot}$). In addition to these stars, the observed evolved stars (blue points) in the light grey region are unexpected as these stars are predicted to have higher nitrogen abundances for their rotational velocities and evolutionary state. Group 1 comprises ~30% of the non-binary sample, two thirds of which are close to the end of their core-hydrogen burning lifetime (blue points).

- The large number of significantly enriched stars in Group 2 (a further 20% of the sample) cannot be explained as fast rotators seen at low inclination angles if these are randomly distributed. The models do not predict strong rotational mixing for slowly rotating stars and in Paper VII we postulate that these may be magnetic stars, equivalent to those discussed by Morel et al. (2006, 2008). We note that we are not referring to magnetic fields produced by dynamo action Spruit (2002) which would be expected to be present in all stars, but rather fields of fossil origin (see Morel et al. 2008, and references therein). Huang & Gies (2006b) also suggest that remnant magnetic fields can account for the peculiar helium abundances of a subset of their sample.

- The supergiant objects appear to be split into two distinct groups. The stars in Group 3 (see Fig. 4.5) have enrichments consistent with the core-hydrogen burning phase — which might be expected if they are their direct descendants. However, the supergiants shown in Group 4 have highly enriched atmospheres. It is postulated that these stars have previously gone through a red supergiant phase. As discussed in Paper VII, our stellar evolution models do predict sufficient enrichment in the red supergiant phase, but the location of these Group 4 objects on the Hertzsprung-Russell diagram cannot be reproduced.

The above summary of the results presented in Paper VII assumes that selection effects in our sample do not introduce a significant observational bias. One such source of bias could be that the rapidly rotating stars will appear brighter when viewed pole on (with low projected rotational velocities) than at high inclination angles (with large projected rotational velocities). This is due to the pole caps being hotter than the equatorial regions as discussed by von Zeipel (1924). Such a bias (Maeder et al. 2009, see also) would affect the Magellanic Cloud samples (which are magnitude limited) and lead to an oversampling of rapidly rotating pole-on stars

(which would populate Group 2 discussed above) and an under-sampling of stars with large projected rotational velocities that could undergo significant nitrogen enhancement and be the precursors to the Group 4 supergiants.

We have investigated this possibility as follows. Martayan et al. (2006, 2007) estimated mean equatorial velocities for B-type stars (i.e. excluding the Be-type stars as has been done for the current sample) in the SMC and LMC ranging from approximately 120 to 160 km s^{-1} with similar values being found in Paper IV. For Galactic targets, the estimated mean values are similar (Strom et al. 2005; Huang & Gies 2006a, Paper III). For the observed B-type stellar populations discussed by Martayan et al. only 8% of their targets have projected rotational velocities of greater than 300 km s^{-1}, in both NGC 330 and NGC 2004. Additionally only two stars (out of a sample of more than 300 objects) were found with a projected rotational velocity of greater than 400 km s^{-1}. Similar results were found for the Magellanic Cloud samples considered here. We have therefore adopted a rotational velocity of 400 km s^{-1} as representative of the most rapidly rotating B-type stars and hence appropriate for investigating the possible consequences of the von Zeipel effect for our sample. We note that this velocity is consistent or larger than the values that have been assumed when modelling rotational mixing in B-type stars (see, for example Heger & Langer 2000; Meynet & Maeder 2000).

Adopting typical physical parameters for an early-B-type main sequence star ($T_{\rm eff} = 25000$ K; $M = 13\,{\rm M}_{\odot}$; $R({\rm pole}) = 5\,{\rm R}_{\odot}$) yields a ratio of the equatorial rotational velocity to the breakup velocity of $v_{\rm eq}/v({\rm crit}) = 0.6$ for $v_{\rm eq} = 400$ km/s. For this ratio we estimate the change in B magnitude between pole-on ($i = 0°$) and equator-on ($i = 90°$) views to be only 0.36 mag, using the methodology outlined by Townsend et al. (2004). This ΔB estimate has very little dependence on B spectral subtype, and hence should be representative of our entire B-type main-sequence sample.

The above example implies that there could be a bias in our sample in the sense that we would preferentially observe fast rotators at low inclination angles. However it should be noted that such objects will be intrinsically very rare for two reasons. Firstly the results of Martayan et al. (2006) and Paper IV indicate that rapidly rotating LMC B-type stars will be intrinsically rare, with those having rotational velocities greater than or equal to 400 km s^{-1} making up less than 1% of an unbiased sample of LMC targets. Additionally the Group 2 stars in Fig. 4.5 have projected rotational velocities of less than 50 km s^{-1}. Assuming that they have a unique rotational velocity of 400 km s^{-1}, the probability of observing them at such a low angle of inclination would be less than 1%; for higher rotational velocities the probability would be even smaller. Hence we estimate that for an LMC population of early B-type stars, the fraction of stars with a rotational velocity greater than or equal to 400 km s^{-1} but

observed to have a projected rotational velocity of less than $50\,\mathrm{km\,s^{-1}}$ would be of the order of one in ten thousand. It was the rareness of such objects that formed the basis of the assumption in Paper VII that most of the Group 2 stars that make up one in five of our sample must be slowly rotating.

We can estimate the amount of bias in our Group 2 sample based on the simulation discussed above. Our approach has been to exclude all stars from the Group 2 sample that lie within 0.36 magnitudes of our photometric cutoff. Hence if all Group 2 stars were rotating at $400\,\mathrm{km\,s^{-1}}$, there would be no bias with respect to similar objects observed equatorially ($i = 90°$). Exclusion of such stars reduces the LMC Group 2 sample from seventeen to thirteen stars. Given our sample size, we would expect on average approximately 0.01 Group 2 stars in our sample compared with the 13 targets found in our corrected sample. Another approach is just to assume that our Group 2 stars are fast rotators and that the von Zeipel effect is far larger than we have calculated. Then we would expect there to be a corresponding very large number of stars (of the order of 10^5) with large projected rotational velocities below our photometric cut-off. The LMC investigation of Martayan et al. (2006) went approximately two magnitudes fainter than our survey but neither in their photometry nor in their projected rotational velocity estimates is there any evidence for these objects.

We note that in our simulations, we have made a number of arbitrary assumptions, for example a single rotational velocity. However relaxing this assumption would be unlikely to change our conclusions. For example, although there would be more stars with lower rotational velocities, the von Zeipel effect would be smaller; conversely more rapid rotators would be very rare as would be the probability of observing them at low angles of inclination. In conclusion, we find that even at rotational velocities as high as $400\,\mathrm{km\,s^{-1}}$, the pole on rotators will appear brighter in the B band by less than 0.4 magnitudes, whilst only approximately one in ten thousand LMC B-type stars should have such rotational velocities with a projected rotational velocity consistent with our Group 2 sample. On the basis of these simulations, we conclude that almost all, if not all, LMC Group 2 stars must be intrinsically slow rotators.

4.4.1 Evolutionary models

As described in Paper VII stellar evolutionary models have been generated to fit the observed LMC data. Briefly, these models have been based on the code of Yoon et al. (2006) and include the effects of rotation (Heger et al. 2000) and angular momentum transport via magnetic torques (Spruit 2002). The code has been updated to include the mass-loss rates of Vink et al. (2001). The magnetically induced chemical diffusion term is not considered as it is not observationally supported (Spruit 2006). An appropriate chemical composition has been chosen, in particular with the light ele-

ments set to the observed values from Paper V. The overshooting parameter (0.335 of the pressure scale height) has been adopted to reproduce the observed trend of rotational velocities from Paper IV. The efficiency parameter for rotational mixing has been set as described in Paper VII. In summary, LMC models were calibrated to best fit the observed data set.

Further evolutionary models have been generated to represent Galactic and SMC compositions with the overshooting and rotational mixing efficiency parameters unchanged as these parameters are not predicted to be metallicity dependent. The light element composition appropriate for these metallicities has again been adopted from Paper V. The full grid of evolutionary models will be discussed in a forthcoming paper (Brott et al. in prep). Here we select models with masses appropriate for our early B-type stellar sample and which cover a range of rotational velocities suitable to make comparisons between the current theory and our observational data set.

4.4.2 Galactic stars

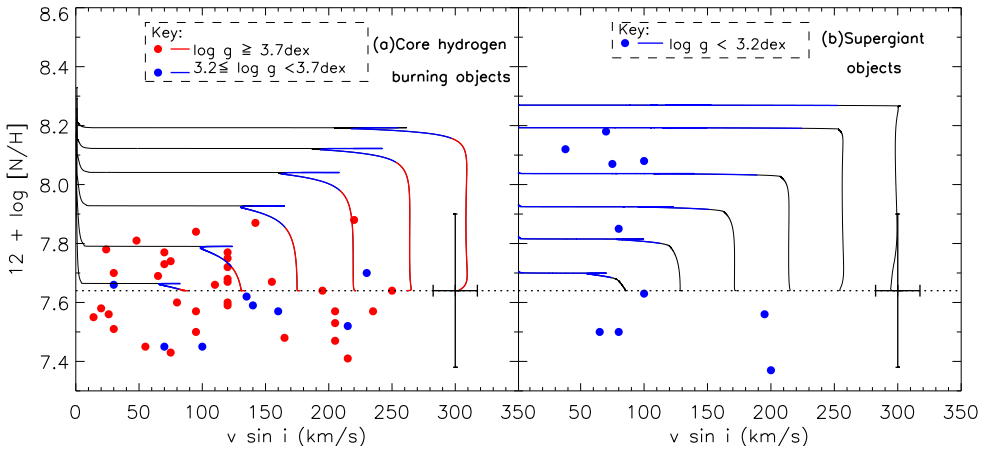

Figure 4.6: Nitrogen abundance (12+log[N/H]) as a function of projected rotational velocity for the Galactic sample of stars. Symbols are equivalent to those in Fig. 4.5. Evolutionary models are plotted for 10 and 20 $M_\odot$ in panels (a) and (b) to represent the mean mass of the two samples.

We plot the nitrogen abundances of the Galactic sample as a function of projected rotational velocity in Fig. 4.6 together with our evolutionary models. Fig. 4.6(a) shows that within the abundance uncertainties no trend of nitrogen abundance with rotational velocity is observed. The evolutionary models suggest that for stars with

initial rotational velocities of 250 km s^{-1} nitrogen abundances up to ~8.0 dex should be observed.

The lack of any significant enrichment amongst the core-hydrogen burning stars is surprising. In a population similar to our observed LMC sample we would expect some nitrogen-rich fast rotators, as — even assuming rotational mixing does not occur — those stars could then be interpreted as spun-up mass gainers in close binaries. Also, we would expect some enriched slow rotators as found in the LMC, as such stars have been identified in the Galaxy recently by Morel et al. (2006, 2008). Indeed, in the Galactic sample we have only included those stars with measurable nitrogen lines and while this introduces a bias against the fastest rotating Galactic stars, it also provides a bias towards the most enriched stars.

The lack of nitrogen-enriched stars may be due to the majority of the core-hydrogen burning stars in our sample being relatively unevolved. As rotational mixing is a continuous process, its effect will be most prominent toward core-hydrogen exhaustion. Also close binary mass transfer is expected much more frequently toward the end of hydrogen burning, since the expansion of core-hydrogen burning stars accelerates in the later stages. Finally, the process which leads to nitrogen enhancement in the slowly rotating early B-type stars is as yet unknown. That we do not find such stars here might imply that the enrichment time scale is of the order of the main sequence life time.

The hypothesis that our sample stars are relatively unevolved is supported by the fact that in Fig. 4.6(a), only eight stars have a surface gravity smaller than 3.7 dex. Note that the limiting gravity between the two classes is set the same as for the LMC core-hydrogen burners, but that the Galactic stars are more metal-rich and have larger radii (and hence lower gravities) than LMC stars of the same mass and evolutionary stage. Despite that, the LMC sample has a majority of stars with $\log g < 3.7$. It should be noted that the observations of the Magellanic Cloud samples have been selected via a magnitude cut (Paper II) which prohibits the observation of zero-age main-sequence stars at the lower masses of the sample. For the Galactic sample this magnitude cut is low enough that the unevolved main sequence stars are not excluded. Additionally there are no blue supergiants with a mass close to the mean sample mass of our core-H burning stars ($\sim 10\,M_\odot$) in our Galactic supergiant sample (Fig. 4.6b). Finally our Galactic sample is mainly composed of cluster stars whereas in the Magellanic Cloud we sample more of the field population which may contain more evolved stars.

Our sample shows seven Galactic core-hydrogen burning objects with low surface gravities (i.e. close to the end of the core-hydrogen burning phase; blue points) and nitrogen abundances lower than that predicted for their evolutionary stage. The two apparently fast rotating supergiants with low nitrogen abundances could also be

placed in this group within the uncertainty in their surface gravities. According to the models we would expect these objects to be nitrogen rich, in particular the fastest rotators. These objects may be analogous to the Group 1 stars shown in Fig. 4.5 and make up ∼20% of the core-hydrogen burning sample, although if we adopt the maximum error several objects could be reconciled with the models. While this group is smaller than that observed in the LMC sample, given the less evolved nature of our Galactic sample this is not unexpected.

In order to determine if we should observe a group of objects similar to Group 2 in Fig. 4.5(a) we have added the mean absolute enrichment of those objects to the Galactic baseline nitrogen abundance (on a logarithmic scale) and find that such a group of objects would appear to have a normal nitrogen abundance within the abundance uncertainties. However, Morel et al. (2008) find slowly rotating magnetic Galactic stars with nitrogen abundances up to 8.0 dex. In Paper VII we considered these stars to be analogous to the Group 2 stars in the LMC and linked fossil magnetic fields to chemical mixing, although the mixing mechanism is unknown. It is unclear why we do not see these stars in our Galactic sample. The Morel et al. sample contains some bias towards such stars and this bias is not present in our Galactic data set. Additionally our Galactic sample is predominantly composed of cluster stars whereas field stars dominate the Magellanic Cloud samples. Wolff et al. (2007) have provided evidence that cluster stars rotate significantly faster than field stars, which is why our Galactic sample contains fewer slower rotators than our Magellanic Cloud samples (see Fig. 4.2). They relate this to differences in the star formation process between cluster and field stars.

We also find some evidence for a difference between field and cluster stars in our LMC sample. The LMC targets lie towards the clusters NGC 2004 and N 11. In the former case almost our entire sample lies beyond the cluster radius and hence is probably a field star population, whereas for N 11 our stars are taken from across the association and the field. While ∼65% of our LMC sample of core-hydrogen burning non-binary stars is taken from the NGC 2004 targets, 80% of the Group 2 stars are from the field of NGC 2004. This may indicate that the Group 2 stars are more likely to occur in the field population and hence explain the lack of such stars in our Galactic cluster sample. However, the significance of the lack of highly mixed slowly rotating core hydrogen burning stars cannot be truly tested.

Figure 4.6(b) suggests that there are two groups of supergiants with different degrees of nitrogen enrichment, in agreement with the situation in the LMC sample, Fig. 4.5(b), although the number of stars in the Galactic sample is limited. Given that no core-hydrogen burning Galactic objects are observed with nitrogen abundance consistent with the highly enriched supergiants, it appears unlikely that these objects have evolved directly from such a phase and hence they should not be used to con-

strain the models of core-hydrogen burning stars. The supergiant sample is further discussed in Sect. 4.4.4.

4.4.3 SMC stars

In Fig. 4.7 we plot the nitrogen abundance as a function of projected rotational velocity for the SMC sample of stars. From the upper panel there appears to be a strong correlation between these two quantities, as would be expected from the theory of rotational mixing. However, for the majority of stars with rotational velocities greater than $100\,\mathrm{km\,s^{-1}}$ only upper limits to the nitrogen abundances have been estimated and such a limit will be correlated with the projected rotational velocity leading to the apparent trend. If we remove these upper limits (lower panel) this correlation disappears. The lack of absolute nitrogen abundances for these fast rotators prevents the observation of a group of stars similar to the Group 1 stars of Fig. 4.5(a). We note that although the estimation of upper limits to the nitrogen abundance is not metallicity dependent, our SMC data is of lower quality (Sect. 4.2) and hence higher upper limits are derived, particularly for the fastest rotators.

A comparison between Fig. 4.7(a) and Fig. 4.5(a) shows that while the majority of the LMC stars have undergone little or no enrichment, many stars in the SMC appear to be significantly enriched. Our mean SMC nitrogen abundance is actually higher than that of the LMC despite the SMC having a lower baseline abundance. However, given that nitrogen lines can only be observed for abundances greater than approximately 6.9 dex for even a moderately rotating star, it is difficult to test the significance of this observation and it should be noted that the mean values are consistent within the uncertainties. Nevertheless, we find 30 of our 70 non-binary core-hydrogen burning stars (excluding upper limits) have such high estimates that, even adopting an average error bar of ± 0.26 dex, they have nitrogen abundances that are inconsistent with the core-hydrogen burning regime of the stellar evolution tracks in Fig. 4.7(a). This is obviously a lower limit as stars with upper limits to their nitrogen abundances could also populate this group if their abundances are indeed higher than the model predictions.

The mean nitrogen abundance of the SMC sample is 7.24 dex and to reproduce this abundance evolutionary tracks with an initial rotational velocity of $\sim 200\,\mathrm{km\,s^{-1}}$ are required. The probabilities of a star rotating at $200\,\mathrm{km\,s^{-1}}$ appearing to have projected rotational velocities of less than 100 and $50\,\mathrm{km\,s^{-1}}$ are 13% and 3% respectively. We observe 19 and 12 stars with such projected rotational velocities but with nitrogen abundances consistent, within their uncertainties, with a $200\,\mathrm{km\,s^{-1}}$ evolutionary track. It is therefore statistically very unlikely that these groups are populated by fast rotators with low angles of inclination. For example, in order to have 12 stars

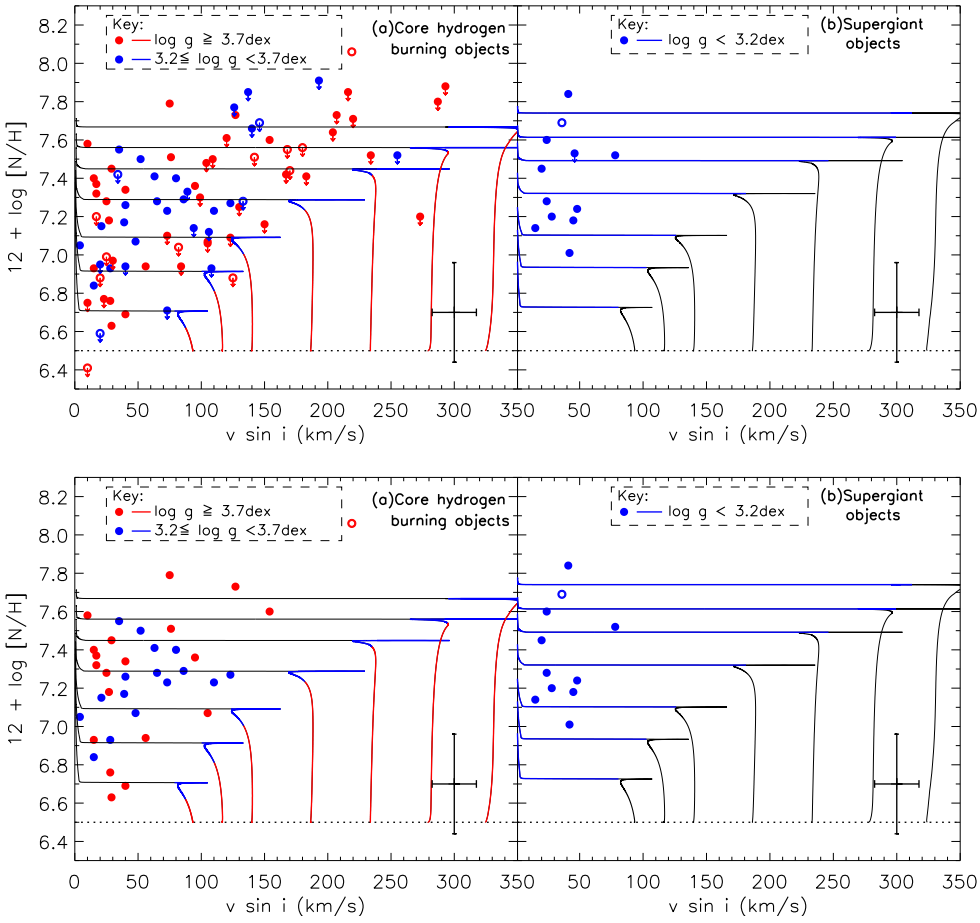

Figure 4.7: Nitrogen abundance (12+log[N/H]) as a function of projected rotational velocity for the SMC sample of stars. Symbols are equivalent to those in Fig. 4.5. The lower panel is equivalent to the upper panel except that upper limits to the nitrogen abundances have been removed. Evolutionary models are plotted for 12 and 13 $M_{\odot}$ in panels (a) and (b).

rotating at 200 km s^{-1} and appearing with rotational velocities of less than 50 km s^{-1} a population of 400 stars would be required with ~260 of these having projected rotational velocities in the range 150-200 km s^{-1}. Such a population clearly does not exist in the upper panel of Fig.4.7 and, although Be-type stars are excluded, there is no bias against normal B-type stars with these velocities. We can therefore conclude that the enriched stars with low projected rotational velocities have intrinsically low

rotational velocities. This is clearly in conflict with the theory of rotational mixing and these stars may be analogous to the LMC stars designated as Group 2 in Fig. 4.5.

There appears to be a gap between the Group 2 stars in the LMC (Fig. 4.5a) and higher velocity stars. Such a gap is not clear in the SMC sample. The significance of this gap is unknown, but if it is real it implies that, whatever the process that is enriching the Group 2 stars, it is efficient at higher velocities in the SMC sample. Alternatively the sample may be populated by two mixing processes, the first being that producing the LMC Group 2 stars while the latter process mixes all the SMC stars to a similar nitrogen abundance. Indeed, it should be noted that the majority of the Group 2 LMC stars are high gravity stars and the same holds true for the analogous sample in the SMC (e.g. projected rotational velocities of less than $50\,\mathrm{km\,s^{-1}}$ and nitrogen abundances greater than 7.2 dex), which is also dominated by a large population of high gravity stars.

Our sample could again be biased by the von Zeipel effect (von Zeipel 1924). To estimate the degree of bias, we have again considered an object with an equatorial rotational velocity of $400\,\mathrm{km\,s^{-1}}$. As discussed above the Group 2 objects are less clearly defined in the SMC sample. However adopting the criteria of a logarithmic surface gravity greater than $\geq$3.2 dex, projected rotational velocity of $\leq$50 $\mathrm{km\,s^{-1}}$ and a nitrogen abundance of $\geq$7.2 dex (corresponding to a nitrogen enhancement of more than 0.6 dex), we find 11 stars. Removing those within 0.36 magnitudes of our B-band magnitude cut-off reduces the sample size to 8 stars. SMC B-type stars have intrinsically larger rotational velocities than their LMC or Galactic counterparts (Martayan et al. 2007, Paper IV) and we would expect approximately 3% to have values of $400\,\mathrm{km\,s^{-1}}$ or more. Again less than 1% of them will have an inclination angle leading to a projected rotational velocity of $\leq$50 $\mathrm{km\,s^{-1}}$. Hence we would expect that approximately one in four thousand SMC B-type stars would have a rotational velocity of $\geq$400 $\mathrm{km\,s^{-1}}$ and a projected rotational velocity of $\leq$50 $\mathrm{km\,s^{-1}}$. In turn, for our SMC sample size, we would then expect on average 0.02 such stars to lie in the same region as the Group 2 LMC stars.

Alternatively, if we assume that all our Group 2 sample are rapidly rotating, we would expect a corresponding population of approximately 30 000 rapidly rotating stars with larger inclination angles. Martayan et al. (2007) study of the SMC cluster NGC 330 goes approximately two magnitudes fainter than our sample and again there is no evidence for this population. Hence we conclude that at least several (and probably most, or all) of the nitrogen-enhanced SMC targets with low projected rotational velocities must be intrinsically slow rotators.

In both Fig. 4.5(b) and Fig. 4.6(b) the supergiant sample consisted of two groups of objects, one mildly enriched (or unenriched) group consistent with the core-hydrogen burning stars and a highly enriched group. This is not observed in the SMC

sample (Fig. 4.7b). However, given that almost all the stars in the core-hydrogen burning sample are significantly enriched, in contrast to the Galactic and LMC samples, this might mask such a distribution. Although the mass of the SMC supergiants ($\sim$13 $M_\odot$) is lower than that of the Galaxy and LMC samples ($\sim$20 $M_\odot$) the correlation of nitrogen abundance with mass is expected to be small (compare evolutionary tracks in Fig. 4.5 a and b) and none is observed in the LMC sample of stars which cover a wide range of masses.

Nevertheless there are a number of supergiant objects with nitrogen abundances greater than 7.6 dex, which is higher than the nitrogen abundance generally observed during the core hydrogen burning phase, indicating that part of the mixing in these supergiants may occur after the hydrogen burning phase.

4.4.4 Supergiants

As discussed above, the supergiants typically show two groups, one highly enriched group and one less enriched (or normal) group, although the effect is less obvious in the SMC sample. In Fig. 4.8 the nitrogen abundance is plotted against the surface gravity (evolutionary status) for each of the three metallicity regimes. It is clear that the lowest gravity supergiants have the highest nitrogen abundances at all metallicities.

As discussed in Paper VII and illustrated in Fig. 4.8, the amount of surface nitrogen enrichment that is obtained during the first dredge-up phase can reasonably reproduce the observed nitrogen abundances of the enriched supergiants in the LMC. This suggests that some of our blue supergiants have previously evolved through a red supergiant stage, with their surfaces enriched through dredge-up. Given that there is little predicted trend with mass and velocity (less than 0.3 dex) for the amount of enrichment during this red supergiant stage, this would imply that all stars which have gone through such a phase should have similar nitrogen abundances regardless of their initial parameters while stars which have not gone through this phase would have lower abundances. Such bimodal distributions are clear in the Galactic and LMC samples. The expected nitrogen enrichment from dredge-up is in excellent agreement with the LMC observations and, while it is slightly higher than our Galactic observations, within the uncertainties it is consistent. The models predict that the nitrogen enrichment from dredge-up in the SMC sample is not significantly greater than that observed for the majority of our core-hydrogen burning sample and hence a bi-modal distribution would not be easily observed. The predicted nitrogen abundance after first dredge-up is lower than that observed for the most enriched SMC supergiants but again, within the uncertainties, the hypothesis that the most enriched supergiants have gone through a red supergiant phase is not unreasonable.

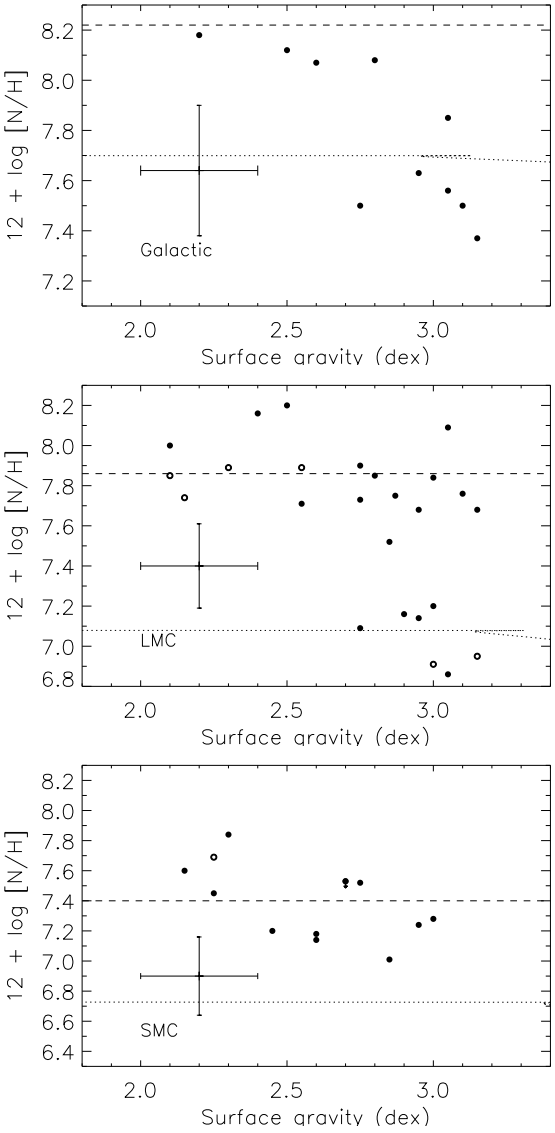

Figure 4.8: Nitrogen abundances of the supergiants in each region. Open symbols represent radial velocity variables. Error bars represent the mean uncertainty in the nitrogen abundance for each of the samples and an uncertainty of 0.2 dex in surface gravity. The dotted line represents the evolutionary track for a model at the mean mass of the sample and a moderate rotational velocity (100 km s^{-1}) although as the main-sequence rotational velocity of these stars is unknown it is not possible to make a detailed comparison with the models. The dashed line represents the nitrogen abundances achieved during the first dredge-up for the same models, although it should be noted that the models do not predict a return to the temperatures and gravities representative for our observations.

However, in order for our enriched supergiants to be explained by such a process it would be necessary for those stars to return to hotter temperatures to allow us to observe them in the blue supergiant stage on a Hertzsprung-Russell diagram. Such a blue-loop was, for example, proposed as the mechanism to explain the progenitor of SN1987A. Whilst these loops are not predicted by our evolutionary models, those in the Geneva models (see, for example Maeder & Meynet 2001) do not extend to high enough masses or to hot enough temperatures to reproduce our observations. If the single star nature of these supergiants can be observationally confirmed it is clear that more extensive blue loops need to be predicted by the evolutionary models. Indeed, such a scenario may also help to bring the expected and observed number of blue supergiants into better agreement (Paper IV).

Venn & Przybilla (2003), a re-analysis of previous work, Venn (1999) have presented similar nitrogen abundances for A-F type supergiants in the Galaxy and SMC and drawn similar conclusions to those presented above.

4.5 Conclusions

Chemical compositions are presented for ∼50 Galactic and ∼100 SMC early B-type stars which cover a broad range of rotational velocities and complement previously published results for ∼130 LMC stars of similar spectral types for which new observationally constrained evolutionary models had been generated. We compare our new observational data sets with the LMC results.

4.5.1 Core-hydrogen burning objects

In both the Magellanic Cloud populations we find a significant excess of slowly rotating nitrogen enriched stars that cannot be explained within the context of rotational mixing, at least for a random distribution of inclination angles; ∼20% in the LMC and ∼40% in the SMC. In the Galactic sample of the FLAMES survey, such stars are not found, although they are present in other Galactic samples (Morel et al. 2006, 2008). While this may be attributed to the early evolutionary stage of the majority of the FLAMES Galactic stars, it would constrain the time scale of the enrichment process for this group — the physics of which is unknown — to be comparable to the main-sequence lifetime.

The LMC sample contains a significant group of stars which are rapidly rotating, but show no significant nitrogen enhancement. Due to the magnitude cut used in our target selection, the zero-age main-sequence is not well sampled at low mass. Hence if only single stars are considered and rotational mixing is assumed to be valid, such nitrogen normal rapid rotators are not predicted by rotational mixing models. A

significant fraction of these stars have gravities that imply that they are close to the end of the core-hydrogen burning phase. The Galactic sample also reveals several fast rotating low gravity stars although they constitute a smaller fraction probably due to the less evolved nature of the Galactic sample. In the SMC, the rather high upper limits on nitrogen abundances for rapid rotators does not allow for their identification.

Finally, the LMC sample contains about 20% of stars which are rather rapidly rotating and nitrogen enriched. Those stars could either be rotationally mixed single stars (Maeder et al. 2009; Brott et al. 2009) if the non-enriched rapid rotators are *all* binary products), or the spun-up mass gainer in mass transfer binaries (Langer et al. 2008). While some such stars may be contained in the SMC sample, they are not found in our Galactic sample. This may be due to the rather unevolved nature of this sample although it should be noted that our Galactic sample contains fewer slow rotators compared to the Magellanic Cloud sample.

The differences in data quality and mean evolutionary state of the samples do not allow clear trends in relative numbers of the various groups of core-hydrogen burning stars to be obtained for each metallicity regime.

4.5.2 Supergiants

In all three metallicity regimes a population of highly enriched supergiant objects have been observed, which are unlikely to be the direct descendants of rotationally mixed core-hydrogen burning stars. The predicted amount of nitrogen after first dredge up reasonably reproduces their nitrogen abundances. However, the position of these stars in the Hertzsprung-Russell diagram cannot be reproduced by our evolutionary models and, if the single star nature of these objects can be confirmed, argues for the occurrence of blue loops at hotter temperatures and higher masses than currently predicted.

In summary we find that both the Galactic and SMC samples support the conclusions made in Paper VII. It should also be noted that we find no evidence for an excess of binary systems in the groups of objects that are in conflict with the rotating single star models although our observations do not allow for complete binary identification. Our results imply that a new nitrogen enrichment process (or processes) other than rotational mixing must be important in massive star evolution. Furthermore, close binary effects may be needed to understand the rapid rotators. Whether rotational mixing is required to understand our results remains an open question at this time, but can be answered by a rigourous study of the binary fraction in those groups of stars which appear to contradict the theory.

Acknowledgements We are grateful to staff from the European Southern Observatory for assistance in obtaining the data. This work, conducted as part of the award 'Understanding the lives of massive stars from birth to supernovae' (SJS) made under the European Heads of Research Councils and European Science Foundation EURYI (European Young Investigator) Awards scheme, was supported by funds from the Participating Organisations of EURYI and the EC Sixth Framework Programme. SJS also acknowledges the Leverhulme Trust. Additionally we acknowledge financial support from STFC (UK Science and Technology Facilities Council), NWO (Netherlands Science Foundation) and DEL (Department of Education and Learning in Northern Ireland).

Appendix

Figure 4.1 and Tables 4.1 and 4.2 are only available in the published online version of this article (published in Astronomy & Astropysics, 2009, 496, 841- 853)

CHAPTER 5

Rotating Massive Main-Sequence Stars II: Simulating a Population of LMC early B-type Stars as a Test of Rotational Mixing

I. Brott, C.J. Evans, I. Hunter, A. de Koter, N. Langer, P.L. Dufton, M. Cantiello, C. Trundle, D.J. Lennon, S.E. de Mink, S.-C. Yoon and P. Anders

Submitted to Astronomy & Astrophysics

Abstract Rotational mixing in massive stars is a widely applied concept, with far reaching consequences for stellar evolution, nucleosynthesis, and stellar explosions. Nitrogen surface abundances for a large and homogeneous sample of massive B-type stars in the Large Magellanic Cloud (LMC) were recently obtained by the ESO VLT-FLAMES Survey of Massive Stars. This sample is the first covering a broad range of projected stellar rotational velocities, with a large enough sample of high quality data to allow for a statistically significant analysis. Here we use the sample to provide the first rigorous and quantitative test of the theory of rotational mixing in massive stars. We have calculated a grid of stellar evolution models, using the VLT-FLAMES sample to calibrate some of the uncertain mixing processes. We developed a new population-synthesis code, which uses this grid to simulate a large population of stars with masses, ages and rotational velocity distributions consistent with those from the VLT-FLAMES sample. The synthesized population is then filtered by the selection effects in the observed sample, to enable a direct comparison between the empirical results and theoretical predictions. Our simulations reproduce the fraction of stars

without significant nitrogen enrichment. However, the predicted number of rapid rotators with enhanced nitrogen is about twice as large as found observationally. Furthermore, two groups of stars (one consisting of slowly rotating, nitrogen-enriched objects and another consisting of rapidly rotating un-enriched objects) can not be reproduced by our single-star population synthesis. Physical processes in addition to rotational mixing appear to be required to understand the population of massive main-sequence stars from the VLT-FLAMES sample. We discuss the possible role of binary stars and magnetic fields in the interpretation of our results. We find that the population of slowly rotating nitrogen-enriched stars is unlikely produced via mass transfer and subsequent tidal spin-down in close binary systems. A conclusive assessment of the role of rotational mixing in massive stars requires a quantitative analysis that also accounts for the effects of binarity and magnetic fields.

5.1 Introduction

Observations of chemically enriched main-sequence stars (e.g. Gies & Lambert 1992; Herrero 1993; Vrancken et al. 2000; Przybilla et al. 2010) have fostered the idea that rotationally induced mixing may bring fusion products from the core of massive stars to their surface during core hydrogen burning. While the potential consequences of rotational mixing for the evolution of massive stars have been shown to be dramatic (Maeder 2000; Yoon & Langer 2005), direct tests of the models have proven to be difficult. A major obstacle of such tests is that observations have typically been restricted to stars that have low projected rotation rates, to minimize any rotational broadening of the stellar absorption lines. However, the often small sample size has allowed the speculation that nitrogen enriched stars might be rapid rotators viewed nearly pole-on. Since the range of observed enrichments was consistent with evolutionary predictions of rapidly rotating stars, this was considered as a confirmation of rotational mixing in massive stars (Heger & Langer 2000; Meynet & Maeder 2000).

It was only in the framework of the ESO VLT-FLAMES Survey of Massive Stars (Evans et al. 2005) that nitrogen abundances were determined for massive main-sequence stars with a wide range of projected rotation rates (Hunter et al. 2007; Trundle et al. 2007). Further analysis of the early B-type stars in the Large Magellanic Cloud (LMC) from this survey revealed the existence of a significant population of nitrogen enhanced stars with *intrinsically* slow rotation (Hunter et al. 2008a). The findings of Morel et al. (2006) argue for a similar population in our Galaxy. The origin of the nitrogen enhancement in these stars is not understood, but, since they are slow rotators, it seems doubtful that rotational mixing can explain it. It is therefore conceivable that samples of enriched stars, with apparently slow rotation velocities

(which substantiated the most convincing direct evidence for rotational mixing in massive main-sequence stars over the past decades), may instead be related to completely different physical processes – e.g. binarity (Langer et al. 2008) or magnetic fields (Morel et al. 2008). In this context, it is worth noting that a wealth of atmospheric and wind properties of massive main-sequence stars are yet to be understood, such as the winds of massive stars with luminosities below $\sim 10^{5.2}\,L_{\odot}$ (e.g Bouret et al. 2003; Martins et al. 2004, 2005; Mokiem et al. 2007; Puls et al. 2008), intermittent discrete absorption components in UV absorption lines (Prinja & Howarth 1988; Kaper et al. 1997), micro- and macro-turbulence (Cantiello et al. 2009; Aerts et al. 2009), and non-thermal X-ray emission (Babel & Montmerle 1997; ud-Doula & Owocki 2002).

Putting the problem of the enriched slow rotators aside, both Hunter et al. (2008a) and Maeder et al. (2009) suggested that the majority of the newly discovered population of rapidly rotating, nitrogen enhanced main-sequence stars in the VLT-FLAMES survey may agree with the predictions of rotational mixing. However, their results remain ambiguous, as the existence of a population of rapidly rotating, nitrogen enriched, apparently single stars is also a prime prediction of close binary evolution models accounting for rotation (Petrovic et al. 2005a; Langer et al. 2008), which is independent of the mechanism of rotational mixing.

In this context, a quantitative effort to reproduce the physical properties of the LMC B-type sample from the VLT-FLAMES survey (see Sec. 5.2) using stellar evolution models for single stars which allow for the effects of rotational mixing, is a logical next step. A future step will be to also account for binary evolution. To achieve the present aim, we use a dense grid of stellar evolution models for main-sequence stars (Brott et al. 2010a, Paper I), for which the initial abundances, convective core overshooting, and rotational mixing were calibrated using the results from the VLT-FLAMES survey. These models are then incorporated in a newly developed population-synthesis code (Sec. 5.3), which we employ in an attempt to reproduce the properties of the LMC sample of B-type stars from the VLT-FLAMES survey. The observed sample is briefly discussed in Sec. 5.2. Our results are described in Sec. 5.4. We draw our conclusions in Sec. 5.5.

5.2 Observational sample

To investigate the predictions of rotational mixing, in this paper we focus on population synthesis of the 107 main-sequence B-type stars in the LMC discussed by Hunter et al. (2008a, 2009a). These were taken from the VLT-FLAMES observations in the two LMC fields – N11 and NGC 2004 (Evans et al. 2006). N11 is the sec-

ond largest H II region in the LMC, with multiple clumps of star formation in which the VLT-FLAMES observations sample a range of stellar ages and spatial structures. NGC 2004 is an older, fairly condensed cluster, in which the targets were mostly in the outer region (the core is too densely populated for the FLAMES-Medusa fibres) and out into the surrounding field population. A total of 225 O- and early B-type stars were observed with VLT-FLAMES in the two LMC pointings.

To constrain our synthesis models we need to understand the selection effects which influenced the original observed sample and the sub-sample considered by Hunter et al. (2008a). The most significant factor in the observed sample was the faint cut-off ($V \leq 15.5^{\rm m}$, to ensure sufficient signal-to-noise in the final spectra), combined with functional issues such as crowding of potential targets.

In the NGC 2004 field we note that, contrary to the statement by Evans et al. (2006), some of the Be-type stars identified by Keller et al. (1999) were actually hardwired out of the input catalogue used for target selection. This could potentially bias the final distribution of Be- relative to B-type stars in this field. However, given the magnitude (and color) constraints on targets, only 18 such stars would have been included in our catalogue of potential targets. Hunter et al. (2008b) investigated the potential for similar selection effects in NGC 330 (in the SMC) using the Fibre Positioner Observation Support Software (FPOSS) with the inclusion of previously excluded stars. We have adopted a similar method for NGC 2004, running FPOSS ten times to compare the resulting configurations. Of the previously excluded stars from Keller et al. (1999), six stars were included in the resulting fibre configuration in two of the test runs, seven stars were included in six of the tests, and eight stars were included in the remaining two tests. Of course, by including some of these previously excluded stars, a corresponding number of the stars actually observed would not have been included, some of which might well be Be-type stars (18 of the 116 stars observed with the Medusa fibres in NGC 2004 are Be-type, i.e. 15%). There may be a weak selection effect relating to the observed sample of Be-type stars, but we believe that this does not unduly bias the overall sample in NGC 2004 – other effects such as the spatial distribution of targets and the magnitude/color cuts would have been more significant. In short, the survey provided a relatively unbiased sample of the bright ($V \leq 15.5^{\rm m}$) main-sequence stars in the observed regions.

5.2.1 Stellar parameters

Physical properties of the LMC B-type stars were determined in a series of papers. The stellar parameters used in our LMC population synthesis (N11 and NGC 2004) are those from Hunter et al. (2008b), which incorporated results for narrow-lined B-

type stars from Hunter et al. (2007) and Trundle et al. (2007), (and for O-type stars from Mokiem et al. 2006).

Physical parameters and abundances for the B-type stars were obtained using the grid of non-LTE model atmospheres described by Dufton et al. (2005), calculated using the TLUSTY code (Hubeny & Lanz 1995). Effective temperatures were estimated from the silicon or helium spectrum, while in those stars where adequate spectral diagnostics were not available, temperatures were adopted on the basis of their spectral classifications using the calibration from Trundle et al. (2007). Surface gravities ($\log g$) were deduced from the hydrogen line profiles. Projected rotational velocities ($v \sin i$) were determined using the profile-fitting methods of Dufton et al. (2006), i.e. using the helium lines (primarily He I at λ4026 Å) in the majority of stars and using metal lines (such as Mg II, Si III) at low $v \sin i$. Surface abundances of C, N, O, Mg, and Si were also determined where possible (Trundle et al. 2007; Hunter et al. 2007, 2008a,b, 2009a).

Results for 107 main-sequence B-type stars were given by Hunter et al. (2009a). From the original sample of 225 O- and early B-type stars: 41 were O-type; 1 was a W-R star; 24 were Be-type (for which N abundances were not determined); 23 additional B-type stars were not analyzed due to doubled-lined binarity, 'shell-like' emission, and low-quality spectra; 29 stars have $\log g < 3.2$. Note however that the observations of the VLT-Flames survey were not optimized for detection of binaries, so some almost certainly remain undetected. In Appendix Awe provide mass and velocity distributions of the observational sample. We refer to Sec. 5.3.3 for a description of how the selection effects are applied to the population synthesis model.

5.3 Stellar models and population synthesis

We have developed the population synthesis code STARMAKER to study the statistical properties of early-type stars for a specified initial rotational velocity, initial mass function (IMF), and given star formation history (SFH). This method can be applied to quantitatively constrain the effects of rotation (and mass loss) on stellar evolution if the dataset to which its results are compared is sufficiently large to provide good sampling of the (random) orientation of rotation axes, and of the velocity and age distribution. On a given grid of stellar evolution models, STARMAKER interpolates model stars of a specified initial mass, age and initial rotational velocity within the grid. In addition to the main stellar parameters (effective temperature, luminosity, radius and surface gravity), the following quantities are also obtained: mass-loss rate, current rotational velocity, current stellar mass, and surface abundances (He, B, C, N, O, Ne, Na, Si). For the simulation presented in this paper, we use the LMC stellar

evolution grid presented in Paper I as input for our population synthesis models. In Sec. 5.3.1 we discuss the implementation method applied, and justify the initial distributions in Sec. 5.3.2. The selection effects applied to both the observed and modeled population are reviewed in Sec. 5.3.3. Note that some aspects of this selection effects are linked to the discussion in Sec. 5.3.2. Sec. 5.3.4 and 5.3.5 discuss stellar evolution models and rotational mixing.

5.3.1 Population synthesis

STARMAKER simulates a prescribed number of stars, with initial mass ($M_{\rm i}$), initial rotational velocity ($v_{\rm ZAMS}$), and age (t) drawn from the corresponding distribution function (IMF, initial distribution of rotational velocities, and SFH). For a given initial triplet ($M_{\rm i}$, $v_{\rm ZAMS}$, and t), four evolutionary sequences from the grid of stellar evolution calculations are selected, and then used to interpolate the stellar parameters using a 3D linear interpolation algorithm.

For a given $M_{\rm i}$ and $v_{\rm ZAMS}$, the interpolation routine first determines the two closest masses above and below $M_{\rm i}$ in the model grid. Then, for each of the two, it chooses the two models with $v_{\rm ZAMS}$ closest to the required value (Fig. 5.1). We found that the algorithm works best when the four selected model sequences form two pairs with equal masses. For example, to interpolate an $18\,{\rm M}_\odot$ model, two $16\,{\rm M}_\odot$ and two $19\,{\rm M}_\odot$ models enter the interpolation. An interpolated track is show in Fig. 5.1 (bottom). Initial masses and initial velocities may be irregularly spaced in the model grid, but for every new mass introduced into the model grid, models of several rotational velocities are required to cover the $v_{\rm ZAMS}$-parameter space considered in the simulation.

As indicated by the arrows in Fig. 5.1, we first interpolate models of equal mass to obtain models with the desired initial velocity, and then we interpolate in mass. We tested our result by changing the interpolation order, and found no significant differences. Adopting the nearest neighbors for interpolation **, i.e the smallest distance** $\sqrt{(\Delta M)^2 + (\Delta v_{\rm ZAMS})^2}$, would often result in selecting models of three or four different initial masses due to the domination of the velocity term in the distance equation (models marked by a triangle in Fig. 5.1). We found this could lead to unsatisfactory results.

Stars with different initial masses and rotation velocities achieve different main-sequence lifetimes. To facilitate the interpolation in time, we use the fractional main-sequence lifetime as the interpolation variable. For all models in the grid their MS-lifetimes have been tabulated so that, for any pair ($M_{\rm i}$, $v_{\rm ZAMS}$), the expected MS-lifetime can be interpolated. To ensure a smooth behavior of isochrones in the HR diagram we fit the MS-lifetime for each initial mass as function of $v_{\rm ZAMS}$ with a

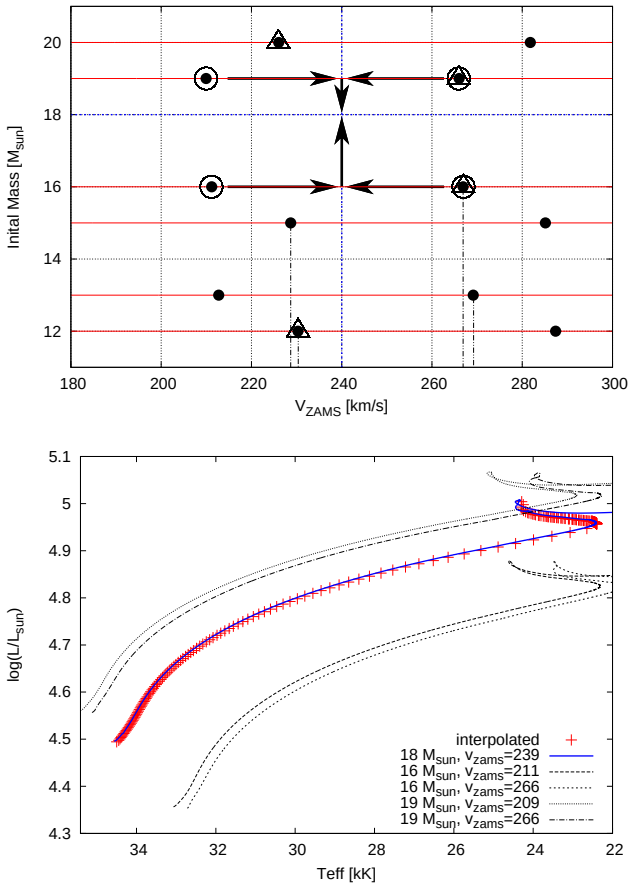

Figure 5.1: Top: Illustration of the interpolation procedure of STARMAKER in the $v_{\rm ZAMS} - {\rm m_i}$ plane. Individual model sequences are indicated by filled circles. Red lines indicate lines of constant mass. In this example, the properties of a star with initial mass $M_{\rm i} = 18\,{\rm M}_\odot$ and initial velocity $v_{\rm ZAMS} = 240$ km/s are determined through interpolation (the intersection of the blue dashed lines). STARMAKER chooses the circled models when interpolating. Models marked by triangles would be chosen if the nearest neighbor method was used. Black arrows indicate the sequence of the interpolation, as described in the text. Dashed lines are intended as guide to the eye to distinguish models of similar velocity. Bottom: Interpolated track (red crosses), resulting from the example given above. The over plotted full blue line shows the model calculated with our stellar evolution code. The four black lines show the evolutionary tracks from which the model has been interpolated.

polynomial, and add a linear fit for masses where quasi-chemically homogeneous evolution is achieved for the largest rotational velocities (Fig. 5.2). The increase in the MS-lifetime for larger rotational velocity is due to rotational mixing of hydrogen into the convective core. This effect saturates when the rotational mixing timescale becomes shorter than the main sequence timescale. At this point the star becomes quasi-chemically homogeneous (e.g. Maeder 1987; Yoon & Langer 2005), implying its interior is well mixed and the star can burn basically all the fuel it contains.

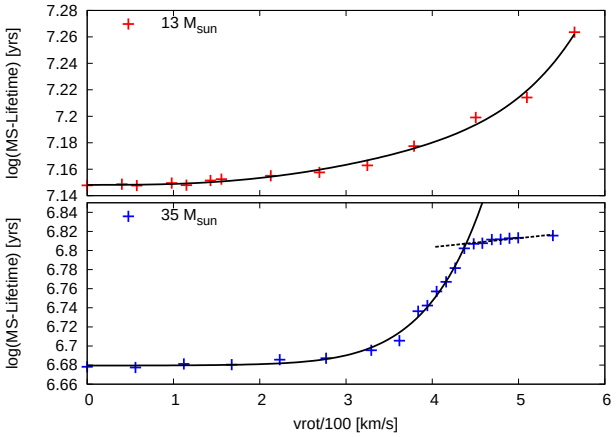

Figure 5.2: The logarithm of the MS lifetime is plotted against the ZAMS rotational velocity for our $13\,M_\odot$ (top) and $35\,M_\odot$ (bottom) sequences. In black we show the polynomial fit to the model data. The bottom panel shows also the linear part (dashed line) used to fit the models evolving quasi-chemically homogeneously.

Any observable can now be interpolated using the four model sequences used for interpolation (Fig. 5.1). As each model sequence is highly resolved in time (with several thousand time steps for the main sequence evolution), the interpolation error in time is negligible.

5.3.2 Initial distribution functions

In our population synthesis we draw the three initial parameters (M_i, v_ZAMS, and t), from the initial distribution functions, which are discussed below. We also adopt an inclination angle for the star, assuming random orientation in space.

Star formation history

We have used our population synthesis code to generate isochrones for non-rotating stars with ages between 0 and 30 Myrs from our stellar evolution grid (see Paper I). In order to evaluate the appropriate star formation history for our population synthesis model, we compare those isochrones with the distribution of the stars of our observational sample in Fig. 5.3.

The N11 region (blue symbols) contains a number of stars with ages younger than ~5 Myr. These are primarily the massive O-type stars, associated with the recent star formation in, e.g. LH 10. Both fields contain older populations with ages in the range of 5 to 25 Myr, and with no obvious preference for a particular age (Fig. 5.3). Given that we do not include the O-type stars in our analysis (see Sec. 5.3.3), we therefore adopt continuous star formation as a good approximation of the observed lower-mass population in our population synthesis models.

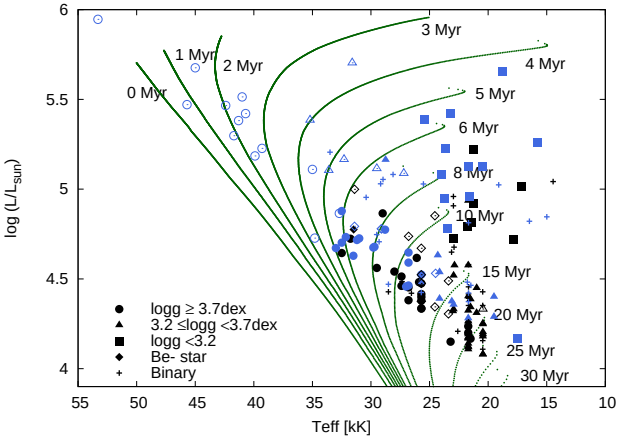

Figure 5.3: Isochrones generated from our non-rotating evolutionary models, compared to the location of stars of our sample, in the H-R diagram. Stars for which nitrogen abundances are available are shown with filled symbols, while we used empty symbols for those for which this is not the case. Black and blue symbols show data from NGC 2004 and N11, respectively.

Initial mass function

As input for our population synthesis we adopted a Salpeter (1955) IMF. The masses are randomly picked from the IMF in the range between 7 and 60 $M_{\odot}$, and the result is plotted in Fig. 5.4 (green, solid line). The present day mass function (PDMF) of our

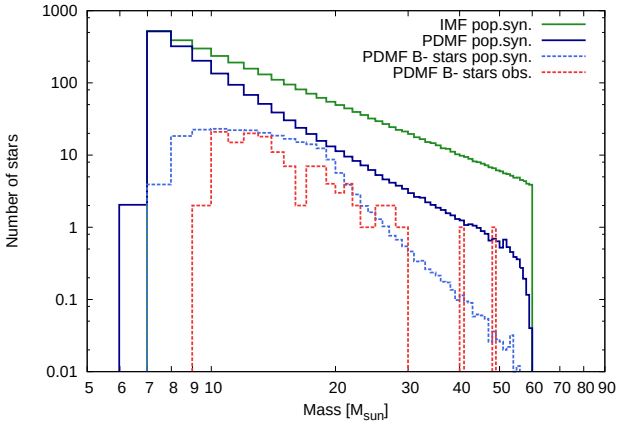

Figure 5.4: Mass functions from the observed sample and our population synthesis simulation. The input initial mass function (IMF) used in the population synthesis is shown in green. The blue solid line represents the present day mass function (PDMF) of all stars in the simulation. The blue dashed line gives the PDMF of the stars which successfully pass our selected effect filters, in comparison the PDMF of all B-type stars of the observed LMC sample, including those for which no nitrogen measurement is available (red line). The synthesized mass functions have been scaled by a factor of 1/500 for ease of comparison with the observed distribution.

population synthesis simulation is also plotted (blue, solid line). It contains only main sequence stars and is calculated assuming continuous star formation. A comparison between the IMF and PDMF shows that mass loss has populated the $6\,M_{\odot}$-bin and that the (negative) slope of the PDMF has increased. The latter is an evolutionary effect: the most massive stars evolve more quickly and once they leave the MS they are removed from the population. At the high mass end the PDMF gets incomplete as mass loss shifts stars to lower mass bins and we do not have stars initially more massive than $60\,M_{\odot}$ in our simulation.

To test if our assumptions on the IMF and the SFH are reasonable, we construct the PDMF of the stars that would pass all observational selection effects in our population synthesis simulation (see Sec. 5.3.3 below). This distribution corresponds to the light-blue dashed line in Fig. 5.4, and is compared to the PDMF of the stars in our sample (red line). A plateau at lower masses develops, since many low mass stars are too faint to be included in the observational sample. At higher masses, the slope steepens further, since the hot O-type stars drop out of the sample (see Sec. 5.3.3). This can be directly compared to the observed sample PDMF, shown as a red, dashed line in Fig. 5.4. Keeping in mind the low number statistics in the observed sample,

it appears that below 30 $M_\odot$ the two curves have approximately the same shape, thus supporting the assumptions made for the simulation.

The lowest mass stars in the observed sample are $9\,M_\odot$ while the lowest mass stars in the simulation are $7\,M_\odot$. This is confirmed in Fig. 5.6, where no stars are observed at the lowest masses. This could imply that the SFH is limited to ~25 Myrs, or — perhaps more likely — that the sample selection concentrated on the brighter stars in the field. This discrepancy between our model and the observational sample might introduce an error in our analysis. However, the error caused in the population numbers of the different regions of the Hunter-diagram by including stars older than 25 Myrs in the simulation is of the order of 1%. We discuss this in more detail in Sec. 5.4.1.

Initial velocity distribution

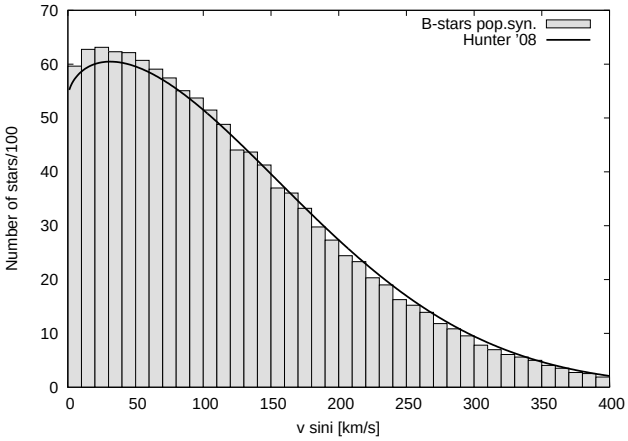

Figure 5.5: The projected rotational velocity distribution found by Hunter et al. (2008b) for non-binary, non-supergiant stars of this sample with masses $\leq 25\,M_\odot$ (black line). This is used as our initial rotational velocity distribution. The gray histogram represents the rotational velocity distribution of our simulated population, after application of all selection effects described in Sec. 5.3.3.

Hunter et al. (2008b) fitted the observed rotational velocity distribution of the LMC sample with a Gaussian function, excluding radial velocity variables, supergiants and stars above $25\,M_\odot$. This mass threshold was used to avoid effects from mass loss induced spin-down on the velocity distribution (see Fig. 5.5). As such, all but the seven lowest mass O-type stars were not included in determining the velocity distribution. Be-stars below the mass threshold are included into the fit to the velocity

distribution. As discussed byHunter et al. (2009b), the width of this function given by Hunter et al. (2008b) is too small and needs to be corrected by a factor $(\pi/4)^{1/4}$. Taking this into account, our ZAMS rotational velocities are selected randomly from the Gaussian function given in Eq. 5.1 (using μ = 100 km/s and σ = 141 km/s), which has been truncated at zero km/s and renormalised (see Hunter et al. 2008b).

$$f(v) \propto \exp\left[-\frac{1}{2}\left(\frac{v-\mu}{\sigma}\right)^2\right]. \tag{5.1}$$

By using this function for our population synthesis, we assume that it is representative of the distribution function of the *initial* rotational velocities. This is justified when the stars rotate close to solid body rotation, which is ensured by including magnetic fields in our models. Also, due to the small mass loss rates for the bulk of the stars in the sample, our models show little change of the rotational velocity over the main sequence evolution. To test this assumption, we have constructed a histogram of the present day projected rotational velocity distribution (PDVD) for the B-type stars from our population synthesis (gray bars in Fig. 5.5). Comparing this for the initial projected rotational velocity distribution (black line) from Hunter et al. (2008b), our simulation predicts only slightly more slow rotators than the input function, but also slightly fewer fast rotators around 200 km/s. The overall shape at lower rotational velocities is preserved in our simulated data. Overall, the observed B-type star velocity distribution seems to be a good approximation to the initial velocity distribution of our population synthesis simulation.

5.3.3 Selection effects

The VLT-FLAMES survey was designed to contain a largely unbiased sample of O- and B-type stars. However, owing to both observational and analytical constraints, there are a number of selection effects present in the final Hunter et al. (2008b) sample (see 5.2), which we attempt to include in our simulation. Specific affected regions in the H-R diagram are highlighted in Fig. 5.6.

Magnitude limit

Our LMC sample is magnitude limited, to ensure sufficient signal-to-noise in each observed spectrum, with about $V = 15.53^{\mathrm{m}}$ for the faintest star. While the limit is not exactly the same in N11 and NGC2004, the limits in each are not significantly different and hence it is reasonable to model these together. In our simulation, we therefore remove all simulated stars that are fainter than this threshold from our simulation, with this region marked in grey in Fig. 5.6. Magnitudes for the simulated

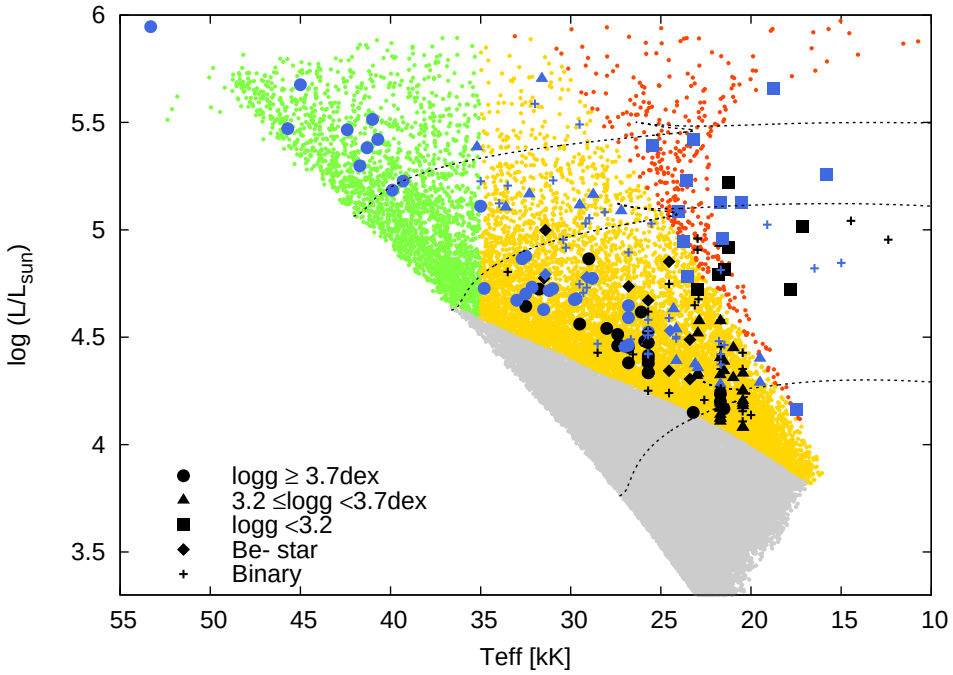

Figure 5.6: H-R diagram of our population synthesis using the initial distributions discussed in Sec. 5.3.2. Regions subject to selection effects (Sec. 5.3.3) are highlighted as: grey – stars too faint for the observed magnitude cutoff; green – stars with $T_{\rm eff} > 35$ kK; red – stars with low surface gravities ($\log g < 3.2$); yellow – remaining stars. Results from Hunter et al. (2009a) are over-plotted (blue: stars in N11; black: NGC 2004; with their shapes indicating their surface gravities). Radial velocity variables and Be-stars that are indicated by crosses and diamonds, respectively. Evolutionary tracks of 10 $M_\odot$, 20 $M_\odot$ and 30 $M_\odot$ of non-rotating models are shown for orientation.

stars have been calculated using:

$$V = M^*_{\rm bol} + \mu + R_{\rm v} \cdot E(B - V) - BC \tag{5.2}$$

$$M^*_{\rm bol} = -2.5 \cdot \log L_{\rm Model} + M_{\rm bol,\odot} \tag{5.3}$$

where $M^*_{\rm bol}$ is the absolute bolometric magnitude of the simulated star. Observational parameters are adopted such that they are consistent with those used by Hunter et al. (2008b) for NGC 2004, i.e., distance modulus $(\mu) = 18.56^{\rm m}$, $E(B-V) = 0.09^{\rm m}$, and a ratio of total-to-selective extinction $R_V = 3.1$. Bolometric corrections (BC) for $T_{\rm eff} < 28172$ K have been adopted from Balona (1994), and for $T_{\rm eff} \geq 28172$ from Vacca et al. (1996).

Exclusion of O-type stars

The dominant nitrogen lines in O-type stars are those from N III. However, this ion is notoriously difficult to model in non local thermodynamic equilibrium due to the need to include di-electronic recombination channels. To date, no large studies of nitrogen abundances in O-type stars are available, although He abundances were studied by Mokiem et al. (2006, 2007). Due to the lack of nitrogen abundances for stars hotter than 35 kK we exclude such hot stars from the simulation (green group in Fig. 5.6), corresponding to spectral types earlier than O9.

Exclusion of low gravity objects

The bulk of the stars have masses in the range of 10 to 20 $M_\odot$. Paper I argues that the surface gravity at the end of the main sequence evolution for these objects is $\log g \simeq 3.2$ (see also Hunter et al. 2008b). While there are some observed stars with lower $\log g$, their nature is unclear (Vink et al. 2010). We therefore exclude post-MS objects, by rejecting all simulated stars with gravities below 3.2 dex (red regime in Fig. 5.6). Note that this implies that we also reject the final part of the main sequence evolution of stars with masses above $\sim 20\,M_\odot$, since the applied overshooting leads to an extension of the main sequence to lower gravities for these objects. We chose to do this because we favor a well defined selection criterion and because the most massive objects have only a small impact on our statistics. Most of the observed stars rejected are luminosity class I supergiants, but this group also contains three class II and two class III objects.

Exclusion of Be stars

Hunter et al. (2009a) did not derive nitrogen abundances for most of the observed Be-type stars (the purple group in Fig. 5.13). For consistency, we excluded a fraction of the most rapid rotators in our simulation. As the mechanism that produces the Be-phenomenon is still being discussed, it is difficult to define a clear criterion to identify simulated stars as Be stars. The Be mechanism appears to be linked with fast rotation and pulsations (e.g. Cranmer 2005). Commonly quoted required fractions of critical rotation for the occurrence of the Be phenomenon are 70-80% (Porter & Rivinius 2003), though values as low as $\geq$ 40% (Cranmer 2005) are also derived. Martayan et al. (2008) finds $\Omega/\Omega_c = 85\%$ in the LMC, and Townsend et al. (2004) argue that Be-stars might actually rotate as fast as 95% of the breakup velocity, since the line broadening due to rotation becomes insensitive to gravity darkening at high rotational velocities.

The fraction of Be/(B+Be) in the observed sample is 13.5%. We can define a theoretical Be fraction within the limits of the yellow region of Fig. 5.6 by dividing the number of stars rotating faster than a specified fraction of break-up rotation by the number of all stars in that region. To match this fraction with the observed one in our sample would require a velocity limit of 55% of the break-up velocity. This number seems too low. As clearly more effects than fast rotation are involved in producing Be stars, we decided to not try to reproduce their number in the population synthesis. In an attempt to simulate the effect of the exclusion of Be-stars from the sample, we chose a more conservative limit and excluded stars with a rotational velocity higher than 90% of their breakup velocity in our simulations. This corresponds to 1.6% of all stars in the yellow region of Fig. 5.6.

In summary, we are unable to reproduce the fraction of observed Be-stars using our cut-off of 90% of breakup velocity. However as we only exclude a small minority of stars from the simulation, we do not expect that this will be a significant source of error.

5.3.4 Stellar evolution models

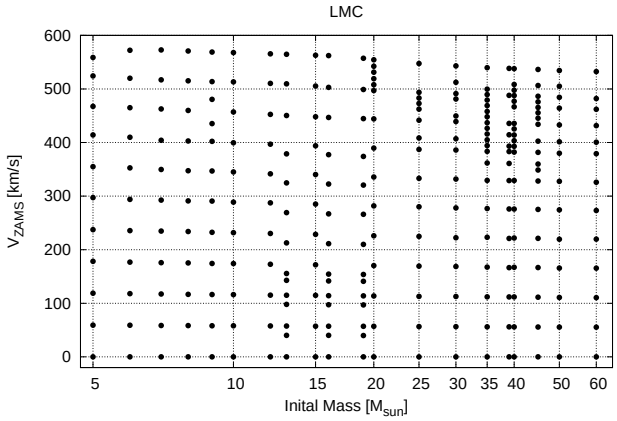

Figure 5.7: Parameter space covered by the LMC evolution grid. Each model sequence is represented by a dot marking its initial mass and rotational velocity.

We calculated a grid of 284 stellar evolution models past core hydrogen exhaustion using a one-dimensional hydrodynamic stellar evolution code, that includes the physics of differential rotation and magnetic fields as described in Paper I; see also

Yoon et al. (2006) and de Mink et al. (2009). The grid spans initial masses of 5–60 $M_\odot$ and rotational velocities ($v_{\rm ZAMS}$) of 0–600 km/s, as shown in Fig. 5.7. The grid is somewhat irregular in rotational velocity since we initialize our models as rigid rotators in a chemically homogeneous state of thermal equilibrium. The subsequent adjustments to achieve CN-equilibrium in the core alter the stellar structure on a thermal time scale and lead to a somewhat different surface rotation rate, which thereafter changes only on the nuclear time scale, and which we designate as $v_{\rm ZAMS}$.

The effect of the centrifugal force on the stellar structure is considered following Endal & Sofia (1976). We consider the transport of angular momentum and chemical elements due to various rotationally induced hydrodynamic instabilities, which include the Eddington-Sweet circulation, the dynamical and secular shear instability, and the Goldreich-Schubert-Fricke instability (Heger et al. 2000). The transport of angular momentum by the Spruit-Tayler dynamo (Spruit 2002) is also implemented. Angular momentum transport and chemical mixing is approximated as a diffusive process.

Convection is treated by the mixing length theory assuming a mixing-length parameter of $\alpha_{\rm MLT} = 1.5$. We follow Langer (1991) for semi-convection, for which rather fast mixing is assumed, with a semi-convection efficiency parameter of $\alpha_{\rm SEM}$=1. We consider convective overshooting using an overshooting parameter of $0.335\,H_P$. This value results from our new calibration using the observed $v \sin i$ drop that is found in our data when we plot $v \sin i$ against the surface gravity (see Paper I) for more details). The rotational mixing efficiency has been calibrated such that the trends in nitrogen of our sample are reproduced well. This leads to adopting $f_c = 0.0228$, which is the ratio of the turbulent viscosity to the diffusion coefficient (see Heger et al. 2000).

We use the recipe of Vink et al. (2000, 2001) for mass loss via stellar winds from O- and B-type stars. To account for the effects of helium enrichment on the stellar wind, we follow the approach of Yoon et al. (2006) (see Paper I for details).

Initial chemical composition

We choose an LMC mixture for the initial chemical composition of our models (Table 5.1). CNO abundances are taken from results for H II regions (Kurt & Dufour 1998). Mg and Si measurements for B-type stars from Hunter et al. (2008b) and B-supergiants of Trundle et al. (2007) are, on average, 0.37 dex lower than the solar values of Asplund et al. (2005). Therefore, we have scaled all other elements from Asplund et al. (2005) by -0.4 dex and adopted the average values of Mg and Si from Hunter et al. (2007) and Trundle et al. (2007) for our stellar models. The resulting metallicity of this mixture is $Z = 0.0047$. We have adopted the OPAL opacity tables

Table 5.1: LMC mixture used in our evolutionary models. The baseline abundances of C, N, O, Mg, Si and Fe are given in the first two columns, i.e. log(C/H) + 12. The total hydrogen (X), helium(Y) and metals (Z) mass fractions are given in the third column.

C	7.75	Mg	7.05	X	0.7391
N	6.90	Si	7.20	Y	0.2562
O	8.35	Fe	7.05	Z	0.0047

(Iglesias & Rogers 1996), for which we use the Fe abundance to interpolate between tables of different metallicities.

We have adopted the helium mass fraction using the primordial helium abundance ($Y_p = 0.2477$) from Peimbert et al. (2007). Assuming the helium abundance to be a linear function of the metallicity Z and fixing it to 0.28 at solar metallicity (Grevesse et al. 1996) results in a value of 0.2562 for our LMC models.

More details on the calibration and choice of the chemical composition for the full evolutionary model grid, which also includes models for Galactic and SMC stars, are presented in Paper I.

5.3.5 Effects of rotational mixing

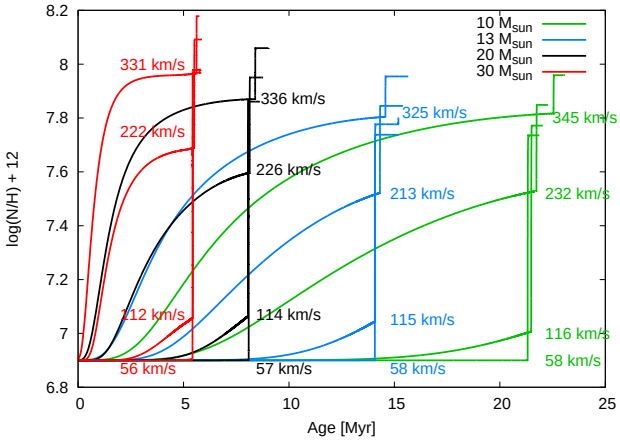

Figure 5.8: Nitrogen surface abundance as a function of time for models with different rotational velocities for 10 $M_\odot$ (green), 13 $M_\odot$ (blue), 20 $M_\odot$ (black) and 40 $M_\odot$ (red) are shown. The model calculations have been ended shortly after the end of core hydrogen burning. The ZAMS velocities are indicated next to each track.

In our models, the strong transport of angular momentum due to the Spruit-Tayler dynamo keeps the star rotating almost rigidly on the main sequence. As a consequence, the shear instability – which is important for non-magnetic models (Heger et al. 2000; Maeder 2000) – is less efficient than the Eddington-Sweet circulation in our models.

The surface abundances of stars can change due to rotational mixing on the main sequence but not all elements are equally well suited for tracing such mixing. While helium is produced in large amounts in the core, the models for moderate rotational velocity show only small enhancements of helium at the surface. This is because the chemical stratification built up by hydrogen burning between the helium enriched core and the hydrogen-rich envelope effectively hinders chemical mixing across the boundary. Only the fastest rotating models ($v_{\rm ZAMS} > 350$ km/s) become significantly helium enriched at the surface, and some of them even follow the quasi-chemically homogeneous evolution if rotational mixing operates faster than hydrogen burning (Yoon et al. 2006). Additionally, helium is already abundant at the stellar surface initially, and the expected enhancement relative to the initial helium abundance is typically small.

Nitrogen, however, can be considerably enhanced at the stellar surface on the MS, even in relatively slow rotators. At the same time, carbon is depleted, but with a smaller relative change than nitrogen, and oxygen remains almost constant. This can be understood in the following way. At the onset of the CNO-cycle, there is a short phase of the CN-cycle in which most of the carbon is transformed to nitrogen. During this phase, hardly any helium is produced, and the mean molecular weight gradient at the outer edge of the core remains small. Therefore, nitrogen produced by the CN-cycle can be efficiently transported into the layers above the convective core. Once the mean molecular weight gradient increases due to helium production, such mixing becomes much slower. As mixing throughout the radiative envelope — i.e. above the major mean molecular weight barrier produced by hydrogen burning — continues during the main sequence evolution, the surface becomes gradually enriched with nitrogen. As the nitrogen abundance at the surface of early B type stars can be measured from optical spectroscopy, nitrogen is one of the best tracers for rotationally-induced chemical mixing.

In Fig. 5.8 we show the surface nitrogen abundance as a function of time for a selection of models from our grid. As the nitrogen enrichment during the main sequence evolution is a monotonic function of time, nitrogen might be used as an age indicator for stars with known initial stellar parameters. In our models, the nitrogen abundance achieved at the end of core hydrogen burning is higher for larger initial rotation velocities, as the Eddington-Sweet circulation operates at a higher flow velocity for faster rotation (Yoon et al. 2006). At the same time, at fixed initial rotation veloc-

ity, the maximum nitrogen abundance increases only slightly with initial mass in the range of 10 to 20 $M_\odot$, but it becomes more sensitive at masses above 30 $M_\odot$. When hydrogen burning stops, the core contracts and the envelope expands and eventually becomes convective, leading to a further dredge-up of nitrogen and a sharp increase of the nitrogen surface abundance as shown in Fig. 5.8.

The abundances of other elements also show variations due to rotational mixing. Sodium is enhanced due to proton captures in the NaNe-cycle, but it is difficult to determine observationally as its lines are weak in this mass range and they are contaminated by interstellar absorption. Boron is strongly depleted, because it is destroyed as it is mixed from the relatively cool outer layers into hotter inner layers (see Paper I), but its spectral lines are weak due to the small initial abundances. Carbon depletion can also be observed in the optical, but it cannot be measured as accurately as nitrogen due to NLTE effects (Hunter et al. 2008b). Fluorine and aluminum are also affected. A full account of this is given in Paper I; in what follows we concentrate on the nitrogen abundances.

5.4 Results

To investigate the role of rotational mixing in massive stars, Fig. 5.9 shows projected equatorial rotational velocities versus nitrogen abundance (hereafter the Hunter plot). The figure contains both observations and theoretical predictions. The observational data includes all stars from our LMC sample for which nitrogen abundances are available (see Sec. 5.2). Radial velocity variables are marked by triangles, while stars with no detected variations are represented with circles. The color coding of the symbol indicates the surface gravity of each object as shown.

The simulation considered 1.5 million stars with initial masses between 7 and 60 $M_\odot$. Only those that remained in the main sequence can be compared to the observational sample. These are plotted in Fig. 5.9. About 45.7% of initial sample have left the main sequence, whilst another 46.3% were excluded due to selection criteria based on magnitude, temperature (spectral type) and surface gravity (see Sec. 5.3.3). The remaining sample contains 120 728 stars.

The most important rejection criterion is the magnitude cutoff, but the age of the simulated star also has a considerable effect. This is easily understood considering that the maximum age of 35 Myr in our SFH corresponds to the MS-lifetime of an 8 $M_\odot$ model. As the MS-lifetime decreases rapidly with increasing initial mass (see Fig. 5.8), the chance that a simulated star is assigned an age greater than its MS-lifetime becomes significant.

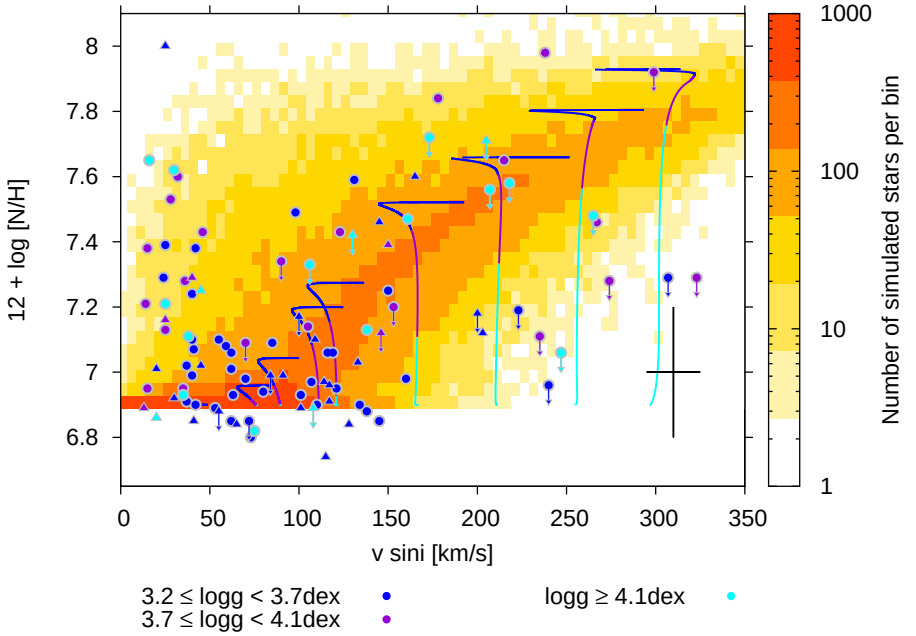

Figure 5.9: Hunter-plot showing projected rotational velocity against nitrogen enhancement. Our population synthesis is shown as a density plot in the background. The color coding corresponds to the number of stars per pixel. Overplotted are data from Hunter et al. (2009a), with surface gravities as indicated by the color (see figure key). Single stars are plotted as circles, radial velocity variables as triangles. Evolutionary tracks of $13\,M_\odot$, corresponding to the average mass of the sample stars, are shown with their surface gravity coded by the same colors as the observations. The velocities of the tracks have been multiplied by $\pi/4$, to account for the average projection effect. The cross in the lower right corner shows the typical error on the observations.

The magnitude cutoff eliminates a large number of simulated stars because the IMF favors lower masses. For instance, models with *less* than $20\,M_\odot$ are too faint to be observed for most of their MS-lifetime. A $12\,M_\odot$ star spends 72% of its MS-lifetime below the magnitude limit, while a $15\,M_\odot$ star is not observable for 35% of its MS-lifetime.

The simulated data have been grouped into 5 km/s $\times\, 0.04$ dex bins to generate a density plot. The color coding represents the number of stars in the bin (see the color bar on the right in Fig. 5.9). We also show evolutionary tracks of $13\,M_\odot$ for comparison. For these tracks the surface gravity is indicated with the same color coding as for the observational data.

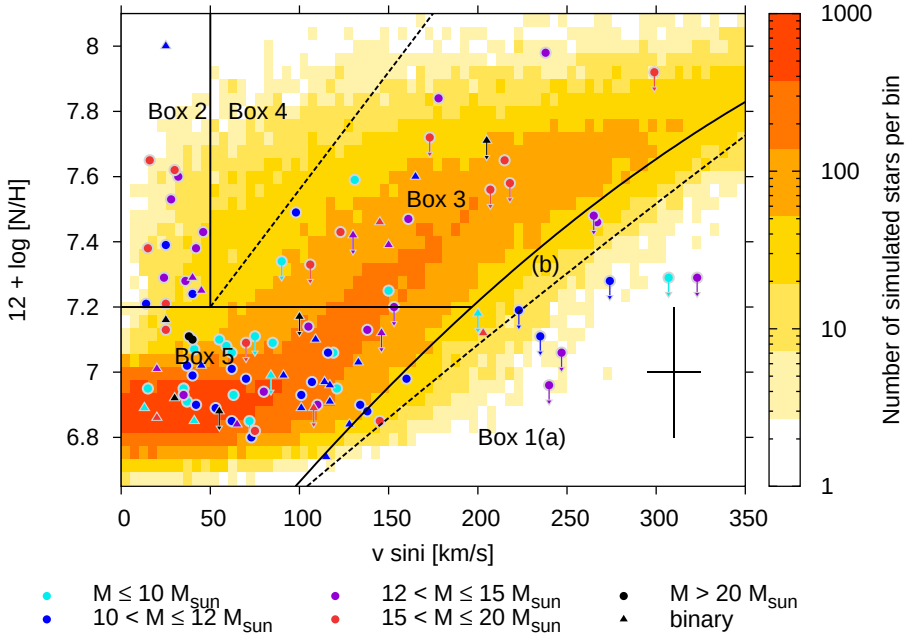

Figure 5.10: As for Fig. 5.9 but with a random error ($\sigma = 0.2$ dex) added to the nitrogen abundances in the simulated data. The observational data have been color coded according to their evolutionary masses (see figure key). For the boxes indicated, in Table 5.2 we give the ratios of the number of observed to simulated stars

Fig. 5.10 shows the same population synthesis simulation as Fig. 5.9, but we have added a random Gaussian error with $\sigma = 0.2$ dex to the predicted nitrogen abundances. This error is characteristic of the spread in the nitrogen abundance determinations of the non-enriched stars. Note that it is smaller than the mean nitrogen error of the entire sample (0.3–0.4 dex; Hunter et al. 2007, 2008b), which is represented by the cross in the lower right corner of Fig. 5.9 and 5.10. We did not include an error for the predicted $v \sin i$ values as the observational values should be reasonably secure. The color coding of the observational data in Fig. 5.10 represents their estimated evolutionary mass.

We have divided the diagram into five regimes:

Box 1(ab) is a region of the diagram at high $v \sin i$ which is predicted to be almost empty. The full line defining box 1(ab) gives the locus where the number of simulated stars per pixel is ~ 40, while this number is ~ 15 for the dashed line defining Box 1b.

Table 5.2: Fraction (in per cent) and absolute number of observed and simulated stars found in each box defined in Fig. 5.10. For the observed stars, in Column 2 we take all stars into account, in Column 3 we only consider those without upper limits. The third column gives the expected number of stars from our population synthesis model. Errors on the number of simulated (Column 6) stars are derived by comparing to simulations with a velocity distribution that was broader or narrower by ±25 km/s.

	observed				modeled	
	all		excl. UL			
	%	#	%	#	%	$\#/10^3$
Box 1ab	14.0	15	7.4	6	$4.6^{+0.8}_{-1.0}$	5.6
Box 1a	5.6	9	0	0	$1.6^{+0.5}_{-0.5}$	2.0
Box 1b	8.4	6	7.4	6	$3.0^{+0.3}_{-0.5}$	3.6
Box 2	15.0	16	19.8	16	$1.2^{+0.0}_{-0.1}$	1.4
Box 3	17.8	19	13.6	11	$35.7^{+4.0}_{-4.6}$	43.1
Box 4	—		—		$2.6^{+0.3}_{-0.5}$	3.1
Box 5	53.3	57	59.3	48	$55.9^{-5.2}_{+6.2}$	67.5
Total		107		81		120.7

Box 2 is a region of the diagram where very few stars are predicted, but where a group of enhanced, slowly rotating stars are observed. This group of stars was already described by Hunter et al. (2009a), and will be discussed further below.

Box 3 encloses the stars in our simulation which have a clear signal of nitrogen enhancement due to rotational mixing.

Box 4 is a region where neither stars are observed, nor a significant number of them is predicted.

Box 5 is the region of the diagram where the un-enriched stars are located. The initial nitrogen abundance is about 6.9 with a typical spread of about 0.2 dex. We chose the upper boundary of 7.2 such that the probability of observed stars found above this line to be truly enriched is large.

In Table 5.2 we present the absolute and relative number of stars populating each box in both the observations and simulations. For the observations we present statistics including and excluding objects for which only an upper limit to the nitrogen abundance was established. A downward revision of the upper limits might reduce the number of observed stars in Box 3, while that in Boxes 5 and 1 might increase. For all stars in Box 1a we only have upper limits, but their presence in this box is not

affected by this. Unless otherwise stated, the numbers quoted in the discussion below include the stars with upper limits to their nitrogen abundances.

We find 53.3% of the total observed sample to be in Box 5, containing the non-enriched stars which do not rotate rapidly. This is in good agreement with the theoretical prediction of 55.9%. Due to the large number of stars in this region, this agreement is not affected by stars with upper limits on their nitrogen abundance. Most of the stars in this box are expected to have a relatively low mass, and in an advanced phase of core hydrogen burning such that they have become sufficiently bright in the optical to be above the magnitude cutoff. Indeed the observed stars with $M \leq 10\,M_{\odot}$ accumulate in Box 5 and appear to have mainly surface gravities of less than 3.7.

We note that a more efficient mixing would reduce the predicted number of stars in Box 5. However, the mixing efficiency is calibrated to best represent the correlation between nitrogen abundance and $v \sin i$ (see above). *The fact that after such a calibration the number of non enriched stars predicted in Box 5 is in very good agreement with the observations supports the theory of rotational mixing.*

Box 3, containing the stars of our simulation which show rotationally induced nitrogen enhancement, is predicted to contain 35.7% of our sample. However only 17.8% of the observed sample is found in this region. Hence we predict approximately twice as many stars to be enriched as are actually observed. Subtracting the stars for which we have only upper limits leaves only 13.6% of the sample stars in Box 3, increasing the discrepancy between theory and observations to almost a factor of three. On the other hand, Fig. 5.11 shows that more observed stars in Box 3 are found in the $12...20\,M_{\odot}$ bin compared to the lower mass bin ($M < 12\,M_{\odot}$), while our models predict similar (absolute) numbers for both mass bins. This may indicate that subdividing our sample into too small sub-samples results in a loss of statistical significance.

While this may show that analyzing sub-samples may lead to effects of small number statistics, it also shows that the overall discrepancy in the predicted and observed number of stars in Box 3 may not be very significant.

Box 2 contains a group of apparently slowly rotating but nitrogen enhanced stars. Theoretical models of rotating single stars predict such enhancements only for fast intrinsic rotation ($v_{\rm ZAMS} > 150$ km/s). Note that all the observed targets in Box 2 cannot be rapid rotators seen nearly pole on. Indeed our simulations (which assume random inclination angles) predict that only 1.2% of the sample (corresponding to one star) would be found in this region. Observationally 16 stars comprising 15% of the sample lie in Box 2. Therefore the projection effect can not populate this part of the diagram. This statement is enforced by the fact that no stars are observed in Box 4, which — if the projection effect were to explain the large number of stars

in Box 2 — should contain more stars than found in Box 2. We conclude that the vast majority of stars in Box 2 are intrinsically slow rotators and their high nitrogen abundance is not explained by our models. The nitrogen enhanced stars in Box 2 appear to have higher masses and to be less evolved. There are no stars with $M \leq 10\,M_\odot$ in this group, even though this is one of the most populated mass bins in the observed sample. With the exception of five stars (of which one is a binary) surface gravities in this group are larger than 3.7 dex. A comparison with the evolutionary tracks in Fig. 5.9 indicates that most stars of this box are in an intermediate or evolved stage of their MS-evolution. *The large number of stars found in Box 2 is not predicted by the theory of rotational mixing in single stars with an overpopulation of observed targets by more than a factor of ten with that predicted.*

Box 1(a+b) contains a group of 15 fast rotating but non-enriched stars (14% of the observed sample). We predict a factor of 3 less stars (4.6%) in this box, with most of them expected to be in Box 1b, i.e. very close to Boxes 3 and 5. In particular the area where the six observed stars in Box 1a are found is predicted to be empty. This prediction is largely due to the adopted observational selection effects, but to a small extent also due to the fast nitrogen enrichment of rapidly rotating stars (Fig. 5.8). Most of the simulated targets populating the diagram started their evolution below the magnitude cutoff. Those which were rapidly rotating have sufficient time (before passing the magnitude limit) to enhance their surface nitrogen abundance so significantly that once they appear in the diagram they show up in Box 3. In Box 1(a or a+b), there does not seem to be a preference for high surface gravities and low masses as suggested by Maeder et al. (2009). The six objects in Box 1a have masses in the range of $9 \ldots 15\,M_\odot$, which is a typical spread for the sample. Their average mass is $12\,M_\odot$ which is similar to the average for all the stars for which nitrogen abundances have been determined of $13.6\,M_\odot$. Additionally the stars cover a range of ages. As the stars in Box 1b have upper limits to their nitrogen abundances, some of them could actually lie in Box 1a, increasing the discrepancy with prediction. *In summary the existence of a significant number of targets in Box 1a cannot be reconciled with the prediction of rotational mixing for single stars that this area should contain effectively no objects.*

Fig. 5.11 indicates that whilst the population of Box 1b is strongly mass dependent, that dependency is less pronounced for Box 1a. The top panel shows simulation and data with $M \leq 12\,M_\odot$. The models of $12\,M_\odot$ spend about 70% of their MS at luminosities below the magnitude limit. When they finally become bright enough, they are already so enriched that they show up in Box 3. Only for models of intermediate mass, as shown in the middle panel (12–20 $M_\odot$), does the interplay between the selection effects and the mixing-timescale allow stars to populate Box 1. Using an even finer mass binning, we find that Box 1a is actually only populated by stars in the

mass range 12–15 $M_\odot$, while Box 1b contains models in the mass range 12–20 $M_\odot$. The bottom panel shows models and observed stars more massive than 20 $M_\odot$. In both cases Box 1 remains empty. Models of 20 $M_\odot$ or more are above the magnitude limit all time, but they have effective temperatures above 35 000 K during their early main sequence evolution, such that the fast rotators, once they have become cool enough to appear in our simulation data, have already achieved a significant nitrogen enrichment.

5.4.1 Model uncertainties

Before we focus on the possible evolutionary implication of our findings, we first discuss the significance of the results summarized in Table 5.2 which are obtained from our population synthesis. The discrepancy between observation and prediction is very large for both Boxes 1 and 2. In contrast, it is smaller for Box 3, being only a factor of approximately two. Hence in discussing our uncertainties, we will focus on how they might affect our simulation of the fractional population of this Box.

These numbers are subject to various uncertainties: *i)* the mixing efficiency in the stellar models, *ii)* the initial velocity distribution, mass function and star formation history, *iii)* the observational biases, and *iv)* exclusion of unsuitable stars.

Mixing efficiency

The calibration of the mixing efficiency is described in detail in Paper I. The models in our stellar evolution grid are calculated with a mixing efficiency parameter of $f_c = 2.28 \times 10^{-2}$ (see Sec. 5.3.4). The impact of a larger mixing parameter f_c is that a larger maximum nitrogen enhancement is achieved for a given initial rotation rate. Therefore, the general trend of nitrogen enhancement versus $v \sin i$ would be shifted to lower rotation velocities and larger nitrogen abundances. In Fig. 5.9, the evolutionary tracks of our 13 $M_\odot$ models show an unaffected nitrogen abundance for $v \sin i < 100$ km/s within the observational error, and a peak value of 7.9 is obtained at $v \sin i \simeq 300$ km/s. This behavior does reflect the general trend of the observed stars in Boxes 5 and 3 quite well: the maximum observed nitrogen abundance, the slope of the nitrogen versus $v \sin i$-relation, and the foot-point at $v \sin i \simeq 100$ km/s are all matched well. We thus believe that the calibration of the mixing efficiency of our models does not contribute significantly to the observed discrepancy.

Input distribution functions

The adopted distribution of initial rotational velocities has been discussed in Sec. 5.3.2. In order to assess the sensitivity of the predictions on the distribution of initial rota-

tional velocities, we investigated the effect of a broader (σ = 166 km/s) and narrower (σ = 116 km/s) width of the underlying Gaussian. A variation of ±25 km/s is consistent with the errors given in Dufton et al. (2006) on the fit to the projected rotational velocity distribution. The relative changes are given as errors on the theoretical percentages in Table 5.2. While we find that the numbers predicted for most boxes do not change significantly, the narrower velocity distribution leading to fewer rapid rotators, shifts about 6% of all modeled stars from Box 3 to Box 5. This reduces the discrepancy for Box 3 (35.7% predicted vs. 17.8% observed) to below a factor of two (29.8% predicted vs. 17.8% observed), but it can not eliminate it.

The initial mass function is assumed to be Salpeter ($\alpha = -2.35$; see Sec. 5.3.2). Given the apparent universal nature of this distribution in the mass range from 10–60 $M_\odot$ (Chabrier 2003; Kroupa 2001), and given the good agreement between the observed and simulated mass functions (see Fig. 5.4) we believe that this is unlikely to be a significant source of error.

As discussed in Sec. 5.3.2, we have assumed continuous star formation in our population synthesis model. Clearly, the star formation history may influence the distribution of stars in Fig. 5.10. For instance, a young co-coeval population will cause the fraction of predicted stars in Box 5 to increase, at the expense of the number of stars in Box 3. However, as Fig. 5.3 appears largely consistent with our assumption of continuous star formation, we do not expect a significant error due to this assumption. We have investigated the case where star formation stopped after 25 Myr (as suggested in Sec 5.3.2) instead of continuing for 35 Myr. The stars that are older than 25 Myr are mainly to be found in Boxes 3 and 5. If we exclude these stars, the number of stars in Boxes 3 and 5 change by about 1%, and by much less in the other boxes.

Observational biases

While we accounted for the observational biases in our population synthesis model, some error may be associated with this. Most relevant in this respect may be the magnitude cut-off applied in the VLT-FLAMES Survey. While Fig. 5.6 shows that indeed no observed stars fainter than our adopted magnitude cut-off are found in the sample, there may be a slight deficit of observed stars near the magnitude cut-off, especially at masses below $\sim$ 10 $M_\odot$. As these stars would be nearly at the end of their main sequence evolution, the ratio of enriched to non-enriched stars amongst them would be larger than average. However, limiting the population synthesis to stars above 9 $M_\odot$ has a very similar effect as limiting the star formation history to 25 Myrs (discussed above), since the main-sequence lifetime of a non-rotating 9 $M_\odot$ model is about 25 Myrs. It changes the number of stars in Box 3 and 5 only by less

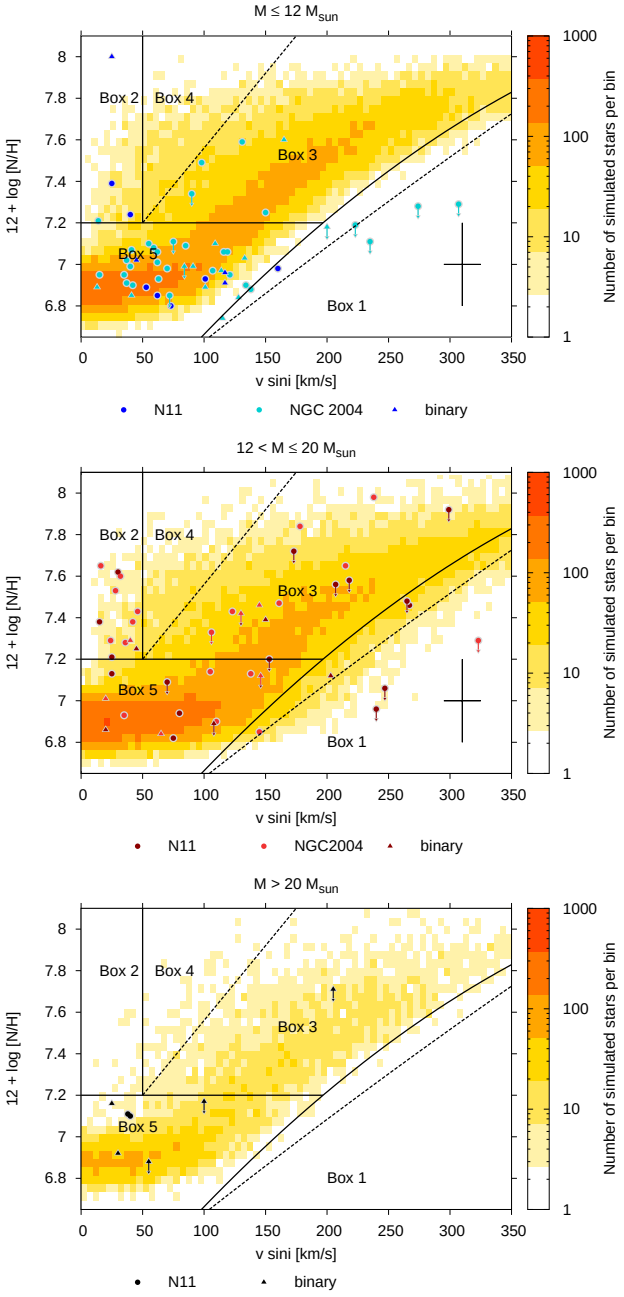

Figure 5.11: Mass dependence of the Hunter-plot. We have separated Fig. 5.10 into three mass bins. Top to bottom: Population synthesis results and observational data for the mass bins $M \leq 12\,M_{\odot}$, $12 \leq M < 20\,M_{\odot}$, $M > 20\,M_{\odot}$ are shown, respectively.

than one percent. The main-sequence lifetime of a non-rotating 9 $M_\odot$ model is about 25 Myrs.

Binary stars are slightly brighter than single stars of a mass or brightness equal to the binary primary. Therefore, some binaries with primaries which would not pass the magnitude limit by themselves might, through the additional light of their companion. A test population simulation where we assumed all stars to consist of binary stars with identical companions convinced us that this effect does not significantly affect any results described below.

For very rapid rotators, the observed brightness and gravity may also depend on the inclination angle due to the latitudinal dependence of gravity darkening. However, the observed and the modeled number of very rapid rotators is so small that this effect is negligible here (see also Hunter et al. 2009a).

Removal of unsuitable stars

In our population synthesis simulation, we have only included single stars computed with a single set of physics assumptions. In reality however, different physical situations may occur. For example, many massive stars are known to have a close binary companion (e.g. Sana et al. 2009) which will modify the evolution during core hydrogen burning. Other massive stars are clearly affected by internal magnetic fields (e.g. Wade et al. 2006). Our model does are therefore only representative of at most a certain fraction of the observed stars.

In order to assess the potential consequences for our conclusions concerning the number of stars in Box 3, let us first assume that the stars in Boxes 1 and 2, which can not be explained well by our model anyway, need to be discarded as "unsuitable" for a comparison with our model. This would reduce the total number of stars to be compared with from 107 to 76, and then render the fraction of observed stars in Box 3 to 25% (rather than 17.8%), which is closer to the predicted fraction of 35.7%.

However, the fraction of observed stars which is "unsuitable" for a comparison with our model may be larger; let us assume it is as large as 50%. As the observed stars in Box 3 agree well with the physics of rotational mixing, let us further assume that none of the 50 or so observed stars to be disregarded would lie in Box 3. Again, we would assume that the observed stars in Boxes 1 and 2 should be disregarded. However, about 20 stars need to be disregarded also from Box 5. For example, this could be fast rotators which can not mix because of strong internal magnetic fields. With such assumptions, we had 37 "suitable" stars left in Box 5, and 19 in Box 3. The latter number corresponds to ~33% of the reduced sample, which then is close to the predicted fraction of 35.7%. While the assumption that we can describe only half of the stars in the observed sample may be extreme, this case can not be ruled

Table 5.3: Expectation value of the numbers of stars and standard deviation for each box as calculated from equations 5.4 and 5.5 given in column one. In the second column these values are expressed in percent of the sample.

	$\mu \pm \sigma$[#]	$\mu \pm \sigma$[%]
Box 1	4.9 ± 2.2	4.6 ± 2.0
Box 2	1.3 ± 1.1	1.2 ± 1.0
Box 3	38.2 ± 5.0	35.7 ± 4.6
Box 4	2.8 ± 1.6	2.6 ± 1.5
Box 5	59.8 ± 5.1	55.9 ± 4.8

out, and it serves as an example of the difficulty in defining a robust observational sample.

Stochastic effects

Here, we assess the spread in the number of stars obtained for each box in Fig. 10 if only 107 stars are drawn randomly from the simulated population. This is equivalent to the following experiment. A pot contains N=120 728 balls, equivalent to the number of simulated stars in Fig. 5.10. The balls in the pot have the colors $c_1 \ldots c_5$. The number of balls in the pot with color c_i is equal to the number of simulated stars in Box i, for $i = 1 \ldots 5$. We draw n=107 balls from this pot, without taking the order into account in which they are drawn. Because of the large number of balls in the pot, the probability p_i to pick a certain color can be approximated as constant, i.e. as the number of balls of color c_i divided by the total number of balls N. This approximation is valid as long the number of balls of color c_i is much larger than the number of balls drawn from the pot.

When the experiment is repeated many times, the result is multinominally distributed(Papoulis 1984, p. 75). The expectation values μ_i for the number balls drawn from each color and its standard deviation σ_i can be calculated by:

$$\mu_i = np_i \tag{5.4}$$

$$\sigma_i^2 = np_i(1 - p_i) \tag{5.5}$$

The expectation values given in Table 5.3 agree with the percentages found in Table 5.2. The standard deviation indicates a rather small spread, which can not cause the discrepancy between observation and simulation discussed above. This is true in particular for the ratio of the number of stars from Box 3 and Box 5.

Overall assessment

We have shown above that the discrepancy of a factor of two in the predicted and observed fraction of stars in Box 3 is not sufficient to rule out rotational mixing for this subsample. Our theoretical mixing calibration, the adopted star formation history, and initial distribution functions for mass and rotational velocity apparently induce little uncertainty. However, the adopted magnitude cut-off and in particular the possibility of applying different physical situations to main sequence stars than assumed in our model allows for a modification of the fractions of stars in Boxes 3 and 5 which may bring theory and observations into agreement.

On the other hand, the possible agreement of the predicted distribution of stars in Boxes 3 and 5 is not sufficient to verify the theory of rotational mixing. This will be discussed further when predictions of massive close binary evolution are included in our considerations, in the next section.

5.5 Discussion

From the previous section, we conclude that overall, the agreement between the population synthesis model and the observed sample is rather poor. While the model predicts stars to be confined to Boxes 5 and 3, the observed stars are much more wide spread. Quantitatively, only in Box 5 is the number of observed stars in good agreement with the predictions. While the stars in Box 3 at least qualitatively agree with the population synthesis model, the stars in Box 1 and Box 2 are completely unexpected and can not be explained by the model. Before any further conclusion, it is thus worthwhile to consider physical and evolutionary processes which could populate Boxes 1 and 2, as those might have effects on Boxes 3 and 4.

5.5.1 Close binary evolution

Though our model assumption is that the diagram is populated only by single stars, it is well known that a significant fraction of stars is part of a binary system (e.g. Mason et al. 2009), with a binary fraction of 0.5 or more found in young star clusters (e.g. Sana et al. 2008, 2009; Bosch et al. 2009), and with a period distribution such that many of them will interact (Sana & Le Bouquin 2010). We emphasize that strong binary interaction (i.e., mass transfer or merging) will often lead to a system that is either a single star or which shows insignificant radial velocity variations. Most observed radial velocity variables in the VLT-FLAMES Survey will likely be pre-interaction systems and thus well suitable for comparison with single star evolution.

The apparent binary fraction in our various observational sub-samples thus give no direct clue to the importance of strong binary interaction for the sub-sample.

In close binaries, the primary star may fill its Roche lobe during the main sequence evolution. This results in the removal of the stellar envelope of the primary star, which is transformed into a (mostly unobservable) helium star. If the entire envelope is added to the companion, the surface nitrogen abundance of this star will increase by a factor of 3 to 5, even when rotational mixing is not taken into account (cf. Fig. 9 in Langer et al. 2008) as in the accretion process the envelope material is well mixed. Subsequent rotational mixing of the mass gainer may enhance the surface nitrogen abundance further on the thermonuclear timescale (cf. Fig. 10 in Langer et al. 2008). If only a small fraction of the material is accreted, the result is no or only a mild N enrichment. During the accretion process not only mass but also angular momentum is transferred to the companion, and it has been found that the accretion of only about 10% of the stellar mass is able to spin-up the star significantly (Packet 1981; Langer et al. 2008).

Therefore, conservative and moderately non-conservative mass transfer would tend to populate the upper right corner in Fig. 5.10 (Box 3), while highly non-conservative mass transfer (e.g. Petrovic et al. 2005a) is likely to move stars to the lower right corner (Box 1) (Langer et al. 2008). Binary interaction leading to a merger is also expected to result in fast rotating objects, likely populating Box 1 or Box 3. Binary evolution is also able to populate Box 2, as post-mass transfer systems may remain so tight that the tidal interaction can spin down the accretion star (Langer et al. 2008).

While quantitative statements requires binary population synthesis models which include a methodology for non-conservative mass transfer (which are not yet available), it is clear that the canonical mass transfer evolution leads to a rapidly rotating, nitrogen-rich main sequence accretion star (Langer et al. 2008). Thus, invoking binaries has the potential to solve the problems with Boxes 1 and 2, but for each star appearing in these boxes, one or more stars would appear in Box 3 due to binary interaction, as binary evolution is expected to lead more often into Box 3 than into Box 1 or 2.

This implies that, using binaries to solve the problems with Box 1a and, in particular, with Box 2, worsens the problem with Box 3, possibly even to the extent that no rotationally mixed single stars are required to explain those found in Box 3. *We conclude that close binary evolution, as far as it is currently understood, is unlikely to be responsible for the slowly rotating nitrogen-rich population of observed stars in Box 2.*

5.5.2 Magnetic fields

Effects of magnetic fields other than the magnetic angular momentum transport implemented in our models may affect a fraction of massive stars. Further down the main sequence, magnetic Ap stars tend to rotate more slowly than non-magnetic A stars and show surface abundance anomalies. Also the ratio of Ap to A stars is about 5-10% (Wolff 1968) which is not far from the percentage of stars which populates Box 2. Furthermore, Morel et al. (2008) recently found magnetic fields in Galactic nitrogen enriched slowly-rotating early B-type dwarfs. All this makes the possibility that magnetic fields play a role in the population of stars in Box 2 an interesting direction of investigation.

A potential magnetic mechanism would not necessarily need to act simultaneously on both the nitrogen abundance and the stellar rotation, as is believed to occur in Ap stars. In fact one could envisage a mechanism that slows stars down through magnetic braking, with rotational mixing occurring whilst the star is still a fast rotator responsible for the nitrogen enrichment. The fact that the number of predicted stars in Box 3 is more or less the sum of the stars observed in Boxes 3 and 2 may be suggestive of a migration process from Box 3 to Box 2. The lack of observed stars in Box 4 then indicates that such a migration needs to occur on a rapid time scale. A massive star example for magnetic braking has been found by Townsend et al. (2010) in the magnetic helium-strong star σ Ori E with a characteristic spin down time of 1.34 Myr. Also, Meynet et al. (2011) have calculated models with a simple description of magnetic braking that leads to slow rotation and produces a nitrogen surface enhancement by inducing strong internal differential rotation.

On the other hand, one may also imagine a migration of stars from Box 5 to Box 2, e.g. through the buoyant rise of magnetic bubbles which carry magnetic flux and nitrogen from the convective core to the surface (MacGregor & Cassinelli 2003). *We conclude that magnetic field effects may play a role, but they are not sufficiently understood to allow secure predictions.*

5.5.3 Comparison with earlier analyses

Some of the conclusions derived in this paper were already obtained by Hunter et al. (2008a), based on the same observational sample as the one scrutinized here, but only based on a subset of the stellar models presented in Paper I rather than on detailed population synthesis. Maeder et al. (2009) argued that the conclusions of Hunter et al. were unwarranted, due to the dispersion of the sample stars in mass, age, rotation, and binarity (we ignore the suggestion of a metallicity spread, which is known to be small in the LMC). In their own analysis, where they reduced the sample size by

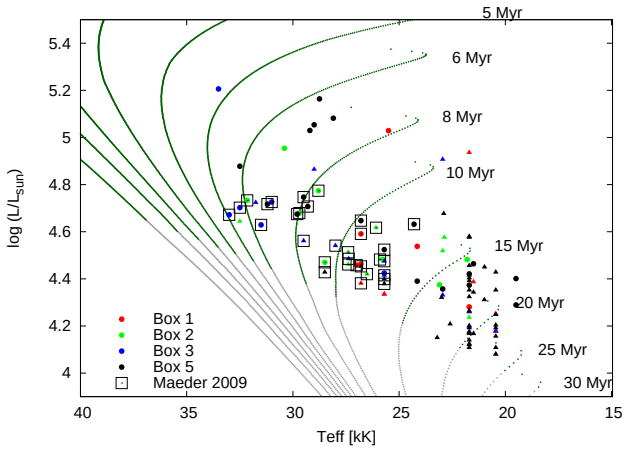

Figure 5.12: HR-diagram of the 107 sample stars in the Hunter diagram. Stars from the N11 and NGC 2004 fields are represented by circles and triangles, respectively. The color coding represents the box into which stars fall in the Hunter diagram. Isochrones made from non-rotating evolution models are shown in green. The isochrone part below the magnitude cut is plotted in gray.

a factor of about 4 to consider only stars of similar mass, they still maintained the dispersion in age (see Fig. 5.12), rotation and binarity, and found their models of rotating single stars to explain the observations satisfactorily.

We find the picture emerging from the reduced sample analyzed by Maeder et al. (2009) and that from Hunter et al. (2008a) not very different. This is in fact not surprising, since the restriction in mass applied by Maeder et al. is not necessary. The mass range of stars in the full sample is already so small (9...25 $M_{\odot}$), that the expected nitrogen enrichment is very similar throughout the considered mass range (cf. Fig. 8, and also Fig. 1 of Maeder et al. (2009)). This is in fact confirmed by their analysis, which shows the bands of potentially rotationally mixed stars in Figs. 3 and 4 of Maeder et al. (2009) being exactly the same, implying that the mass dependance is negligible. While Maeder et al. conclude that the stars in Box 3 agree with single star models, we do the same, only we note that binary evolution provides an alternative explanation for these stars.

Maeder et al. also find stars in Box 2 in their reduced samples, with a similar proportion as they occur in the full sample. While Maeder et al. argue that they may occur due to binary effects and thus do not disturb the agreement of single star predictions with the observations, Meynet et al. (2011) argue that massive slowly rotating nitrogen-rich main sequence stars could be single stars undergoing magnetic

braking, as proposed by Hunter et al. (2008a). Only the fraction of rapidly rotating stars without strong nitrogen enrichment (Box 1) in the Maeder et al. (2009) sample is smaller than in the full sample, which is due to the small size of the samples of Maeder et al. However, of course, all Box 1 stars in the full sample remain to be explained.

In any case, we developed the population synthesis approach as presented in this paper in order to construct a tool to analyze also diverse stellar samples in a statistically sound way. The spread in age, mass and rotation (and in principle, metallicity) is fully accounted for by our method. Our new results reinforce the uncomfortable conclusions of Hunter et al. (2008a) that two significant groups of massive core hydrogen burning stars stand out as being in conflict with evolutionary models, posing a challenge to the concept of rotational mixing.

5.6 Conclusions

Through detailed single star population synthesis modeling, we have tried to reproduce the properties of the largest homogeneous sample of early B-type stars in the LMC. This sample is the first for which nitrogen surface abundances have been determined for a large range in projected rotational velocities. Uncertain mixing parameters in the underlying stellar evolution models (overshooting and rotational mixing) have been calibrated such that they reproduce the observed main-sequence widening deduced from the sharp drop in rotational velocities (Paper I, Vink et al. 2010), as well as the observed pattern of nitrogen enrichment as a function of the projected rotation velocity in the majority of fast rotators (Hunter et al. 2008a).

We confirm quantitatively the result of Hunter et al. (2008a) that two sub-populations of stars, namely rapidly rotating, unenriched stars and slowly rotating, nitrogen-rich stars (Boxes 1a and 2 in Fig. 5.10), are not reproduced by a population synthesis model for single stars.

While the group of rapidly rotating nitrogen-rich stars (Box 3) is, by construction, in qualitative agreement with our simulation, only about half of the number of predicted stars are found to be present in the observational sample. Although possibly explained by uncertainties in our method (see Sec. 5.4.1), predictions of close binary evolution models, which also produce nitrogen-rich rapid rotators, tend to increase this discrepancy.

We find it unlikely that the group of slowly rotating nitrogen-rich stars (Box 2 in Fig. 5.10) is produced via mass transfer and subsequent tidal spin-down in close binary systems, as a binary population which could produce these stars would likely overpopulate the group of rapidly rotating nitrogen-rich stars (see Sec. 5.5.1). At

present, it appears plausible that some of the unexplained slowly rotating, nitrogen-rich stars are affected by magnetic fields (cf. the magnetic field measurements for Galactic stars with similar properties; Morel et al. 2008).

While a detailed physical prescription of possible magnetic effects in stellar models is currently not available, several binary effects are much better understood. Therefore, it appears promising to perform a binary population synthesis of massive main sequence stars in the near future, which will give quantitative constraints on the relative importance of binaries in the various sub-groups. In fact, this appears to be required in order to arrive at solid conclusions on the nature of the group of rapidly rotation nitrogen-rich stars, and, thereby, obtain clear evidence for the universality of rotational mixing in massive stars.

Further light should be shed on this by the ongoing Tarantula Survey (Evans et al. 2010), which has targeted over 1000 stars in the 30 Doradus of the LMC. 30 Dor is the largest H II region in the Local Group, containing a large number of very massive stars. The new survey is tailored for the detection of binarity, so will help sample the mass range above 30 $M_{\odot}$, where mixing effects should be more significants, and therefore more easily detectable.

Acknowledgements We thank Georges Meynet, the referee of this paper, for many helpful comments and suggestions. SdM acknowledges support for this work provided by NASA through Hubble Fellowship grant HST-HF-51270.01-A awarded by the Space Telescope Science Institute, which is operated by the Association of Universities for Research in Astronomy, Inc., for NASA, under contract NAS 5-26555.

Appendix A: The LMC Sample

In Fig. 5.13 we show the mass and projected rotational velocity distributions of our sample. In the upper panels, the targets are divided into the VLT-FLAMES fields. The rotational velocity distributions in both fields are very similar. The total mass distribution is dominated by N11 stars at high masses, while NGC 2004 contributes mainly to the lower-mass end.

We divided our sample into single and binary stars, as shown in the middle and lower panels of Fig. 5.13, respectively. The color coding corresponds to our selection effects that are later applied to each star of our population synthesis (see discussion in Sec. 5.3.3). The single star velocity distribution is well represented by those stars with measured nitrogen abundances (yellow panels). Around 50 km/s is a peak of low gravity objects (orange), which is somewhat sensitive to our overshooting calibration.

A value of 50 km/s is also the order of the line broadening due to macro turbulence, therefore, these stars could be rotating at lower velocities.

The mass distribution of single stars with measured nitrogen abundances is also representative of the mass distribution of the total single star sample. Nitrogen abundances were not determined for the limited sample of the most massive stars owing to the problems of modeling the N III line. The binary velocity distribution shows three peaks (at 30, 100 and 200 km/s), which may well be not statistically significant given the small number of stars.

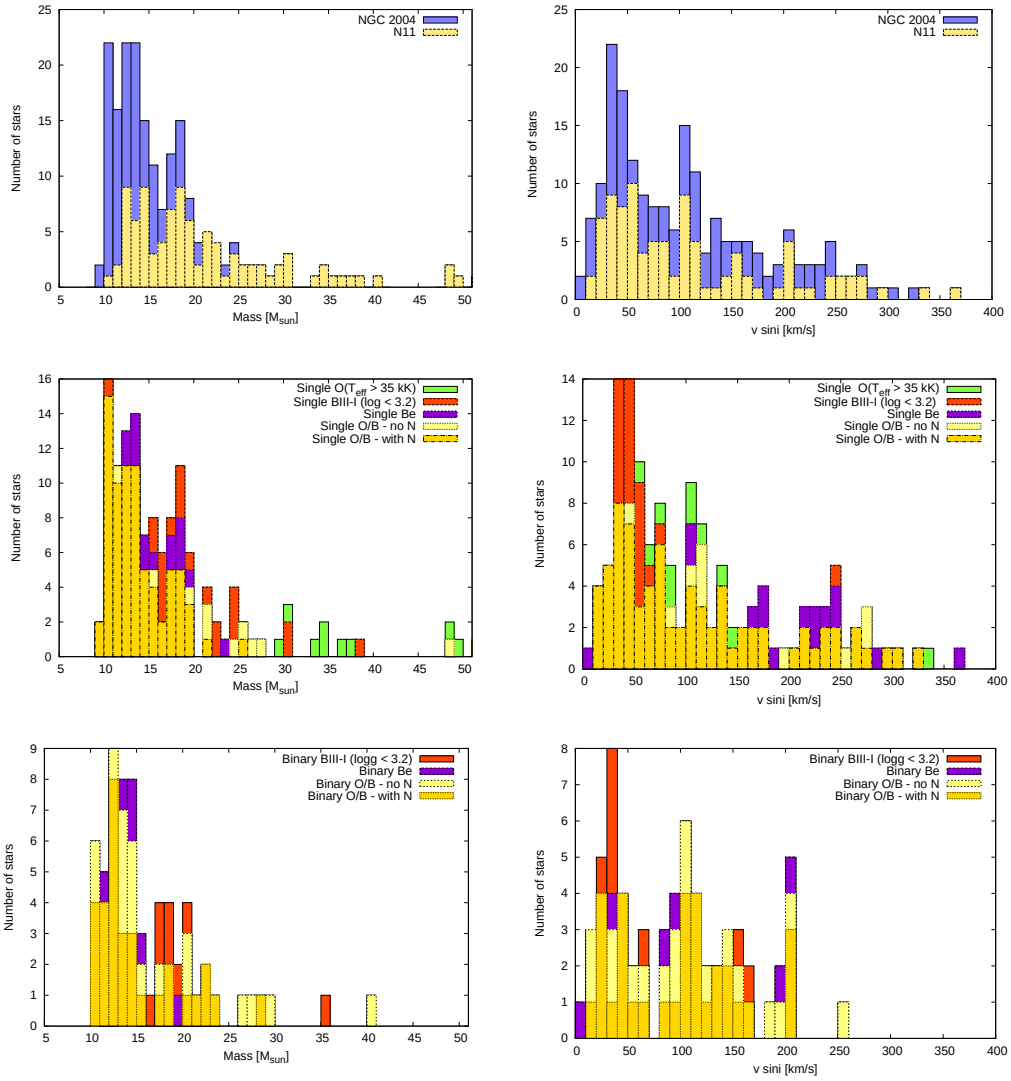

Figure 5.13: Distribution of evolutionary masses (left) and projected rotational velocities (right) of O- and B-type stars from Hunter et al. (2009a) in the NGC 2004 and N11 VLT-FLAMES fields. *Top panels:* The contributions from each VLT-FLAMES field are shown in yellow (N11) and blue (NGC 2004); *Middle:* Apparently single stars; *Bottom:* Radial velocity variables. The selection effects discussed in Sec 5.3.3 are color-coded as per the legend in each plot. For the objects in light yellow we do not have nitrogen measurements for various reasons. The stars shown with gold panels are those with measured nitrogen abundances that are the primary focus of the current analysis. Not shown in the mass histogram are two O-type stars, with masses of 62 and 83 $M_{\odot}$.

CHAPTER 6

The Nature of B Supergiants: Clues From a Steep Drop in Rotation Rates at 22 000 K – The possibility of Bi-stability braking

Jorick S. Vink, **I. Brott**, G. Gräfener, N. Langer, A. de Koter, D.J. Lennon

Published in Astronomy & Astrophysics, 2010, 512, L7

Abstract The location of B supergiants in the Hertzsprung-Russell diagram (HRD) represents a long-standing problem in massive star evolution. Here we propose their nature may be revealed utilising their rotational properties, and we highlight a steep drop in massive star rotation rates at an effective temperature of 22 000 K. We discuss two potential explanations for it. On the one hand, the feature might be due to the end of the main sequence, which could potentially constrain the core overshooting parameter. On the other hand, the feature might be the result of enhanced mass loss at the predicted location of the bi-stability jump. We term this effect "bi-stability braking" and discuss its potential consequences for the evolution of massive stars.

6.1 Introduction

The large number of B supergiants as well as their location in the Hertzsprung-Russell diagram represents a long-standing problem in massive star evolution (e.g. Fitzpatrick & Garmany 1990). Even the most basic question of whether B supergiants are core

hydrogen (H) burning main sequence (MS) or helium burning objects has yet to be answered. Here we propose their nature may be revealed utilising their rotational properties.

On the MS, O-type stars are the most rapid rotators known (with $v\sin i$ up to 400 km/s), but B supergiants rotate much more slowly (with $v\sin i \lesssim 50$ km/s), which has been attributed to the expansion of the star after leaving the MS. Hunter et al. (2008b) noted a steep drop in rotation rates at low gravities ($\log g < 3.2$) and suggested the slowly rotating B supergiants to be post-MS. The steep drop was also used to constrain the core overshooting parameter $\alpha_{\rm ov}$ in massive star models (Brott et al. 2010). The slowly rotating B supergiants are also cooler (with $\log T_{\rm eff}$ below ~22 000 K) and $v\sin i$ is observed to drop steeply below this $\log T_{\rm eff}$. Here we introduce an alternative explanation for the slow rotation of B supergiants: wind-induced braking due to bi-stability, or bi-stability braking (BSB).

Mass loss plays a crucial role in the evolution of massive stars. Whilst a large amount of attention has been directed towards the role of stellar winds in terms of the *loss of mass*, as winds "peel off" the star's outer layers (Conti 1976), much less effort has been dedicated to understanding the associated *loss of angular momentum* (but see Langer 1998; Meynet & Maeder 2003). Yet the angular momentum aspect of these winds may be equally relevant for understanding massive stars as the loss of mass itself, possibly in a mass range as low as ~10-15 $M_\odot$.

We first recapture the physics of bi-stable winds and BSB (Sect. 6.2.1), before presenting the current knowledge of rotational velocities of massive stars. We note a steep drop at ~22 000 K (Sect. 6.3) and propose two possible explanations for it. In the first one, the drop is due to the separation of MS objects from a second population of slow rotators (Sect. 6.4.1), whilst in the second one the slow rotation is the result of BSB (Sect. 6.4.2).

6.2 The physics of the mass loss bi-stability jump

The BS-Jump (Pauldrach & Puls 1990) is a theoretically predicted discontinuity where wind properties change from a modest $\dot{M}$, fast wind, to a higher $\dot{M}$, slow wind, when the effective temperature drops below ~22 000 K. Vink et al. (1999) predicted an increase in the mass-loss rate by a factor of ~5-7 (see the blue dotted line in Fig. 6.1) and a drop in the terminal wind velocity by a factor of ~2. Here the reason for the jump is an increased flux-weighted effective number of iron lines due to the recombination of Fe IV to Fe III (and not necessarily related to the optical depth of the Lyman continuum). In fact, the temperature of the BS-Jump was found to be weakly density dependent, with the BS-Jump starting as high as ~26 kK for the higher mass

models and dropping to ~22.5 kK for the lower mass models at ~20 $M_\odot$ (Vink et al. 2000).

Whilst the predicted drop in terminal wind velocity across the BS range has been confirmed (Crowther et al. 2006), the issue of a jump in mass loss is controversial. The jump may have been confirmed in radio data that suggest a local $\dot{M}$ maximum at the predicted temperature (Benaglia et al. 2007), but the predicted rates on the cool side of the jump are up to an order of magnitude larger than those found from state-of-the-art NLTE models (Vink et al. 2000; Trundle & Lennon 2005; Crowther et al. 2006; Markova & Puls 2008; Searle et al. 2008). To gain more insight into this mass-loss discrepancy one way forward is to search for other physical effects in the bi-stability region, which might assist us to unravel whether B supergiant mass-loss rates are as high as predicted, or as low as the spectral modelling suggests. Here we outline one such approach, involving stellar rotation rates in the region of the BS-Jump. Vink (2008) pointed out that the temperature of the bi-stability jump coincides with the position where the rotational velocities drop to smaller values (below 100 km/s), and suggested this might be due to BSB.

6.2.1 Bi-stability braking (BSB)

Employing stellar evolution models which include mass loss and rotation, we test whether the predicted increase in $\dot{M}$ at the bi-stability jump might lead to slower rotation. Figure 6.1 shows the run of the mass-loss rate and predicted rotational velocity as a function of temperature for a 40 $M_\odot$ star with an initial rotational velocity of 275 km/s. It shows a drastic drop in surface rotation rates for massive stars around 22 000 K, which is due to BSB in our models. When we do not increase the mass loss due to the BS-Jump, the stars remain rotating rapidly – despite the stellar expansion, as angular momentum is transferred from the core to the envelope. Bi-stability braking can only be efficient if the star spends a significant amount of time, i.e. part of its MS evolution, on the cool side of the BS-Jump. In our present standard models BSB only occurs above a critical mass of ~30 $M_\odot$ for the Galaxy, ~35 $M_\odot$ for the Large Magellanic Cloud (LMC), and ~50 $M_\odot$ for the Small Magellanic Cloud (SMC). In these models we employed a core overshooting parameter $\alpha_{\rm ov}$ of 0.335 of a pressure scale-height. A higher value of $\alpha_{\rm ov}$ lowers the critical mass. For instance, in a test calculation with $\alpha_{\rm ov}$=0.5 at LMC metallicity, BSB occurs already for a 20 $M_\odot$ star.

6.3 The steep drop in rotational velocity at 22 000 K

Howarth et al. (1997) catalogued $v\sin i$ values for 373 OB stars, with roughly half of them being supergiants (luminosity class I; red diamonds). We plot the $v\sin i$ values

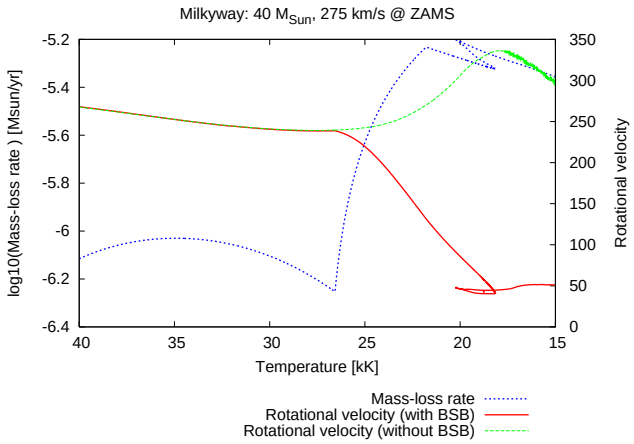

Figure 6.1: Mass-loss rate (blue dotted) and rotational velocities for a 40 $M_\odot$ star with an initial rotational velocity of 275 km/s, including the predicted BS-Jump (red solid) and without it (dashed green). A core overshooting parameter α_{ov} of 0.335 was employed in these models.

of this large and uniformly determined data-set in Fig. 6.2. The figure shows a drop in $v\sin i$ for stars hotter than 22 kK with values as high as ~400 km/s for all objects and as high as ~250 km/s for the supergiants only to values that *all* fall below 100 km/s for the cooler objects. In other words, we identify a general absence of rapidly rotating B supergiants[1]. As the stars in this data-set have not been analysed in detail, we resort to the results from the FLAMES Survey of massive stars (Evans et al. 2008), which involves data from the Galaxy, the LMC, and the SMC.

Figure 6.3 shows $v\sin i$ versus effective temperature for the FLAMES data, where we again note a steep drop in $v\sin i$ from values as high as ~400 km/s to values below 100 km/s. The data selection is a non-trivial undertaking, as we wish to optimise the sample size to sample homogeneity – in the presence of selection effects. The reason we employ a cut-off mass at 15 $M_\odot$ is that for the largest subset, i.e. that of the LMC, there is a detection limit that runs from ~20 $M_\odot$ at the hottest temperatures to ~10 $M_\odot$ at the cool part of the HRD (see Brott et al. 2010). For this reason, we choose an intermediate value of 15 $M_\odot$ as a minimum value. If we had chosen a higher mass cut-off, the drop feature would shift to a somewhat higher log $T_{\rm eff}$ (up to 27 kK). If we had opted for a lower mass cut-off, the feature shifts to log $T_{\rm eff}$ = 20 kK. Having noted this, tens of manual trials have shown that the sheer drop feature itself does not

[1]Note that the remaining broadness in the B supergiant spectra may (partly) be due to macro-turbulence in addition to, or instead of, rotational broadening (Conti & Ebbets 1977; Aerts et al. 2009).

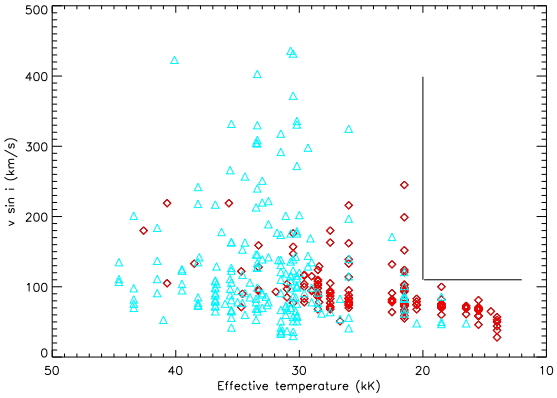

Figure 6.2: Projected rotational velocity $v\sin i$ of the Howarth et al. (1997) dataset of Galactic OB supergiants (red diamonds) and non-supergiants (blue triangles) as a function of log $T_{\rm eff}$ (Martins et al. 2005; Crowther et al. 2006, converted from spectral types using). We note that $v\sin i$ drops from values as high as ~400/250 km/s to values below 100 km/s at ~22 kK.

depend on a particular choice of mass range, and given the presence of the drop in both Figs. 6.2 and 6.3, as well as data presented in Fraser et al. (2010), we argue the drop feature is ubiquitous in the entire mass range ~10-60 $M_\odot$.

The dark grey lines overplotted in Fig. 6.3 show evolutionary tracks for the intermediate metallicity of the LMC with $v_{\rm rot}$ = 250 km/s by Brott et al. (2010) for masses of 15, 20, 30, 40 and 60 $M_\odot$. The black tick-marked dots on the tracks represent evolutionary time-steps of 10^5 years, and are intended to facilitate the comparison with observations.

6.4 Two possible interpretations for the drop in $v\sin i$

In Sect. 6.3, we highlighted the steep drop in the rotation rates of massive stars, but we have yet to provide an explanation for it. The question is whether the absence of rapidly rotating B supergiants is the result of BSB, or if the cooler slow rotators form an entirely separate population from the hotter MS stars.

6.4.1 The case for two populations

The cool objects (red asterisks) in Fig. 6.3 and the HRD of Fig. 6.4 are supergiants of luminosity class I, whilst the fast rotators are dominated by dwarfs (blue pluses).

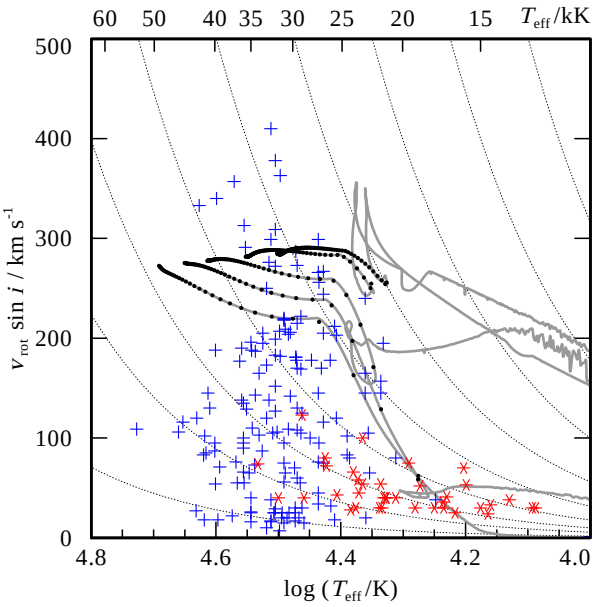

Figure 6.3: Rotational velocities vs. log $T_{\rm eff}$ for all FLAMES objects with evolutionary masses above 15 $M_{\odot}$. Luminosity classes are shown as blue pluses (luminosity classes II-V) and red stars (luminosity class I). The LMC evolutionary tracks including the predicted BS-Jump are shown in grey with initial $v_{\rm rot}$ = 250 km/s for five masses of 15, 20, 30, 40 and 60 $M_{\odot}$. It can be noted that the critical mass for BSB is ~35 $M_{\odot}$ in the LMC. The steepness of these tracks can be compared to the angular momentum conservation case, drawn as grey dotted background lines. The black dots on the tracks represent 10^5 year time-steps.

Although it is by no means obvious that supergiants cannot be in a H burning phase, the division in log$g$ might imply that we have a population of rapidly rotating MS objects on the one hand, whilst observing a population of slowly rotating evolved supergiants – which have somehow lost their angular momentum – on the other hand. Currently, we do not have sufficient information with respect to the evolutionary state of these cool supergiants. In principle, this part of the HRD can be populated with the products of binary evolution, although this would normally not be expected to lead to slowly rotating stars. Alternatively, one could envision the cooler objects to be the product of single star evolution, e.g. post-RSG or blue-loop stars, but the key point is that within the context of the two population interpretation, they are *not* core H burning.

A potential distinguishing factor between the "two population scenario" and BSB is that of the chemical abundances. We present LMC N abundances versus effective

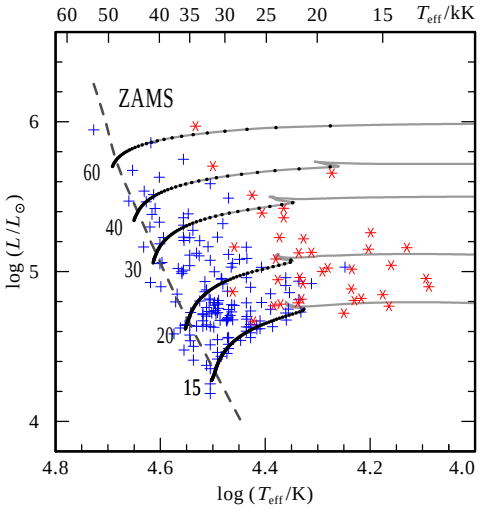

Figure 6.4: HRD of the FLAMES survey of massive stars. See the caption of Fig. 6.3 for an explanation of the symbols.

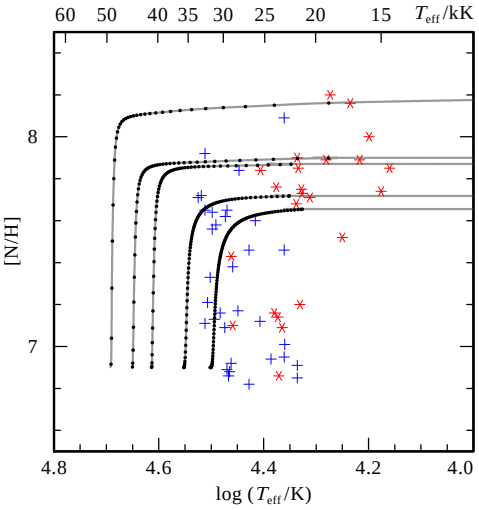

Figure 6.5: Nitrogen abundance vs. log $T_{\rm eff}$ for the LMC subset. See the caption of Fig. 6.3 for an explanation of the symbols.

temperature in Fig. 6.5, noting that N abundances could only be derived for a subset of our objects shown in Figs. 6.3 and 6.4. As the LMC baseline [N/H] equals ~6.9, the vast majority of slow rotators is found to be strongly N enhanced. Although rotating models can in principle account for large N abundances, the fact that such a large number of the cooler objects is found to be N enriched suggests an evolved nature for these stars.

6.4.2 The case for BSB

The second explanation for the steep drop in rotation rates is that both the objects cooler and hotter than 22 000 K reside on the MS, and that it is BSB that explains the slow rotation of the cooler B supergiants. The main argument for BSB is that it is predicted at the temperature where the rotational velocities are found to drop steeply. The evolutionary tracks in Fig. 6.4 indicate that the MS for the highest mass stars indeed appears rather broad, reaching as far as the BS-Jump temperature at 22 kK, and beyond. Therefore, mass loss seems capable of removing a considerable amount of angular momentum during the MS evolution for the highest mass stars.

6.5 Discussion

In principle it is possible that both effects of "two populations" and BSB occur simultaneously at 22 000 K, with BSB occurring above a certain critical mass, and the "two population" scenario taking over in the lower mass (10-20 $M_{\odot}$) range, but this situation might appear somewhat contrived. The strongest argument for the "two population scenario" are the large N abundances of the B supergiants, whilst the strongest argument for BSB is that the drop is observed at the correct location (whilst no such coincidence would be expected for the alternative interpretation).

Using our standard models, BSB can only operate above a certain critical mass and would not be able to explain the steep drop in rotational velocities of stars below the critical mass. The reason BSB does not operate at lower masses in our standard models (of Fig. 6.3) is that the drop feature has been used to constrain the core overshooting parameter of $\alpha_{\rm ov} = 0.335$. The applicability of BSB could be pushed to lower masses if the MS lifetime were extended. This could be achieved by increasing $\alpha_{\rm ov}$. When we enlarge $\alpha_{\rm ov}$ to 0.5, BSB also occurs at 20 $M_{\odot}$ for our Galactic and LMC models. What is clear is that the critical mass is model-dependent. For instance, the solar-metallicity models of Meynet & Maeder (2003) show BSB in the lower ($\sim$15-20 $M_{\odot}$) range.

We point out that if BSB were the correct explanation for the drop feature all the way down to $\sim$10 $M_{\odot}$, we would require a very large core overshooting parameter, and the consequences would be far-reaching. For instance, it would imply that B (and even A) supergiants are MS objects burning H in their cores. This would potentially solve the long-standing problem of the presence of such a large number of B supergiants. Moreover, if BSB could work for the entire mass range, it would also have profound implications for the Blue to Red (B/R) supergiant ratio that has been used to constrain massive star models as a function of metallicity for decades. Furthermore, if the absence of rapidly rotating B supergiants is due to BSB, one might wonder what this would imply for the evolutionary state of the presumably rapidly rotating B[e] supergiants. The rapid rotation of these extreme objects could possibly be related to close binary evolution or merging (Pasquali et al. 2000), but this requires future investigation.

If BSB would indeed occur in the lower mass range (down to $\sim$10 $M_{\odot}$), one should be aware that the derived overshooting parameter of 0.335 becomes a lower limit and that the real value becomes larger. Although this would be consistent with the suggested increase in $\alpha_{\rm ov}$ with stellar mass (Ribas et al. 2000), such a large value of $\alpha_{\rm ov}$ might be considered uncomfortable, as the highest mass data-point in Ribas et al. is based on one binary star, V380 Cyg, for which the results have been challenged (Claret 2003).

To summarise, we have presented two potential explanations for the steep drop in rotation rates at 22 000 K. Currently, we have insufficient information to decide which one is correct. In any case, our study demonstrates the important role of mass loss for massive star evolution, and especially the importance of *specifics* in its dependence on the stellar parameters. Furthermore, we have highlighted the significant influence of mass loss on the angular momentum transport in massive stars. Last but not least, BSB may offer a novel method of diagnosing the effects of mass loss via its influence on the angular momentum. Current analyses yield controversial results with respect to the existence of a BS jump. On the one hand, the predicted drop in terminal wind velocity across the BS range has been confirmed (Crowther et al. 2006). On the other hand, for temperatures below the BS-Jump, the mass-loss rates obtained from spectral modelling are generally much lower than predicted (Vink et al. 2000; Crowther et al. 2006).

A simultaneous investigation of the abundances, mass loss, and rotational properties of a large sample of massive stars, e.g. with the FLAMES II Tarantula survey (Evans et al. 2010), would be most helpful to settle these issues.

Bibliography

Abt, H. A., Levato, H., & Grosso, M. 2002a, ApJ, 573, 359

Abt, H. A., Levato, H., & Grosso, M. 2002b, ApJ, 573, 359

Aerts, C., Puls, J., Godart, M., & Dupret, M. 2009, A&A, 508, 409

Arnould, M., Goriely, S., & Jorissen, A. 1999, A&A, 347, 572

Asplund, M., Grevesse, N., & Sauval, A. J. 2005, in Astronomical Society of the Pacific Conference Series, Vol. 336, Cosmic Abundances as Records of Stellar Evolution and Nucleosynthesis, ed. T. G. Barnes, III & F. N. Bash, 25

Babel, J. & Montmerle, T. 1997, A&A, 323, 121

Balog, Z., Rieke, G. H., Su, K. Y. L., Muzerolle, J., & Young, E. T. 2006, ApJL, 650, L83

Balona, L. A. 1994, MNRAS, 268, 119

Bastian, N., Covey, K. R., & Meyer, M. R. 2010, ARA&A, 48, 339

Benaglia, P., Vink, J. S., Martí, J., et al. 2007, A&A, 467, 1265

Bertoldi, F. 1989, ApJ, 346, 735

Böhm-Vitense, E. 1958, ZAp, 46, 108

Bosch, G., Terlevich, E., & Terlevich, R. 2009, AJ, 137, 3437

Bouret, J., Lanz, T., Hillier, D. J., et al. 2003, ApJ, 595, 1182

Bourge, P., Théado, S., & Thoul, A. 2007, Communications in Asteroseismology, 150, 203

Braithwaite, J. 2006, A&A, 449, 451

Braithwaite, J. & Spruit, H. C. 2004, Nature, 431, 819

Briquet, M., Morel, T., Thoul, A., et al. 2007, MNRAS, 381, 1482

Bromm, V. & Larson, R. B. 2004, ARA&A, 42, 79

Bromm, V., Yoshida, N., Hernquist, L., & McKee, C. F. 2009, Nature, 459, 49

Brott, I., de Mink, S. E., Cantiello, M., et al. 2010a, A&A, submitted

Brott, I., Evans, C. J., Hunter, I., et al. 2010b, A&A, submitted

Brott, I., Hunter, I., Anders, P., & Langer, N. 2008, in American Institute of Physics Conference Series, Vol. 990, First Stars III, ed. B. W. O'Shea & A. Heger, 273–275

Brott, I., Hunter, I., de Koter, A., et al. 2009, Communications in Asteroseismology, 158, 55

Cantiello, M., Langer, N., Brott, I., et al. 2009, A&A, 499, 279
Chaboyer, B. & Zahn, J.-P. 1992, A&A, 253, 173
Chabrier, G. 2003, PASP, 115, 763
Charbonnel, C., Meynet, G., Maeder, A., Schaller, G., & Schaerer, D. 1993, A&AS, 101, 415
Chiosi, C. & Maeder, A. 1986, ARA&A, 24, 329
Claret, A. 2003, A&A, 399, 1115
Claret, A. 2007, A&A, 475, 1019
Conti, P. S. 1976, Memoires of the Societe Royale des Sciences de Liege, 9, 193
Conti, P. S. & Ebbets, D. 1977, ApJ, 213, 438
Cranmer, S. R. 2005, ApJ, 634, 585
Crowther, P. A., Hillier, D. J., Evans, C. J., et al. 2002, ApJ, 579, 774
Crowther, P. A., Lennon, D. J., & Walborn, N. R. 2006, A&A, 446, 279
Crowther, P. A., Schnurr, O., Hirschi, R., et al. 2010, MNRAS, 408, 731
Daflon, S., Cunha, K., Butler, K., & Smith, V. V. 2001, ApJ, 563, 325
de Koter, A., Heap, S. R., & Hubeny, I. 1997, ApJ, 477, 792
de Mink, S. E., Cantiello, M., Langer, N., et al. 2009, A&A, 497, 243
de Mink, S. E., Langer, N., & Izzard, R. G. 2010, ArXiv e-prints
Douglas, L. S., Bremer, M. N., Stanway, E. R., Lehnert, M. D., & Clowe, D. 2009, MNRAS, 400, 561
Dufour, R. J., Shields, G. A., & Talbot, Jr., R. J. 1982, ApJ, 252, 461
Dufton, P. L. 1972, A&A, 16, 301
Dufton, P. L., Ryans, R. S. I., Trundle, C., et al. 2005, A&A, 434, 1125
Dufton, P. L., Smartt, S. J., Lee, J. K., et al. 2006, A&A, 457, 265
Endal, A. S. & Sofia, S. 1976, ApJ, 210, 184
Endal, A. S. & Sofia, S. 1978, ApJ, 220, 279
Evans, C., Hunter, I., Smartt, S., et al. 2008, The Messenger, 131, 25
Evans, C. J., Bastian, N., Beletsky, Y., et al. 2010, in IAU Symposium, Vol. 266, IAU Symposium, 35–40
Evans, C. J., Lennon, D. J., Smartt, S. J., & Trundle, C. 2006, A&A, 456, 623
Evans, C. J., Smartt, S. J., Lee, J.-K., et al. 2005, A&A, 437, 467
Ferrario, L. & Wickramasinghe, D. 2006, MNRAS, 367, 1323
Fitzpatrick, E. L. & Garmany, C. D. 1990, ApJ, 363, 119
Fraser, M., Dufton, P. L., Hunter, I., & Ryans, R. S. I. 2010, MNRAS, 404, 1306
Fryer, C. L. 2003, Classical and Quantum Gravity, 20, 73
Gallart, C., Zoccali, M., & Aparicio, A. 2005, ARA&A, 43, 387
Garnett, D. R. 1999, in IAU Symposium, Vol. 190, New Views of the Magellanic Clouds, ed. Y.-H. Chu, N. Suntzeff, J. Hesser, & D. Bohlender, 266
Georgy, C., Meynet, G., Walder, R., Folini, D., & Maeder, A. 2009, A&A, 502, 611
Getman, K. V., Feigelson, E. D., Luhman, K. L., et al. 2009, ApJ, 699, 1454
Gies, D. R. & Lambert, D. L. 1992, ApJ, 387, 673
González, J. F., Ostrov, P., Morrell, N., & Minniti, D. 2005, ApJ, 624, 946
Grevesse, N., Noels, A., & Sauval, A. J. 1996, in Astronomical Society of the Pacific Conference Series, Vol. 99, Cosmic Abundances, ed. S. S. Holt & G. Sonneborn, 117

Grevesse, N., Sauval, A. J., & Blomme, R. 1994, in IAU Symposium, Vol. 154, Infrared Solar Physics, ed. D. M. Rabin, J. T. Jefferies, & C. Lindsey, 539
Haiman, Z. & Loeb, A. 1997, ApJ, 483, 21
Hamann, W., Koesterke, L., & Wessolowski, U. 1995, A&A, 299, 151
Heger, A. & Langer, N. 2000, ApJ, 544, 1016
Heger, A., Langer, N., & Woosley, S. E. 2000, ApJ, 528, 368
Heger, A., Woosley, S. E., & Spruit, H. C. 2005, ApJ, 626, 350
Herrero, A. 1993, Space Science Reviews, 66, 137
Hertzsprung, E. 1911, Publikationen des Astrophysikalischen Observatoriums zu Potsdam, 63
Howarth, I. D., Siebert, K. W., Hussain, G. A. J., & Prinja, R. K. 1997, MNRAS, 284, 265
Howarth, I. D. & Smith, K. C. 2001, MNRAS, 327, 353
Huang, W. & Gies, D. R. 2006a, ApJ, 648, 580
Huang, W. & Gies, D. R. 2006b, ApJ, 648, 591
Hubeny, I. & Lanz, T. 1995, ApJ, 439, 875
Hunter, I., Brott, I., Langer, N., et al. 2009a, A&A, 496, 841
Hunter, I., Brott, I., Lennon, D. J., et al. 2008a, ApJL, 676, L29
Hunter, I., Dufton, P. L., Smartt, S. J., et al. 2007, A&A, 466, 277
Hunter, I., Lennon, D. J., Dufton, P. L., et al. 2008b, A&A, 479, 541
Hunter, I., Lennon, D. J., Dufton, P. L., et al. 2009b, A&A, 504, 211
Iglesias, C. A. & Rogers, F. J. 1996, ApJ, 464, 943
Kaper, L., Henrichs, H. F., Fullerton, A. W., et al. 1997, A&A, 327, 281
Keller, S. C., Wood, P. R., & Bessell, M. S. 1999, A&AS, 134, 489
Kilian, J. 1992, A&A, 262, 171
Kippenhahn, R. & Thomas, H. 1970, in IAU Colloq. 4: Stellar Rotation, 20
Kippenhahn, R. & Weigert, A. 1990, Stellar Structure and Evolution (A&ALibary)
Korn, A. J., Keller, S. C., Kaufer, A., et al. 2002, A&A, 385, 143
Korn, A. J., Nieva, M. F., Daflon, S., & Cunha, K. 2005, ApJ, 633, 899
Kroupa, P. 2001, MNRAS, 322, 231
Kudritzki, R. P., Urbaneja, M. A., Bresolin, F., & Przybilla, N. 2008, Physica Scripta Volume T, 133, 014039
Kurt, C. M. & Dufour, R. J. 1998, in Revista Mexicana de Astronomia y Astrofisica, vol. 27, Vol. 7, Revista Mexicana de Astronomia y Astrofisica Conference Series, ed. R. J. Dufour & S. Torres-Peimbert, 202
Langer, N. 1991, A&A, 252, 669
Langer, N. 1998, A&A, 329, 551
Langer, N., Cantiello, M., Yoon, S.-C., et al. 2008, in IAU Symposium, Vol. 250, IAU Symposium, ed. F. Bresolin, P. A. Crowther, & J. Puls, 167–178
Langer, N., El Eid, M. F., & Fricke, K. J. 1985, A&A, 145, 179
Langer, N., Fricke, K. J., & Sugimoto, D. 1983, A&A, 126, 207
Langer, N. & Maeder, A. 1995, A&A, 295, 685
Lee, H. & Chen, W. P. 2007, ApJ, 657, 884
Lennon, D. J., Dufton, P. L., & Crowley, C. 2003, A&A, 398, 455
Lennon, D. J., Dufton, P. L., Keenan, F. P., & Holmgren, D. E. 1991, A&A, 246, 175

MacGregor, K. B. & Cassinelli, J. P. 2003, ApJ, 586, 480
Maeder, A. 1987, A&A, 178, 159
Maeder, A. 1999, A&A, 347, 185
Maeder, A. 2000, New Astronomy Review, 44, 291
Maeder, A. & Meynet, G. 1987, A&A, 182, 243
Maeder, A. & Meynet, G. 2000, ARA&A, 38, 143
Maeder, A. & Meynet, G. 2001, A&A, 373, 555
Maeder, A. & Meynet, G. 2005, A&A, 440, 1041
Maeder, A., Meynet, G., Ekström, S., & Georgy, C. 2009, Communications in Asteroseismology, 158, 72
Markova, N. & Puls, J. 2008, A&A, 478, 823
Marquez-Lugo, R. A. & Phillips, J. P. 2010, MNRAS, 407, 94
Martayan, C., Diago, P., Gutiérrez-Soto, J., et al. 2008, ArXiv e-prints
Martayan, C., Frémat, Y., Hubert, A., et al. 2006, A&A, 452, 273
Martayan, C., Frémat, Y., Hubert, A., et al. 2007, A&A, 462, 683
Martins, F., Schaerer, D., & Hillier, D. J. 2002, A&A, 382, 999
Martins, F., Schaerer, D., & Hillier, D. J. 2005, A&A, 436, 1049
Martins, F., Schaerer, D., Hillier, D. J., & Heydari-Malayeri, M. 2004, A&A, 420, 1087
Mason, B. D., Hartkopf, W. I., Gies, D. R., Henry, T. J., & Helsel, J. W. 2009, AJ, 137, 3358
Massey, P., Bresolin, F., Kudritzki, R. P., Puls, J., & Pauldrach, A. W. A. 2004, ApJ, 608, 1001
Massey, P., Puls, J., Pauldrach, A. W. A., et al. 2005, ApJ, 627, 477
McKee, C. F. & Ostriker, E. C. 2007, ARA&A, 45, 565
McKibben, W. P., Bagnuolo, Jr., W. G., Gies, D. R., et al. 1998, PASP, 110, 900
McWilliam, A. 2010, ArXiv e-prints
McWilliam, A. & Rauch, M. 2004, Origin and Evolution of the Elements
Mermilliod, J. & Maeder, A. 1986, A&A, 158, 45
Meynet, G., Eggenberger, P., & Maeder, A. 2011, A&A, 525, L11+
Meynet, G. & Maeder, A. 1997, A&A, 321, 465
Meynet, G. & Maeder, A. 2000, A&A, 361, 101
Meynet, G. & Maeder, A. 2003, A&A, 404, 975
Meynet, G. & Maeder, A. 2005, A&A, 429, 581
Meynet, G., Maeder, A., Schaller, G., Schaerer, D., & Charbonnel, C. 1994, A&AS, 103, 97
Mitalas, R. & Falk, H. J. 1984, MNRAS, 210, 641
Mokiem, M. R., de Koter, A., Evans, C. J., et al. 2007, A&A, 465, 1003
Mokiem, M. R., de Koter, A., Evans, C. J., et al. 2006, A&A, 456, 1131
Morales, M. F. & Wyithe, J. S. B. 2010, ARA&A, 48, 127
Morel, T., Butler, K., Aerts, C., Neiner, C., & Briquet, M. 2006, A&A, 457, 651
Morel, T., Hubrig, S., & Briquet, M. 2008, A&A, 481, 453
Napiwotzki, R., Schoenberner, D., & Weidemann, V. 1991, A&A, 243, L5
Nieuwenhuijzen, H. & de Jager, C. 1990, A&A, 231, 134
Nieva, M. F. & Przybilla, N. 2006, ApJL, 639, L39
Nieva, M. F. & Przybilla, N. 2008, A&A, 481, 199
Ohkubo, T., Nomoto, K., Umeda, H., Yoshida, N., & Tsuruta, S. 2009, ApJ, 706, 1184

Packet, W. 1981, A&A, 102, 17
Papoulis, A. 1984, Probability, Random Variables, and Stochastic Processes (New York: McGraw-Hil)
Pasquali, A., Nota, A., Langer, N., Schulte-Ladbeck, R. E., & Clampin, M. 2000, AJ, 119, 1352
Pauldrach, A. W. A. & Puls, J. 1990, A&A, 237, 409
Peimbert, M., Luridiana, V., & Peimbert, A. 2007, ApJ, 666, 636
Penny, L. R. & Gies, D. R. 2009, ApJ, 700, 844
Petrovic, J., Langer, N., & van der Hucht, K. A. 2005a, A&A, 435, 1013
Petrovic, J., Langer, N., Yoon, S., & Heger, A. 2005b, A&A, 435, 247
Pinsonneault, M. 1997, ARA&A, 35, 557
Pinsonneault, M. H., Kawaler, S. D., Sofia, S., & Demarque, P. 1989, ApJ, 338, 424
Plyusnina, L. A. 2010, Solar Physics, 261, 223
Porter, J. M. & Rivinius, T. 2003, PASP, 115, 1153
Prandtl, L. 1925, Z. angew. Math. Mech, 5
Prinja, R. K. & Howarth, I. D. 1988, MNRAS, 233, 123
Przybilla, N., Firnstein, M., Nieva, M. F., Meynet, G., & Maeder, A. 2010, A&A, 517, A38
Przybilla, N., Nieva, M., & Butler, K. 2008, ApJL, 688, L103
Puls, J., Vink, J. S., & Najarro, F. 2008, A&A Rev., 16, 209
Reitermann, A., Stahl, O., Wolf, B., & Baschek, B. 1990, A&A, 234, 109
Ribas, I., Jordi, C., & Giménez, Á. 2000, MNRAS, 318, L55
Rolleston, W. R. J., Smartt, S. J., Dufton, P. L., & Ryans, R. S. I. 2000, A&A, 363, 537
Russell, H. N. 1913, The Observatory, 36, 324
Salpeter, E. E. 1955, ApJ, 121, 161
Sana, H. & Evans, C. J. 2010, ArXiv e-prints
Sana, H., Gosset, E., & Evans, C. J. 2009, MNRAS, 400, 1479
Sana, H., Gosset, E., Nazé, Y., Rauw, G., & Linder, N. 2008, MNRAS, 386, 447
Sana, H. & Le Bouquin, J. 2010, in Revista Mexicana de Astronomia y Astrofisica Conference Series, Vol. 38, Revista Mexicana de Astronomia y Astrofisica Conference Series, 27–29
Savaglio, S. 2006, New Journal of Physics, 8, 195
Schaerer, D., Meynet, G., Maeder, A., & Schaller, G. 1993, A&AS, 98, 523
Schröder, K., Pols, O. R., & Eggleton, P. P. 1997, MNRAS, 285, 696
Searle, S. C., Prinja, R. K., Massa, D., & Ryans, R. 2008, A&A, 481, 777
Serenelli, A. M. 2010, Ap&SS, 328, 13
Shaver, P. A., McGee, R. X., Newton, L. M., Danks, A. C., & Pottasch, S. R. 1983, MNRAS, 204, 53
Sigut, T. A. A. 1996, ApJ, 473, 452
Simón-Díaz, S. & Herrero, A. 2007, A&A, 468, 1063
Slettebak, A. 1968, ApJ, 154, 933
Spruit, H. C. 2002, A&A, 381, 923
Spruit, H. C. 2006, ArXiv Astrophysics e-prints
Stothers, R. B. 1991, ApJ, 383, 820
Strom, S. E., Wolff, S. C., & Dror, D. H. A. 2005, AJ, 129, 809

Suijs, M. P. L., Langer, N., Poelarends, A., et al. 2008, A&A, 481, L87
Tassoul, J. 1978, Theory of rotating stars (Princeton: University Press)
Townsend, R. H. D., Oksala, M. E., Cohen, D. H., Owocki, S. P., & ud-Doula, A. 2010, ApJL, 714, L318
Townsend, R. H. D., Owocki, S. P., & Howarth, I. D. 2004, MNRAS, 350, 189
Trundle, C., Dufton, P. L., Hunter, I., et al. 2007, A&A, 471, 625
Trundle, C. & Lennon, D. J. 2005, A&A, 434, 677
ud-Doula, A. & Owocki, S. P. 2002, ApJ, 576, 413
Vacca, W. D., Garmany, C. D., & Shull, J. M. 1996, ApJ, 460, 914
Venn, K. A. 1995, ApJS, 99, 659
Venn, K. A. 1999, ApJ, 518, 405
Venn, K. A. & Przybilla, N. 2003, in Astronomical Society of the Pacific Conference Series, Vol. 304, Astronomical Society of the Pacific Conference Series, ed. C. Charbonnel, D. Schaerer, & G. Meynet, 20
Villamariz, M. R. & Herrero, A. 2005, A&A, 442, 263
Vink, J. S. 2008, in IAU Symposium, Vol. 252, IAU Symposium, ed. L. Deng & K. L. Chan, 271–281
Vink, J. S., Brott, I., Gräfener, G., et al. 2010, A&A, 512, L7
Vink, J. S. & de Koter, A. 2005, A&A, 442, 587
Vink, J. S., de Koter, A., & Lamers, H. J. G. L. M. 1999, A&A, 350, 181
Vink, J. S., de Koter, A., & Lamers, H. J. G. L. M. 2000, A&A, 362, 295
Vink, J. S., de Koter, A., & Lamers, H. J. G. L. M. 2001, A&A, 369, 574
von Zeipel, H. 1924, MNRAS, 84, 665
Vrancken, M., Hensberge, H., David, M., & Verschueren, W. 1997a, A&A, 320, 878
Vrancken, M., Hensberge, H., David, M., & Verschueren, W. 1997b, A&A, 320, 878
Vrancken, M., Lennon, D. J., Dufton, P. L., & Lambert, D. L. 2000, A&A, 358, 639
Wade, G. A., Fullerton, A. W., Donati, J., et al. 2006, A&A, 451, 195
Walborn, N. R. 1970, ApJL, 161, L149+
Walter, D. K., Dufour, R. J., & Hester, J. J. 1992, ApJ, 397, 196
Wellstein, S., Langer, N., & Braun, H. 2001, A&A, 369, 939
Wolff, S. C. 1968, PASP, 80, 281
Wolff, S. C., Strom, S. E., Dror, D., & Venn, K. 2007, AJ, 133, 1092
Woosley, S. E. & Heger, A. 2006, ApJ, 637, 914
Yoon, S. & Langer, N. 2005, A&A, 443, 643
Yoon, S.-C., Langer, N., & Norman, C. 2006, A&A, 460, 199
Zahn, J. 1992, A&A, 265, 115
Zahn, J., Brun, A. S., & Mathis, S. 2007, A&A, 474, 145
Zinnecker, H. & Yorke, H. W. 2007, ARA&A, 45, 481

Samenvatting in het Nederlands

Sterren worden gevormd met een breed scala aan massa's, te beginnen bij een paar tienden van de massa van onze zon ($M_\odot$) tot misschien zelfs honderden $M_\odot$ (Crowther et al. 2010, zie ook Fig. 1.1). Dit proefschrift richt zich op de zwaarste sterren. Zij zijn ook de helderste sterren, zichtbaar tot op enorme afstanden in het lokale universum (Kudritzki et al. 2008) en in het geïntegreerde licht van ster-vormende sterrenstelsels bij hoge roodverschuivingen (Douglas et al. 2009). Er wordt geschat dat er $\sim 10^{11}$ sterren in ons melkwegstelsel zijn. Zware sterren[2] vertegenwoordigen slechts een klein deel van dit aantal. In andere grote sterrenstelsels wordt een vergelijkbare situatie verwacht. Voor stellaire normen is de gemiddelde levensduur van een zware ster erg kort, slechts een paar miljoen jaar. Hoewel het aantal zware sterren in het heelal relatief klein is en hun levens heel kort zijn, hebben zware sterren niettemin een sterke invloed op hun omgeving door hun uitstromende atmosferen, straling en explosieve dood. Ondanks het belang van zware sterren is hun evolutie nog steeds slecht begrepen. Voor de lage- en middelbare-massa sterren zijn evolutionaire modellen redelijk succesvol in het weergeven van de belangrijkste waarneembare eigenschappen, zie bijv. Gallart et al. (2005) voor een review over de interpretatie van kleur-magnitude diagrammen met behulp van sterevolutieberekeningen, of Serenelli (2010) omtrent het standaardmodel voor de zon. In tegenstelling hiermee, blijft het voor zware sterren een grote uitdaging om zelfs maar de verdeling van sterren in het Hertzsprung-Russell diagram te reproduceren. Zo voorspellen evolutiemodellen een duidelijk gedefinieerde koele rand van de hoofdreeksband en een 'kloof' tussen sterren die in hun kern waterstof fuseren (de hoofdreekssterren) dan wel helium fuseren. Observationele steekproeven tonen deze scherpe overgang echter niet. De door evolutiemodellen voorspelde kloof wordt door vele O-en B-superreuzen bevolkt waarvan de evolutionaire fase onduidelijk is (bijv. Fitzpatrick & Garmany 1990; Evans et al. 2006; Vink et al. 2010). Als een mogelijke oplossing voor dit dilemma werd in sterevolutieberekeningen rotatie geïntroduceerd (bijv. Heger et al. 2000; Meynet & Maeder 1997). Alle sterren draaien,

[2] sterren die zwaarder zijn dan ongeveer $8\,M_\odot$

een eigenschap die jonge sterren erven van de moleculaire wolken waarin ze zijn geboren. De zon is een zeer trage rotator. Slechts eens in de ongeveer 27 dagen draait ze rond haar as (Plyusnina 2010), hetgeen op een equatoriale rotatiesnelheid van ongeveer 2 km/s neerkomt. Zware hoofdreekssterren draaien gemiddeld met veel hogere snelheden, in de orde van 100 km/s (Hunter et al. 2008b; Martayan et al. 2006, 2007; Penny & Gies 2009).

In de context van rotatie zijn met name de hoeveelheden helium en stikstof die aan het oppervlak worden aangetroffen van bijzonder belang. In sommige zware O- en B-type sterren en in reuzen en superreuzen worden deze elementen verrijkt aangetroffen ten opzichte van de initiële hoeveelheden van dit materiaal (Gies & Lambert 1992; Herrero 1993; Vrancken et al. 2000; Przybilla et al. 2010). Tot recentelijk (maar zie dit proefschrift) zijn bepalingen van de chemische samenstelling van de atmosferen van zware sterren veelal beperkt gebleven tot objecten met lage geprojecteerde rotatiesnelheden. Voor die sterren die verrijkt waren in stikstof werd geconcludeerd dat het snelle rotators moesten zijn die vrijwel recht op hun pool werden gezien in overeenstemming met de fysica van rotationele menging in snel draaiende sterren.

Het grootste deel van het in dit proefschrift beschreven werk richt zich op evolutionaire modellen van de fase van waterstofverbranding van zware roterende sterren. We concentreren ons op de gevolgen van de rotatie voor de oppervlakte abundanties, met name die van stikstof. Wij presenteren de resultaten voor stikstofmetingen van de VLT-FLAMES Survey van Zware Sterren (FLAMES Survey), voor set van snel en langzaam roterende B-type sterren. Onze evolutionaire modellen worden vergeleken met, en geijkt aan, deze metingen. We maken hiervoor gebruik van gedetailleerde populatie-synthese modellen, die het mogelijk maken het effect van verschillende inclinatiehoeken en diverse selectie-effecten op de waarnemingen te onderzoeken. Het grote aantal (meer dan driehonderd) B-sterren dat in de context van de FLAMES Survey is waargenomen en geanalyseerd biedt een unieke kans om de huidige theorie van rotationele menging op een werkelijk kwantitatieve manier te testen.

De hoofdstukken in dit proefschrift

In hoofdstuk 2 introduceren we set evolutionaire modellen die we zullen gebruiken voor de analyse van de FLAMES Survey data. Hoofdstuk 3 beschrijft een eerste analyse van vroege B-type sterren in de Grote Magelhaense Wolk (LMC) met behulp van de evolutionaire modellen van hoofdstuk 2. Hoofdstuk 4 presenteert de analyse van de Klein Magelhaense Wolk sterren (SMC) en de Galactische sterren en vergelijkt deze met modellen. We presenteren een verfijnde vergelijking van de LMC steekproef in hoofdstuk 3. In hoofdstuk 5 beschrijven we onze nieuw ontwikkelde populatie synthese code STARMAKER, waarmee voor een statistisch significante groep sterren de verdeling van stereigenschappen zoals oppervlakte abundanties en rotatiesnelheden kan worden voorspeld voor willekeurige stervormingsgeschiedenis. Met deze code kunnen we de theorie van rotationele menging testen.

Hoofdstuk 6 onderzoekt twee alternatieve scenario's die verantwoordelijk zouden kunnen zijn voor een waargenomen daling in de rotatie snelheid van B-sterren zodra die een oppervlakte temperatuur hebben die lager is dan 22 000 K. We bespreken of de daling van

de rotatiesnelheid het gevolg is van het bereiken van het eind van de hoofdreeks of van een sterke toename van een bij deze temperatuur plotseling sterk toenemend massaverlies.

Hoofdstuk 2: Evolutionaire modellen en isochronen

We presenteren een raster met meer dan 600 stellaire modellen die zijn geëvolueerd voorbij het einde van de hoofdreeksfase. De modellen hebben initiële massa's tussen 5 en 60 $M_{\odot}$ en initiële rotatiesnelheden tussen 0 en 550 km/s. Voor dit netwerk van modellen hebben we een op de abundanties van H II gebieden gebaseerde initiële chemische samenstelling gebruikt, die past bij sterren in de SMC, LMC en de Melkweg. Er is bijzondere aandacht besteed de initiële (of basislijn) abundanties omdat de mate van stikstof-verrijking tijdens de daaropvolgende evolutie zeer afhankelijk is van de initiële waarden van de CNO-elementen. Van bijzonder belang voor hoofdstuk 6 is de övershooting"calibratie in dit grid, die wij baseren op een waargenomen daling van de projecteerde rotatiesnelheid als functie van de oppervlaktezwaartekracht.

Verder presenteren we in dit hoofdstuk een uitgebreide set van isochronen. Isochronen voor gelijke leeftijd maar variabele rotatiesnelheid vormen een gebied in het HR-diagram in plaats van een lijn, wat interessante nieuwe inzichten over stellaire populaties opleverd. Deze nieuwe isochronen maken ook een verfijning van de huidige populatie synthese modellen van jonge clusters mogelijk.

Hoofdstuk 3: Rotatie en stikstof-verrijking als sleutel voor het begrijpen van de evolutie van zware sterren

In dit hoofdstuk presenteren we stikstof-abundanties voor de LMC sterren in de FLAMES Survey data. De resultaten worden vergeleken met de voorspellingen beschreven in hoofdstuk 2. Al in deze eerste studie wordt duidelijk dat er twee groepen van sterren bestaan die in strijd zijn met de verwachtingen die voortvloeien uit sterevolutieberekeningen. Wij vinden een groep van niet-verrijkte sterren met hoge projecteerde rotatie snelheden. De zwaartekrachten aan het oppervlak van deze sterren geven aan dat zij dicht bij het einde van waterstof verbranding zijn. Omdat de projecteerde rotatiesnelheid slechts een ondergrens voor de ware rotatiesnelheid levert, wordt voor deze groep een sterke verrijking verwacht. Verder vinden wij ook een groep verrijkte sterren met zeer lage projecteerde rotatie snelheden. Hoewel sommige daarvan snelle rotators zouden kunnen zijn, is het uiterst onwaarschijnlijk dat de rotatieas van al deze objecten vrijwel precies in de richting van de aarde is georiënteerd. Beide groepen zijn in strijd met ons begrip van rotationele menging in enkelvoudige niet-magnetisch zware sterren.

Hoofdstuk 4: Evolutie van de chemische samenstelling van snel roterende B-type sterren in het Melkwegstelsel en de Magelhaense Wolken

In dit hoofdstuk breiden we de analyse van de FLAMES Survey data uit naar B sterren in ons Melkwegstelsel en de Kleine Magelhaense Wolk. In de SMC is er ook een groep van langzaam draaiende in stikstof verrijkte sterren, vergelijkbaar met de overeenkomstige groep

in de LMC. Voor de snel roterende niet-verrijkte groep kan geen tegenhanger worden geïdentificeerd, mogelijk omdat er voor de snelst draaiende sterren rotators slechts bovengrenzen voor de stikstof hoeveelheid beschikbaar zijn. Een verbetering ten opzichte van de vorige hoofdstuk is de her-definiëring van de problematische groep van niet-verrijkte snel roterende objecten. In de groep galactische sterren vinden we geen significante verrijking. Echter, slechts en kleine fractie van de snelle rototors in deze groep is voldoende geëvolueerd om verrijking te laten zien. We concluderen dat om een beter inzicht te krijgen in de rol van rotationele menging het belangrijk is om van de geanalyseerde sterren te achterhalen of ze deel uitmaken van een dubbelstersysteem, met name of de problematische groepen (stikstof rijke langzaam draaiende sterren en stikstof arme snel draaiende sterren) een opvallend hoge fractie van dit soort dubbelsterren kent.

Hoofdstuk 5: Het simuleren van een LMC populatie van jonge B-type sterren als test voor menging door rotatie

We presenteren de nieuw ontwikkelde populatie synthese code STARMAKER en gebruiken dit computerprogramma om de groep jonge B-type sterren in de LMC (beschreven in hoofdstuk 4) te simuleren. De set van stellaire evolutiemodellen beschreven in hoofdstuk 2 wordt als input voor onze populatie synthese simulatie gebruikt. De onderliggende geschiedenis van de stervormingen en de verdeling van de beginsnelheden zijn empirisch bepaald (Hunter et al. 2008b). Om een eerlijke vergelijking mogelijk te maken, gebruiken wij voor onze simulatie dezelfde selectie-effecten als in de waargenomen steekproef voorkomen. Onze simulaties reproduceren de fractie van sterren die niet verrijkt zijn in stikstof, maar voorspellen twee keer zoveel verrijkte snelle rotators als zijn waargenomen. De groepen van de niet-verrijkte snelle rotators en verrijkte trage rotators (zie hoofdstuk 3) kan niet worden gereproduceerd door onze populatie synthese, waarin is aangenomen dat alle sterren enkelvoudig zijn. We beargumenteren dat het onwaarschijnlijk is dat de groep van verrijkte trage rotators door dubbelster evolutie geproduceerd wordt. Mogelijk zijn effecten ten gevolge van magnetische velden nodig om deze groep te begrijpen.

Hoofdstuk 6: De aard van B superreuzen – aanwijzingen voor een steile daling in de rotatiesnelheden bij 22 000 K en de mogelijkheid van *"bi-stability"breaking*

B-type sterren koeler dan 22 000 K hebben altijd een waargenomen geprojecteerde rotatiesnelheid die lager is dan ongeveer 100 km/sec. Hetere O- en B-type sterren kunnen veel hogere waarden hebben, tot meer dan 400 km/sec. We onderzoeken de mogelijkheid dat de waargenomen daling van de projecteerde rotatie snelheid als functie van de effectieve temperatuur, maar die zich ook manifesteerd als functie van de oppervlaktezwaartekracht, kan worden veroorzaakt door een plotselinge toename in de massaverlies (de zogenaamde "bistabiliteit jump") bij ongeveer 22 000 K, (Vink et al. 2000, 2001). Een sterk sterwind kan effectief draaiimpulsmoment afvoeren waardoor een ster langzamer gaat draaien. In hoofdstuk 2 wordt het waargenomen in geprojecteerde rotatiesnelheid gebruikt om de *overshooting* parameter te kalibreren, i.e. er wordt aangenomen dat als sterren langzamer gaan draaien als ze van de hoofdreeks af evolueren. We hebben vast gesteld dat het alternatieve massaverlies

scenario een soortgelijk effect kan veroorzaken wanneer de *overshooting* parameter zo groot is dat sterren al op de hoofdreeks de *bi-stability jump* ondergaan. In onze berekeningen is dit het geval voor sterren met een initiële massa die groter is dan 30 $M_{\odot}$. Bij lagere massa's zou het massaverlies scenario ook kunnen werken mits een veel grotere overshooting parameter wordt aangenomen dan die wij in onze modellen (hoofdstuk 2) toepassen.

Acknowledgements

. . .

Try sitting yourself in an office chair,
and turn around a few times with a lot of flair.

Imagine it is past noon and you had lunch,
then I think you will get a hunch.

Because a star who is heavy,
obviously has a full belly.

And, perhaps bored, he is spinning around fast,
his happy demeanor will no longer last.

His spectrum will slowly become green-shifted,
because with illness he has now become afflicted.

The mass he has so voraciously collected,
will confuse his stomach and ultimately be ejected!

So I hope I have made you aware,
that you should be careful on your office chair.

. . .

I got this poem for Sinterklaas 2007, together with the five pointed star shown on the back-cover. It describes the subject of this thesis in a way I would have never thought of. Unfortunately, I still don't know who wrote the poem, but it inspired me throughout my PhD. Thanks a lot to whoever wrote this poem. It's gorgeous.
Many people have contributed over the last years to the success of this work. Even more helped me over the last decade to let my dream, to become an Astronomer, come true. There are many people to thank, more than I can name here.

My undergraduate years at the Hamburg Observatory were certainly an important phase on the way to become an astronomer. I would like to thank Peter Hauschildt for being an excellent supervisor during that time and Andreas Schweizer for teaching me most tricks about Linux, BSD and program compiling I know. I'm happy that I can count you to my

friends ever since and I'm looking forward to be able to work more with you two again in the near future. Thanks also go to my old colleagues from the Hamburg Observatory, Alex, Knopi, Costa, Matze, Andy, Dieter, Caro, Michi, the A-Team (Annette, Angelika und Anke). In particular I want to say thank you to Norbert Christlieb and Volker Beckmann. @Volker: It's now a bit more than 10 years ago that you finished your PhD and were my supervisor during the school internship. Now you are building your own institute and I have finished my own PhD. Thank you for all the advice, motivation and help you gave me over the years. Let's see where we are in 10 years from now. @Norbert C.: About 10 years ago, when you where finishing your PhD, me and a friend from school came to the Observatory to learn what a spectrum is. That was the day when I learned that a spectrum has spectral lines, and consist not only of pretty colors. You also gave us the priceless advice to go to the International Astronomical Youth Camp (IAYC), which became so important to me. Without that camp I would never have become the international vagabond I am today. I treasure the memories of the IAYC summers and I still come across someone from those camps everywhere I go. Kalle, Nadi, Ingo, Aarnoud, Betti, Jeroen, Francesca, Anne, Rolf, Jojo, Holger and Markus thank you for meeting since more than ten years for birthday parties, in which every country they are.

I also want to thank my master thesis supervisor Thierry Courvoisier for having me over in Geneva and the new friends I made at the INTEGRAL Science Data Centre. Peter and Bärbel Kretschmar, Ingo Kreykenbom and JC Leyder thanks for your support.

Regarding the more recent past, I would like to thank my PhD supervisors Norbert Langer and Alex de Koter for their advice and guidance in the process of writing this thesis. It was not always easy, sometimes the work was truly nerve-wracking. But I think we managed to bring it to a good end and I'm proud of this book. Special thanks goes to Chris Evans and Paul Dunstall for our many skype discussions at any hour of day or night. @Chris: I will never forget when one day at midnight my skype chat popped open and you started discussing with me some massive star science after you came back from a pub evening with Mark. I really enjoyed these discussions and hope that we will have many more of them in the future. @Paul: I'm sorry that I caused Philip to make you analyze Be stars, but I think we got some very interesting results and I enjoyed working with you. For me this was definitely a highlight of my time in Utrecht. Also not to be forgotten, Ian, Danny, Philip, Jorick Vink, Selma, Matteo and Lianne, it was great working with you. @Lianne and Alex: I stopped counting how often we drove to Bonn together. However, I learned a lot about dutch and latin american politics from our discussions in Alex car. And football not to forget. Thanks for those rides. Thanks to Enrique and Hilding for being my Bonn office mates the last months of this thesis. @Karen and Markus: thanks for showing me the nice sides of Bonn and Cologne outside the Argelander-Insitute. @Rob Izzard: Thanks for letting me stay at your flat, and stay as you are.

@Matteo, Bob, Joke, Carlo and Jos: Thanks for being my Utrecht office mates in the past years. @Sandra: I'd always go with you on a coffee break again, especially with cake. @Peter A.: I don't remember how many discussions we had over isochrones, stellar populations etc. Thanks for helping me with all my programming problems and uncountable chocolate breaks. Thanks also to my colleagues from the Astronomical Insitute Utrecht: Eveline, Frans, Carlo, Sabina, Helena, Hector, Anna, Maria, Catherine, Theodora, Remco, Diederik, Michiel,

Esteban, Nikola, Sander, Evert and Tim. Special thanks to Onno, Henny and Christoph for their advice and support. @Onno: and for packing our kitchen equipment.

@Vir, Saskia, Joke, Jonas, Peter, Frank, Liz, Josh, and Badger for the many nights of slaughtering orks, kobolts and undead creatures, fighting elementals and outer-plain aberrations with sharp steel, flapping wings and sometimes the help of a singing harp. I will miss our D&D, gaming and pizza evenings. You made Utrecht into a home for me.

Also special thanks to everybody who was directly involved with the finishing of this book. Alex, Joke and Eveline for helping with the Dutch translation, Liz and Lyn for spellchecking my introduction and Liz for getting the references in order. @Matteo: I guess you will recognize the layout, thanks for the tex-files of your thesis manuscript. @Gloria: Thanks for your moral and creative support whenever needed. Your tip with writing emails to friends (even though you never send them) helped me to overcome the daily writers block. Some of the early tex files of my papers are full with those letters. Hope no one will read them ever.

And some people I want to mention, but have not done so far: @Adrian: I didn't believe you when you told me you gonna through me around in Paris. Now I do. RnR rocks. My teachers, especially Frau Sahlmann, Ulli and Herr Brühning, who accompanied me over the first years of my scientific education. @Frau Sahlmann: I remember how I asked you in class, if there is no better way to explain magnetism, than the little magnets picture that orientate themselves in the magnetic field. Back then I found your answer a bit unsatisfactory, but now I understand that explaining magnetism to a student in the 8 or 9th grade without the knowledge of the structure of matter is indeed very challenging.

I also want to mention my new colleagues in Vienna: Manuel, Armin, Christian, Peter W., Simon, and Steffi. Thank you for welcoming me so nicely, I already feel at home. And especially Armin for helping unloading the overloaded truck on midnight of January 1st.

Last but not least, I would like to thank my parents and my sister, who have always encouraged me to follow my dreams. And not to forget: Katha, Cata, Amy, Yoshi, Jan and Maike Haza for being my friends since now almost 20 years. @Jakob: Thank you for coming to live with me in the Netherlands and now moving along to Austria. I'm looking forward to the years to come.

Curriculum Vitae

Born:	6 February 1981, Hamburg, Germany
Master of Science:	Physics & Astronomy, University Hamburg, Germany (2000 – 2006) INTEGRAL Science Data Centre (ISDC), University Geneva Switzerland (2004 – 2005) Thesis: An Extragalactic Deep Field Observation with *INTEGRAL/IBIS* Supervisors: Peter H. Hauschildt, Thierry J.-L. Courvoisier
Doctorate:	Astrophysics, Astronomical Institute, Utrecht University The Netherlands (2006 – 2010) Thesis: Modeling Populations of Rotationally Mixed Massive Stars Supervisors: Norbert Langer, Alex de Koter
Postdoc:	Institute for Astronomy, University of Vienna, Austria (2011 – current) Research area: Star formation Supervisor: Manuel Guedel

List of Publications

Published in refereed journals

- Vink, J. S., **Brott, I.**, Gräfener, G.,et al. 2010, The nature of B supergiants: clues from a steep drop in rotation rates at 22 000 K. The possibility of Bi-stability braking, A&A,512,L7
- Sordo, R., Vallenari, A., Tantalo, R.,et al. 2010, Synthetic stellar and SSP libraries as templates for Gaia simulations, Ap&SS, 2, 38
- Cantiello, M., Langer, N.,**Brott, I.**, et al. 2009, Sub-surface convection zones in hot massive stars and their observable consequences, A&A, 499, 279
- Hunter, I., **Brott, I.**, Langer, N, et al. 2009, The VLT-FLAMES survey of massive stars: constraints on stellar evolution from the chemical compositions of rapidly rotating Galactic and Magellanic Cloud B-type stars, A&A 496, 841
- de Mink, S. E., Cantiello, M., Langer, N., et al. 2009, Rotational mixing in massive binaries: detached short-period systems, A&A, 497,243
- Cantiello, M., Langer, N., **Brott, I.**, et al. 2009, On the origin of microturbulence in hot stars, CoAst 158, 61
- **Brott**, I., Hunter, I., de Koter, A., et al. 2009, Rotational mixing in Magellanic clouds B stars - Theory versus observation, CoAst158, 55
- Hunter, I., **Brott**, I., Lennon, D. J., et al. 2008, The VLT FLAMES Survey of Massive Stars: Rotation and Nitrogen Enrichment as the Key to Understanding Massive Star Evolution, ApJL, 676, 29
- Kučinskas, A., Hauschildt, P. H., **Brott, I.**, et al. 2006, Broad-band photometric colors and effective temperature calibrations for late-type giants. II. Z < 0.02, A&A, 452, 1021

- Kučinskas, A., Hauschildt, P. H., Ludwig, H.-G., et al. 2005, Broad-band photometric colors and effective temperature calibrations for late-type giants. I. Z = 0.02, A&A, 442, 281

Submitted to refereed journals

- **Brott, I.**, de Mink, S. E., Cantiello, M., et al., Rotating Massive Main-Sequence Stars I: Grids of Evolutionary Models and Isochrones, submitted to A&A
- **Brott, I.**, Evans, C. J., Hunter, I., et al., Rotating Massive Main-Sequence Stars II: Simulating a Population of LMC early B-type Stars as a Test of Rotational Mixing, submitted to A&A

Published in conference proceedings

- Lennon, D. J., Evans, C., Hunter, I., et al. 2010, The VLT-FLAMES Survey of Massive Stars, Proc. of "Hot and Cool: Bridging Gaps in Massive Star Evolution", ASP 425, 29
- Lennon, D. J., Trundle, C., Hunter, I., et al. 2010, B-Type Supergiants in the Magellanic Clouds, Proc. of "Hot and Cool: Bridging Gaps in Massive Star Evolution", ASP 425, 23
- Langer, N., **Brott, I**., Cantiello, M., et al. 2010, Light elements in massive single and binary stars, Proc. of "Light Elements in the Universe", IAU Sym. 268, 411
- Vallenari, A., Sordo, R., Tantalo, R., et al. 2010, Synthetic Stellar libraries and SSP simulations in the Gaia Era, Proc. of "Stellar Populations Planning for the Next Decade", IAU Sym. 262, 444
- Evans, C. J., Bastian, N., Beletsky, Y., et al. 2010, The VLT-FLAMES Tarantula Survey, Proc. of "Star clusters: basic galactic building blocks throughout time and space", IAU Sym. 266, 35
- Anders, P., Kotulla, R., Izzard, R., et al. 2010, GALEV Evolutionary Synthesis Models: Why Are They Special?, AAS, 42,443
- Sordo, R., Vallenari, A., Bouret, J. C., et al. 2009, New high resolution synthetic stellar libraries for the Gaia Mission, Proc. of "52 Sait Meeting'", Memorie della Societa' Astronomica Italiana 10, 80, 130
- de Mink, S. E., Cantiello, M., Langer, N., et al. 2008, Rotational mixing in close binaries, Proc. of "The Art of Modeling Stars in the 21st Century", IAU Sym. 252, 365
- Evans, C. J., Hunter, I., Smartt, S., et al. 2008, The VLT-FLAMES Survey of Massive Stars, Msngr, 131, 25

- **Brott**, I., Hunter, I. , Anders, P., et al. 2008, How Efficient is Rotational Mixing in Massive Stars ?, Proc. of "'First Stars II", AIP Conference Proc. 990, 273
- Langer, N., Cantiello, M., Yoon, S.-C., et al. 2008, Rotation and Massive Close Binary Evolution, Proc of "Massive Stars as Cosmic Engines", IAU Sym. 250, 167
- Kučinskas, A., Hauschildt, P. H., Ludwig, et al. 2006, Photometric colors of late-type giants: theory versus observations, Proc. of "'The Scientific Requirements for Extremely Large Telescopes", IAU Sym. 232, 276
- **Brott, I.**,Kreykenbohm, I., Lubinski, P., et al. 2006, A Deep Study of the 3C273 Field in γ-rays, Proc, of "Populations of High Energy Sources in Galaxies", IAU Sym. 230, 459
- **Brott, I.**, Swank, J., Mowlavi, N., & Shrader, C. 2005, INTEGRAL follow-up of GRO J1655-40, ATel 432
- Kučinskas, A., **Brott, I.**, Hauschildt, P. H., et al. 2005, Theoretical Modelling of Late-Type Giant Atmospheres: Preparing for Gaia, Proc. of "The Three-Dimensional Universe with Gaia", ESA SP-576, 591
- **Brott, I.** & Hauschildt, P. H. 2005, A PHOENIX Model Atmosphere Grid for GAIA, Proc. of "The Three-Dimensional Universe with Gaia", ESA SP-576, 565